Development of novel polysaccharide based adsorbents for precious metal recovery

by © Xiangpeng Gao submitted

to the School of Graduate Studies in partial fulfillment of the

requirements for the degree of

Doctor of Philosophy

Faculty of Engineering and Applied Science

Memorial University of Newfoundland

March, 2018

St.John's Newfoundland and Labrador

Abstract

Biosorption is a green, efficient, and low cost method to recover precious metals from aqueous solutions compared to conventional methods. Over the past two decades, great efforts have been made to fabricate biosorbents to recover precious metals from natural polysaccharides in batch adsorption process. However, most of the studies were focused on mono-metallic solutions, while biosorption from multi-metallic solutions should be addressed as it is more closely parallels the real life scenario. In addition, the adsorption mechanism is not clearly defined, especially for the competitive adsorption of multi metal ions. Moreover, most of the polysaccharide based adsorbents synthesized are not suitable to be packed into fixed-bed columns for large-scale processes due to their poor mechanical strength, improper particle sizes, and extremely slow mass transfer rates. To fill these research gaps, this study mainly focuses on fabrication of polysaccharide based adsorbents with good selectivity as well as physical structure and mechanical strength, understanding the selective adsorption mechanism, and dynamic adsorption in fixed-bed column.

In this work, five polysaccharide-based adsorbents have been synthesized for selective adsorption of precious metals from multi-metallic solutions. Three adsorbents have been synthesized by cross-linking (or gelatinization) the polysaccharides (cellulose or sodium alginate), and then grafting functional groups onto the surface of the adsorbents. These adsorbents have exhibited outstanding selectivity towards precious metals as well as high capacities. Biosorption of Au (III) in acidic media are mediated by the electrostatic and

covalent interactions between Au (III) and hydroxyl, carboxyl, amino, and –C=S functional groups. Porous epichlorohydrin/thiourea modified alginate adsorbent (PETA) has been synthesized by direct templating method. PETA has shown great capacities and selectivity as well as remarkable improvement in adsorption kinetics than the nonporous adsorbent. In order to achieve a smaller diameter for the purpose of fixed-bed adsorption test, a microsphere adsorbent (ETA) has been synthesized by facile emulsion method of a water-in-oil emulsion of modified alginate. ETA microspheres were packed into a fixed-bed column and a mathematical model was applied to describe the breakthrough curves of Pd (II) and Cu (II) ions under different experimental conditions.

Several characterization methods were applied to investigate the adsorption mechanism. The polysaccharides, synthesized adsorbents, and the adsorbents after adsorption were characterized by FT-IR spectroscopy to identify the chemical bonds and functional groups. Scanning electron microscope (SEM) images were recorded to observe the surfaces and structures of the adsorbents. X-ray photoelectron spectroscopy (XPS) was used to determine the electron donors and acceptors from the shift of their binding energies. X-ray diffraction (XRD) was used to detect the reduced gold particles.

A transport-dispersive model with a linear driving force kinetics equation was utilized to predict breakthrough curves of Pd (II) and Cu (II) in the fixed-bed packed with ETA microspheres. A pH-dependent competitive Langmuir isotherm was developed and used in the simulation. Effects of flow rates, feed concentrations, and pH values were studied and experimental data were used to validate the mathematical model. The good agreement between the simulated and experimental breakthrough curves confirms that

transport–dispersive model is capable of predicting the dynamic adsorption performance over wide operating range.

Acknowledgments

First and foremost, I would like to thank my supervisors, Dr. Yan Zhang and Dr. Yuming Zhao, for their extraordinary, patience, and selfless guidance throughout this research project. I am extremely grateful to them for spending so much time on this work and share their broad and profound knowledge with me. I also would like to thank Dr. Stephen Butt, who is a member of my Ph.D committee, for his feedback and assistance. My appreciation also goes to Dr. Shafiq Alam for the supervision and support in the first two years of my program.

I am also grateful to Dr. Manju Gurung and Dr. Hari Paudyal for their instructions and suggestions on this project. My gratitude also goes to Dr. Wanda Aylward, Adam Gerald Beaton, Dave Grant, and Nicholas Ryan for their help with experimental analysis. I would give my appreciation to all group members in the Hydrometallurgy lab for their cooperative work and patience with me. The financial support from Memorial University of Newfoundland and RDC is also gratefully acknowledged.

I would like to thank my parents and my wife, for their consistency understanding, unconditional love, and support which makes everything possible. Any laudatory and appreciation words are not excessive to express my gratitude to them.

Table of Contents

List of Tables

List of Figures

List of Abbreviations and Symbols

AG	Aminoguanidine
AuNPs	Gold nanoparticles
BE	Binding energy
BET	Brunauer-Emmett-Teller surface area analysis
BJH	Barrett-Joyner-Halenda pore size and volume analysis
DMF	Dimethylformamide
DOEs	Design of experiments
ECH	Epichlorohydrin
ECH-AG-cellulose	Epichlorohydrin cross-linked N-aminoguanidine modified cellulose
ETA	Epichlorohydrin/thiourea modified alginate
ETSA	Epichlorohydrin/thiourea modified sulfuric acid gelatinized alginate
FT-IR	Fourier-transform infrared spectroscopy
HASB	Hard and soft acids and bases
ICDD	International Center for Diffraction Data
ICP-OES	Inductively coupled plasma-optical emission spectrometry
IR	Infrared spectroscopy
MTZ	Mass transfer zone
NETA	Nonporous epichlorohydrin/thiourea modified alginate
NTA	Nanoparticle Tracking Analysis
PDF	Powder diffraction files

PETA	Porous epichlorohydrin/thiourea modified alginate
PZC	Point of zero charge
SEM	Scanning electron microscope
Suf-AG-cellulose	Concentrated sulfuric acid cross-linked N-aminoguanidine modified cellulose
UV-Vis	Ultraviolet-visible spectroscopy
XPS	X-ray photoelectron Spectra
XRD	Powder X-ray diffraction
XRF	X-ray fluorescence
b	Langmuir constant related to adsorption affinity, L/mmol
c_t	Concentration of metal ions at time t, mmol/L
C_e	Equilibrium concentration of metal ion in the solution, mmol/L
C_i	Initial concentration of metal ion in the solution, mmol/L
$C_{i,\exp}$	Experimental concentration at point i of the breakthrough curve, mmol/L
$C_{i,\mathrm{mod}}$	Model prediction concentration at point i of the breakthrough curve, mmol/L
C_P	Concentration of the solute inside the pores, mmol/L
C_s	Concentration of the component in the stationary phase, mmol/L
d_p	Diameter of the adsorbent, cm
D_a	Apparent dispersion coefficient, cm^2/min

D_L	Axial dispersion coefficient, cm^2/min
D_m	Molecular diffusion, cm^2/min
D_P	Diffusion coefficient of the solute in the particle pores, cm^2/min
F	Phase ratio
$F_{(p)}$	Error function for parameter optimization
k_1	Pseudo-first-order rate constant, h^{-1}
k_2	Pseudo-second-order rate constant, g $mmol^{-1}$ h^{-1}
k_a	Adsorption rate constant
k_d	Desorption rate constant
K_a	Adsorption equilibrium constant
k_f	Lumped mass transfer coefficient, cm/min
M_F	Mass flux pf solute from the bulk solution to the external surface of the particle
n	Constants from Freundlich isotherm equation
q	Amount of metal ions adsorbed per mass unit of adsorbent, mmol/g
q_e	Amount of metal ions adsorbed per mass unit of adsorbent at equilibrium, mmol/g
q_m	Maximum adsorption capacity, mmol/g
q_s	Column saturation capacity, mmol/g

q_t	Amounts of metal ions adsorbed per mass unit of adsorbent at time t, mmol/g
Q	Flow rate, mL/h
t	Time, min
u	Interstitial velocity, cm/min
V	Volume of the solution, mL
V_t	Volume of the solution at time t, mL
W	Mass of the adsorbent, mg
ε	Porosity of fixed-bed
ε_p	Internal porosity of the particle

Chapter 1 Introduction

1.1 Problem Statement

Precious metals have been widely used in electrical, medical, architecture, aerospace, and jewelry industries due to their excellent bio-compatibility, conductivity, and appearance. The increasing demand for precious metals has attracted considerable concern towards the recovery and reuse of these metals from mining wastes and industrial effluents. Biosorption, a physicochemical process which is defined as the passive uptake of substances from solution by dead or inactive biological materials (i.e., biosorbents) is a promising technology for precious metal recovery (Das, 2010; Wang & Chen, 2014; Won, Kotte, Wei, Lim, & Yun, 2014). Over the last two decades, great efforts have been made to fabricate cost-effective biosorbents from various biomass resources (Dodson et al., 2015; Fiset, Blais, & Riveros, 2008; Won et al., 2014). Among the biomass resource pool, polysaccharides (e.g., cellulose, chitin and chitosan) extracted from plants, animals, and microorganisms are good candidates as adsorbents for metal ions (Benguella & Benaissa, 2002; Gurung, Adhikari, Gao, Alam, & Inoue, 2014; Zhang et al., 2013; Zhang, Zhang, & Helleur, 2015).

Polysaccharide-based biosorbents demonstrated higher adsorption capacity and selectivity for metal ions due to various functional groups (hydroxyl, carboxyl or amino) present in polymer chains (Bailey, Olin, Bricka, & Adrian, 1999; Liu, Wang, Yu, & Meng, 2013; O'Connell, Birkinshaw, & O'Dwyer, 2008; Varma, Deshpande, & Kennedy, 2004). However, polysaccharides in their natural forms cannot be used as biosorbents directly

due to their poor chemical resistance and mechanical strength. Chemical modifications through surface grafting and cross-linking of natural polysaccharides are the most widely used methods to fabricate biopolymer based adsorbents.

Most of the reported polysaccharide-based adsorbents prepared by surface grafting and cross-linking are normally in the forms of fine powder or nonporous hydrogels (Klimmekand, Stan, Wilke, Bunke, & Buchholz, 2001; Minamisawa, Minamisawa, Yoshida, & Takai, 2005; Parajuli & Horita, 2009), not suitable to be used as the stationary phase in a fixed-bed adsorption column because of their low porosity, poor reusability and hydrodynamic limitations. Development of porous polysaccharide-based resins (adsorbents) is the key to large-scale adsorption process of precious metal ions. So far, chitosan, a cationic polysaccharide obtained by partial deacetylation of chitin, the major component of crustacean shells has been widely used as the building block to fabricate polysaccharide-based biosorbents in different physical forms (Chen & Wang, 2012; Donia, Atia, & Elwakeel, 2007; Guibal, 2004; Zhang et al., 2015). Developing sustainable, environmentally-friendly biosorbents from the more abundant biopolymers, i.e., cellulose and alginate deserves further study.

Adsorption of precious metal ions by polysaccharide-based sorbents involves complex sorption mechanisms. Understanding the binding mechanism is thus important because it enables the possibility for further improving the adsorption performance (e.g., capacity, selectivity and adsorption rate). Generally, the binding of metal ions by biosorbents are mainly through electrostatic attraction, ion exchange and chelation. Due the influence of solution pH, polysaccharide-based adsorbents can be either positively or negatively

charged, leading to different sorption mechanisms under different pH values. Identification of the potential sorption mechanism of metal ions by means of IR, SEM, XPS and XRD analyses of metal loaded sorbents is of great importance.

It is also noticed that comprehensive study on modelling and simulation of the fixed-bed adsorption of metal ions by polysaccharide-based adsorbents are seldom reported. The dynamic column adsorption process is preferred compared to batch adsorption because it is more efficient and productive. Modelling and simulation of fixed-bed adsorption is an excellent alternative to experimental investigation for a good prediction on the adsorption of metal ions under different operating conditions. Development of proper isotherm and mass transport models which are capable of predicting adsorption of metal ions in packed-beds over wide operating conditions is valuable because it helps to optimize the adsorption performance without running many experiments.

To address these issues, the present work endeavors to develop various biosorbents using cellulose and alginate as the building blocks to selectively adsorb precious metal ions from multi-metallic solution. Development of cost-effective technologies to recover precious metals from electrical waste and mining effluent will help to build a circular route for recovery and reuse of these valuable elements.

1.2 Objective and Scope of Study

The objectives of this research are to a) develop facile fabrication methodologies to prepare polysaccharide-based adsorbents which demonstrate high uptake capacity, good selectivity, easy accessibility and good reusability; b) characterize the functional groups

involving the metal binding and the binding mechanisms; and c) develop mathematical tools which facilitate the design and optimization of large-scale recovery process in fixed-bed adsorption.

In order to achieve these objectives, the scope of this study covers:

- Biosorbent preparation

Cellulose and alginate were selected as the raw biomass to prepare adsorbents for the recovery of precious metal ions in both batch and fixed-bed adsorption processes. Surface grafting, cross-linking and direct-templating methods were employed to construct five different types of biosorbents. Characterization of the fabricated biosorbents was carried out using FT-IR, XPS and SEM-EDS.

- Adsorption isotherm and kinetic studies

Adsorption isotherm quantifies the amount of adsorbate on the adsorbent as a function of its concentration at constant temperature. Adsorption isotherm illustrates the equilibrium uptake of metal ions by the prepared adsorbent at different initial metal concentrations. Adsorption kinetics, which reflects the rate of mass transfer of metal ions from liquid phase to solid phase, is an indicator of efficiency for an adsorption process. Static adsorption of metal ions by the synthesized adsorbents was carried out for the adsorption isotherm and kinetics studies.

- Identification of biosorption mechanism

Metal uptake through biosorption is a complex process which involves electrostatic interaction, ion exchange, chelation/complexation and/or chemical reduction. Thus, potential implementation strategies should be involved to support the results of adsorption equilibrium and kinetics, such as FT-IR, XPS, XRD, and SEM, which are essential to identify the interaction between metals and adsorbents.

- Modelling and experimental verification of fixed-bed adsorption

The transport-dispersive model was selected to simulate the breakthrough adsorption of palladium and copper ions by modified alginate microspheres. Inverse method was adopted to derive the model parameters, followed by the validation of the mathematical model and model parameters by experimental results under different flow rate, initial metal concentration and solution pH. To address the influence of pH on the breakthrough curves, a pH-dependent competitive Langmuir isotherm was developed and used in the simulation.

1.3 Thesis Outline

This thesis includes seven chapters. Chapter 1 is the introduction which covers the background, the scope, and the objectives of this study. Chapter 2 gives an overall review on the most relevant research with respect to the biosorption of precious metals. Chapter 3 focuses on the selective adsorption of gold ions by chemically modified cellulose. Detailed adsorption equilibrium, kinetics and the potential adsorption mechanism are presented. Following Chapter 3, biosorption and reduction of Au (III) to gold nanoparticles by modified alginate was introduced in Chapter 4. Different methods to

characterize gold nanoparticles are addressed. Chapter 5 presents the fabrication of porous modified alginate microbeads by direct templating method. Fast adsorption kinetics of gold ions by the porous adsorbent was observed. Chapter 6 shows the modelling and simulation of breakthrough adsorption of palladium and copper ions in a fixed-bed column packed with modified alginate microspheres. The model and model parameters were validated using experimental results obtained under various operation conditions. Major conclusions from this study and recommendations for future work are summarized in Chapter 7.

Chapter 2 Literature Review

2.1 Precious metal recovery and biosorption

Precious metals, such as gold, silver, platinum, and palladium are rare, naturally occurring metallic chemical elements of high economic value. The development of precious metals recovery technology has become attractive because of the growing demand for these precious metals in industrial processes and jewelry markets. Over past decades, due to the gradual depletion of high-grade ore resources and the passage of increasingly stringent environmental legislation, significant proportions of precious metals are obtained through secondary resources, such as electronic wastes and industrial effluents (Widmer, Oswald-Krapf, Sinha-Khetriwal, & Schnellmann, 2005).

Traditional methods for the recovery of precious metals include ion exchange, chemical precipitation, and membrane filtration. The advantages and disadvantages of these methods are listed in table 2.1. Biosorption, a physicochemical process in which the passive uptake of pollutants by dead or inactive biological materials occurs, is a promising technology for the recovery of precious metal ions from waste solutions. Over the past two decades, great efforts have been made to fabricate biosorbents from various biomass resources including bacteria, fungi, yeast, and algar. Usually, biomass in its original form cannot be used as a biosorbent due to its low uptake capacity and poor mechanical strength. Chemical modification (though cross-linking and surface grafting) of raw biomass has been widely explored to prepare the low-cost biosorbents. Through chemical modification of biomass materials or extracted biopolymers, these biosorbents

possess metal-sequestering property and can be used to concentrate precious metals or remove heavy metals. Compared to traditional metal recovery methods, biosorption has high capacity, fast kinetics, as well as possible selectivity depending on the synthesis methods; therefore it is an ideal candidate for the treatment of high volume and low concentration complex wastewaters or industrial effluents (Wang & Chen, 2009).

Table 2.1 Advantages and disadvantages of traditional methods for recovery of precious metals

Technology	Advantages	Disadvantages	Reference
Ion-exchange	Metal selective Limited pH tolerance High regeneration	High initial capital cost High maintenance cost	Aderhold, Williams, & Edyvean, 1996
Chemical precipitation	Process simplicity Not metal selective Inexpensive capital cost	Large amount of sludge containing metals Sludge disposal cost High maintenance cost	Aderhold et al., 1996
Membrane filtration	Low solid waste generation Low chemical consumption Small space requirement Possible to be metal selective	High initial capital cost High maintenance and operation cost Membrane fouling Limited flow rates	Madaeni & Mansourpanah, 2003 Qin, Wai, Oo, & Wong, 2002

2.2 Biosorbents

In the biosorption process, the focus is on the interaction and immobilization by sequestering of the metallic elements through their deposition in the microbial-based biosorbents (Volesky, 1990). According to Volesky (1990), biosorption processes are mainly applied to the toxicity removal, which is an environmental aspect; and recovery of valuable metals, which is a technological aspect. Ideal biosorbents should have the following characteristics: good stability under application conditions, high capacity for the objective metals, good selectivity, easy separation from aqueous solution, and easy to

regenerate (Wang & Chen, 2014). Recovery of precious metals using polysaccharide-based adsorbents has long been a focus of study. Among polysaccharides, cellulose and alginate are widely used as the base matrices for the adsorption of precious metals (Abdolali et al., 2014; O'Connell, Birkinshaw, & O'Dwyer, 2008).

Cellulose from wood and cotton has been used for thousands of years as an energy source, a building material, and clothing (O'Connell et al., 2008). The molecular structure of cellulose is a carbohydrate polymer that consists of repeating β-D-glucopyranose units which are covalently linked through acetal functions between the OH group of the C_4 and C_1 carbon atoms (Gurung et al., 2014). Currently, two main approaches are used in the preparation of cellulose-based biosorbents. The first method directly modifies the cellulose backbone by introducing chelating or metal binding functionalities that produce a range of heavy metal adsorbents. The second method grafts selected monomers to the cellulose backbone either by directly introducing the metal binding capacity or by the subsequent functionalization of these grafted polymer chains with known chelating moieties (O'Connell et al., 2008). Most of the cellulose based biosorbents exhibited high capacities toward metal ions. Some of these biosorbents have good selectivity towards precious metals in very low pH conditions (Adhikari et al., 2007, 2008a, 2008b; Dwivedi, Dubey, Hokkanen, Fallah, & Sillanpaa, 2014; Pangeni et al., 2012). The equilibrium time for these biosorbents ranged from 5 hours to 40 hours. In these studies, cellulose based biosorbents were usually modified with amino, sulfonic, or sulfhydryl groups for a better sorption performance. These biosorbents, in the form of powder or flakes, have limited

applications due to their low mechanical strength and may cause clogging problems in industrial columns.

Alginate, also called alginic acid, is a linear copolymer with homopolymeric blocks of (1-4)-linked β-D-mannuronate (M) and C-5 epimer α-L-guluronate (G) residues, respectively, covalently linked together in different sequences or blocks. This polymer is extracted by treating seaweed with a sodium carbonate solution and recovered by precipitation as alginic acid or sodium salt (Fiset et al., 2008). It is inferred that the carboxyl groups and the pyranose oxygen atoms from the alginate will form stable five membered chelates with metal ions (Ghimire, Inoue, Ohto, & Hayashida, 2008; Paudyal et al., 2013). Due to its chemical properties, alginate can be fabricated into both powder and bead form biosorbents. Sodium alginate can be first dissolved into water and then injected into calcium chloride solution to form solid calcium alginate beads, which exhibit good sorption performance for cationic metal ions (Torres et al., 2005). However, calcium alginate beads are hydrogels which do not have porous structures and are slow in mass transfer rate. Table 2.2 lists some cellulose and alginate based biosorbents for precious metal recovery.

Table 2.2 List of cellulose and alginate based biosorbents for precious metals

	Biosorbent	Adsorption capcity (mg/g)	Reference
Cellulose based biosorbents	Taurine modified cellulose	Au(III) 34.5	Dwivedi et al., 2014
	Taurine modified cellulose	Ag(I) 55	Dwivedi et al., 2015
	Dehydrated date palm leaves	Pd(II) 192.3 Pt(II) 49.5	El-Shafey, 2013
	Oxidized hemp fibers	Ag(I) 198.48	Kostic, Milanovic, Baljak, Mihajlovski, & Karmar, 2014
	Iminodiacetic acid-modified waste paper	Au(III) 649.97 Pd(II) 151.12	Adhikari et al., 2007
	Dimethylamine modified waste paper	Au(III) 906.06 Pd(II) 223.48 Pt(IV) 175.57	Adhikari et al., 2008a
	P-aminobenzoic acid-modified paper gel	Au(III) 1004.50 Pd(II) 159.63 Pt(IV) 97.54	Adhikari et al., 2008b
	Cotton cellulose gel	Au(III) 1223.12	Pangeni et al., 2012b
	Cross-linked pure cellulose gel	Au(III) 1089.19	Pangeni et al., 2012a
	Organodiphosphonic acid modified spent buckwheat hulls	Au(III) 465.16	Xu et al., 2013
	Biomolecule-cellulose complexes	Pd(II) 175.44	Yunus & Tsai, 2015
	Tertiary-amine modified cedar wood	Pd(II) 148.99	Parajuli & Hirota, 2009
Alginate based biosorbents	Sargassum fluitans	Au(I) 0.63	Niu & Volesky, 1999
	Ca-alginate beads	Au(III) 290 Ag(I) 52	Torres et al., 2005
	L-cysteine impregnated alginate capsules	Au(III) 298.2	Kotte & Yun, 2014
	Turbinaria conoides	Au(III) 34.5	Vijayaraghavan, Mahadevan, Sathishkumar, Pavagadhi, & Balasubramanian, 2011
	Fucus vesiculosus	Au(III) 68.94	Mata et al., 2009
	Chlorella vulgaris	Ag(I) 56.7	Cordery, Will, Atkinson, & Wills, 1994
	Sargassum sp.	Au(III) 32.94	Sathishkumar, Mahadevan, Vijayaraghavan, Pavagadhi, & Balasubramanian, 2010

In some studies, raw materials containing cellulose or alginate were washed, dried, and grinded into powder to function as biosorbents (Mata et al., 2009; Niu & Volesky, 1999; Sathishkumar et al., 2010; Vijayaraghavan et al., 2011). These biosorbents are

inexpensive and easy to prepare, however, it is difficult to explain the mechanisms for these sorbents because of their complex chemical components. Furthermore, in order to increase the capacity of biosorbents, biopolymers are preferred because they contain more useful sorption sites.

2.2.1 Evaluation of biosorbents

The conventional metal recovery methods suffer with incomplete metal removal, high capital cost, high energy requirement, and a disposal of the secondary wastes generated (Mack et al., 2007). Therefore, a feasible biosorption process is an alternative and effective method to recover precious metals from the waste solutions. Several required specifications were considered to evaluate the performance of biosorbents including capacity, selectivity, regeneration, mass transfer kinetics, cost, and process applicability.

Capacity is the amount of metal ions sequestered per unit mass of biosorbents. Precious metal biosorption mechanism is generally regarded as physico-chemical interactions between metal ions and the functional groups present on the surface of biosorbent. This includes electrostatic interactions, ion exchange, chelation or complexation, microprecipitation, and reduction. Carboxyl, hydroxyl, amine, and phosphoryl functional groups presented on the biosorbent account for such interactions (Won et al., 2014). Metal uptake capacity is strongly dependent on the pH value of the metal ion solutions. Competition between cations and protons for binding sites means that biosorption of metals like Cu, Cd, Ni, Co, and Zn is often reduced at low pH values. Conversely for

anionic metal species including $Au(CN)_2^-$, $PtCl_4^{3-}$, CrO_4^{2-}, and SeO_4^{2-}, increasing uptake capacity can be observed at lower pH values (Gadd, 2009).

Selectivity is an important criterion for evaluating the adsorption performance, especially for multi-metallic solutions which is common in wastewater and industrial effluents. As long as selective biosorbents are available, the separation of precious metals becomes simple and cost effective. Selectivity can be achieved by modifying surface functional groups of the biosorbent, or adjusting the solution pH value. It is worth noticing that for precious metals including Au, Pt, and Pd, the species existing in high chloride environments are chloride complexes. Therefore, the complex ionic species must be considered because of the metal binding mechanism is different as simple metal ions (Mack et al., 2007). However, developing selective biosorbents is still very challenging as co-existing metal ions compete with targeted metal ions for binding sites.

In industrial applications, biosorption needs to be performed in sequential cycles with uniform performance. Regeneration of biosorbent is thus important for saving time and reducing capital cost in the process. The biosorption need to be washed by specific solution to remove the adsorbed metal ions, therefore exposing the sorption sites, regenerated for a new adsorption-desorption cycle. The capacity of biosorbents will show a gradual decay after sequential cycles, due to the aging and poisoning of the biosorbents.

The adsorption-desorption time depends on the mass transfer of metal ions from bulk solution phase to the binding sites on the biosorbents. Combination of film diffusion in the aqueous phase and intra-particle diffusion in the adsorbents is termed as mass transfer

kinetics (Won et al., 2014; Kanai, Oshima, & Baba, 2008). In general, intra-particle diffusion is the rate determining step in the sorption process. Therefore, modifying the biosorbent to increase the intra-particle diffusion rate is an efficient approach for achieving faster mass transfer kinetics (Won et al., 2014).

In the past decades, microorganism-based biosorbents were prepared which have good sorption capacities towards precious metals (El-Shafey, 2013; Kostic et al., 2014; Pangeni et al., 2012). However, these biosorbents have small particle size, poor mechanical strength, difficulty in solid-liquid separation, and severe pressure drop in the column system. The solution of such problems is to apply proper immobilization technique. Immobilization provides a biosorbent the right size, mechanical strength, rigidity, and good porosity (Vijiayaraghavan & Yun, 2008; Won et al., 2014).

2.2.2 Chemical modification

Physical and chemical treatments are used for biomaterial modification, which include autoclaving, steaming, thermal drying, grinding, mechanical disruption, washing with detergents, and acid or alkali treatment (Gautam, Mudhoo, Lofrano, & Chattopadhyaya, 2014). These methods were generally used as a pre-treatment process for biosorbents. The purpose of pre-treatment of biomaterial is to remove impurities or to activate the binding sites. Chemical pre-treatments have been preferred because of their simplicity and efficiency (Vijayaraghavan & Yun, 2008). Some researchers reported that by acid or alkali pretreatment, the sorption capacity was enhanced by rupture on the surface wall

(Akar & Tunali, 2006) or elimination of impurities blocking the binding sites (Won et al., 2014).

Chemical modification is usually involved in the preparation of biosorbents after pre-treatment, which generally includes cross-linking and surface grafting. The purpose of crosslinking is to increase chemical stability and mechanical strength while surface grafting can enhance the sorbent selectivity and increase the metal uptake capacity.

Cross-linking is the most common procedure to treat with biomass or biopolymers to build a 3D structure, therefore changing their solubility and enhance their mechanical strength. However, cross-linking usually decreases the metal uptake capacity because some sorption sites on the biomass or biopolymers are consumed in the reaction.

Several cross-linkers have been used in the preparation of sorbents including glutaraldehyde (Ruiz, Sastre, & Guibal, 2000; Wang et al., 2012), epichlorohydrin (Ghimire, Inoue, Ohto, & Hayashida, 2007; Gurung et al., 2014; Huo, Su, & Tan, 2009; Laus, Costa, Szpoganicz, & Favere, 2010; Zhou, Wang, Liu, & Huang, 2009), calcium chloride (Bertagnolli et al., 2014; Ghimire et al., 2007; Paudyal et al., 2013), formaldehyde (Ghimire et al., 2007), concentrated sulfuric acid (Gurung et al., 2014), triphosphate (Laus et al., 2010), and thiourea (Dai, Ren, &Tao, 2012).

Glutaraldehyde is used as the cross-linker for chitosan as the biosorbents toward gold and palladium, respectively (Ruiz et al., 2000; Wang et al., 2012). It is inferred that chitosan can react with glutaraldehyde to form double imine bonds (C=N) and double ethylenic bonds (C=C) (Monteiro Jr & Airoldi, 1999; Poon, Wilson, & Headley, 2014).

Glutaraldehyde can be used to cross-link chitosan through imine linkages between the amine groups of chitosan and the aldehyde groups of the cross-linking agent (Ruiz et al., 2000).

Epichlorohydrin is used as the cross-linker in seaweed, chitosan, and cellulose (Ghimire et al., 2007; Gurung et al., 2014; Huo et al., 2009; Laus et al., 2010; Zhou et al., 2009). Epichlorohydrin is effective in grafting sulfur groups in cross-linking of cellulose (Ghimire et al., 2007). The cross-linking mechanism of epichlorohydrin is inferred by Simkovic et al. (Simkovic, Laszlo, & Thompson, 1996) when cross-linking starch. Epichlorohydrin cross-linking occurs on the C-6 alcohol groups of glucopyranose units when ammonium hydroxide (or sodium hydroxide) exists.

Calcium chloride is used to cross-link alginate to prepare biosorbents (Bertagnolli et al., 2014; Ghimire et al., 2007; Paudyal et al., 2013). Calcium chloride cross-linked alginate has good selectivity towards divalent ions but the performance on monovalent ions is poor (Paudyal et al., 2013). When alginic acid reacts with calcium ions, a cross-linking effect takes place, which gives the resulting alginate gel a significant structural strength (Nestle & Kimmich, 1996). The cross-linking is caused by a polyvalent ion binding with two or more carboxylic groups on adjacent polymer chains, and this can be accompanied by chelation of the ion by the hydroxyl and carboxyl groups of the polymer chains (Shimizu & Takada, 1997).

Concentrated sulfuric acid is used in the cross-linking of pure cellulose on the hydroxyl groups by Gurung et al. This reaction makes the biopolymer rigid and highly amorphous

(Gurung et al., 2014). However, some biopolymers are carbonized rather than cross-linked when treated with concentrated sulfuric acid.

Formaldehyde and triphosphate are also reported as cross-linkers in some research (Dai et al., 2012; Ghimire et al., 2007; Laus et al., 2010). Formaldehyde was used in the cross-linking of seaweed by Ghimire et al. to compare the performance with epichlorohydrin and calcium chloride (Ghimire et al., 2007). Triphosphate is a non-toxic multivalent anion that cross-links chitosan by the positively charged amino groups and the negatively charged counterions of the triphosphate molecules (Laus et al., 2010).

Biomass can be cross-linked into powder form or microsphere form, which has their own properties for biosorption applications. For powder or flake form biosorbents, the metal uptake capacity is usually very high due to high density of sorption sites. These biosorbents also have superior sorption kinetics because of their large surface area which would increase the contact chance of biosorbents with metal ions. However, powder form biosorbents are not suitable to be packed in a column for applications at preparative scale because they may cause clogging problems, a huge pressure drop or serious hydrodynamic limitations. Therefore, microsphere biosorbents were preferred as they have good physical properties for dynamic column adsorption.

Microsphere biosorbents can be prepared through gelation, which can occur by either by physical linking or chemical cross-linking. The physical gel involves physical bonds, while chemical gelation involves covalent bonds. For cellulose and alginate, dropping

procedures or dispersion procedures can be applied in the synthesis of microsphere biosorbents (Gericke, Trygg, & Fardim, 2013).

Microsphere beads can be obtained by the formation of spherical droplets of a polysaccharide solution and solidification of these droplets in a coagulation bath of a non-solvent. This synthesis method generally is applied by pressing the solution through a syringe nozzle, forming a droplet when the combined forces of gravity and pressure used for injection exceed a certain value determined by surface tension and capillary forces (Gericke et al., 2013). Optimization of ejection speed, falling height, and solution viscosity are consequently important for the preparation of microsphere using a dropping procedure (Sescousse, Gavillon, & Budtova, 2011; Trygg, Fardim, Gericke, Mäkilä, & Salonen, 2013). The diameter of microspheres obtained by dropping procedure is limited to approximately 0.5-3 mm, which is restricted to the size of droplets that can be prepared.

Dispersion procedure is a relatively advanced method compared to dropping procedure as the diameter ranges from 10 to 800 μm. In this procedure, a solution is dispersed in an immiscible solvent of opposite polarity under high rotational speed results in the formation of emulsions that can be stabilized with the aid of surfactants (Karbstein & Schubert, 1995). The diameter of the droplets is determined by mixing speed, type, amount of surfactant, ratio of hydrophobic to hydrophilic solvent, and viscosity (Kotoulas & Kiparissides, 2006; Maggioris, Goulas, Alexopoulos, Chatzi, & Kiparissides, 2000).

Synthesized microsphere biosorbent have been applied in the dynamic column adsorption (Du, 2017; Jang et al., 2018; Kondo, Hirayama, & Matsumoto, 2013; Liu et al., 2012).

These biosorbent illustrated much better applicability in the column adsorption than powder or flake biosorbents. However, because of slow mass transfer kinetics, microsphere biosorbents without porous structure have limitations in the feed flow rate and initial concentration. Therefore, synthesis of porous microsphere biosorbents has been a focus of study due to their superior mass transfer kinetics and mechanical structures.

Surface grafting of functional groups on the biopolymer can increase the metal capacity as well as enhance the selectivity toward specific metal ions. The HASB (hard and soft acids and bases) theory explains the functional group binding affinity with metals. “Soft” or “hard” and “acid” or “base” is assigned to chemicals. “Hard” applies to species which are small, highly charged (which applies mainly to acids and to a lesser extent to bases), and are weakly polarizable. “Soft” applies to species which are large, lowly charged, and are strongly polarizable (Jolly, 1984). The theory states that soft acids react faster and form stronger bonds with soft bases, whereas hard acids react faster and form stronger bonds with hard bases. For precious metals and toxic metals, Cr^{3+}, Cr^{6+}, and Au^{3+} are hard acids, Pt^{2+}, Pd^{2+}, Ag^{+}, Au^{+}, and Cd^{2+} are soft acids, and Cs^{+} and Pb^{2+} are borderline acids. OH^{-}, RO^{-}, F^{-}, Cl^{-}, and NH_3 are common hard bases; RS^{-}, SCN^{-}, and CN^{-} are common soft bases, whereas pyridine, nitrate, and sulfate anions are borderline bases (Jolly, 1984). Proper functional groups can be chemically grafted onto the biopolymer to adsorb certain metals from solution. Nitrogen, sulfur, and oxygen containing groups have shown great performance in biosorption towards different precious metal ions (Adhikari et al., 2008a; Donia et al., 2007; Dong, Liu, Yuan, Yi, & Zhao, 2016; Wang et al., 2012; Won et al.,

2014). In these studies, amine, carboxyl, hydroxyl, sulfonate, phosphonate, and Schiff base were proven to be efficient in binding precious metals. These functional groups work as electron donors that donate electrons to precious metal ions, forming covalent or ionic links.

Amine functional groups which are responsible for binding of anionic solutes were introduced to the carboxyl groups of brown macroalga by reacting with propylamine (Kousha, Daneshvar, Sohrabi, Jokar, & Bhatnagar, 2012). The uptake of acid orange II was approximately two times higher than the un-treated biomass. Radiation was used to grafting amine groups and hydroxyl groups on cellulose microsphere (Dong et al., 2016). The resulting biosorbent was effective in binding $AuCl_4^-$ by ion exchange and chelation. It is also reported that amine functional groups showed improvement of capacity on precious metals (Adhikari et al., 2008a; Elwakeel, El-Sayed, & Darweesh, 2013; Gurung et al., 2013).

Carboxyl groups provide binding sites for cationic solutes, which were commonly grafted on the biomass surface by reacting with citric acid (Marshall, Wartelle, Boler, Johns, & Toles, 1999; Vaughan, Seo, & Marshall, 2001). Citric acid can react with hydroxyl groups of the biomass to form an ester linkage. Carboxyl functional groups can be introduced to chitosan-based biosorbents by carboxymethylation, which can dramatically increase the metal uptake capacity (Wang et al., 2016; Zhang et al., 2015). Other grafting approaches include treated by succinic anhydride (Vijayaraghavan, Won, Mao, & Yun, 2008), in situ radical polymerization of divinylbenzene and acrylic acid (Gomes, Dutta, & Bhaumik, 2014), and grafting by maleic and phtalic (Abdolali et al, 2014).

Hydroxyl groups are rich in polysaccharides which are the main functional groups of biosorbents. Therefore, pre-treatment of raw biomaterials is the main methodology to expose hydroxyl groups on the surface of biosorbents. Washing by acid, alkali, or detergent are effective approaches for this purpose (Gautam et al., 2014). Sulfonate groups and phosphonate groups can be grafted on the polymer surface by reacting with sulfonic acid, phosphonic acid, or their salts (David, Ortega, Chougrani, Manseri, & Boutevin, 2011; Lu et al., 2011; Vaquette et al., 2013; Villemin et al., 2001).

2.2.3 Synthesis of porous microsphere biosorbents

Biosorbents in the form of porous microsphere have good physical properties for the column test. Metal ion containing solutions can transport in the pores of these sorbents, therefore creating more contact chances with sorption sites, which lead to faster sorption kinetics than conventional hydrogel beads. However, pore generation remains to be the main problem in porous microsphere biosorbents fabrication. Various attempts have been made to synthesis porous polymers including direct templating, block copolymer self-assembly, and direct synthesis methodologies (Wu et al., 2012).

The direct templating methodology is a simple and versatile approach for preparation of porous polymers. Direct templating is a molding or casting technique for the direct replication of the inverse structure of the preformed templates with stable morphology (Thomas, Goettmann, & Antonietti, 2008). The direct templating synthesis can generate a variety of porous networks with a wide range of pore sizes, well-defined morphologies on controllable length scales, and various chemical functionalities to match the needs of

different applications (Zhao et al., 2005). The general route for direct templating includes the following steps: template preparation, directed synthesis of target materials using the template, and template removal (Liu, Goebl, & Yin, 2013; Tran, Naseri, Kolasnikov, Bai, & Yang, 2011). A template is the most influencing parameter to the surface area, porosity, and morphology of the beaded polymer (Mane, 2015). Various templates, including sodium chloride, silica, paraffin spheres, sugar crystals, gelatin, and polymers have been successfully used to fabricate porous structures (Bencherif, Braschler, & Renaud, 2013; Draghi, Resta, Pirozzolo, & Tanzi, 2005; Wu et al., 2012). The template selection depends on the polarity and solubility parameter of monomer, polymer, and the interaction between them (Liu et al., 2013; Mane, 2016). Hard templates, which have a solid structure, usually yield better control of the product but the removal of the templates are difficult and in most cases environmental-unfriendly. In comparison, soft templates including surfactant and some polymers, are easier to eliminate from the product. The direct templating method synthesis is relatively easy, since the template structure is fixed, and the precise control over meso-/macropore structure can be achieved (Wu et al., 2012).

The block copolymer self-assembly methodology is very useful for synthesis mesoporous or macroporous polymer, especially materials with long-range order due to the microphase separation of incompatible blocks yielding mesoscale structures (Hillmyer, 2005; Olson, Chen, & Hillmyer, 2008). Block copolymers suitable for self-assembly can be regarded as hybrid macromolecules consisting of two or more chemically immiscible homopolymers that are covalently linked together (Wu et al., 2012). The phase separation occurs via self-assembly because of the thermodynamic incompatibility of these segments

to minimize contact energy between the segments of the copolymer. However, the separation is restricted to the nanometer scale because of the segment chain connectivity (Kim, Yang, Lee, & Kim, 2010). Generally, the block copolymer can function as the pore template, which is a sacrificial component that self-assembles with polymer precursors; or the block polymer can serve as the source of framework for the porous polymers (Olson et al., 2008; Wang & Li, 2011). Porous polymers synthesized by block copolymer seld-assembly have well-defined pore architectures and long-range order; however, the synthesis is usually hard to scale up due to high cost (Wu et al., 2012).

The direct synthesis methodology can directly generate pores during polymerization, followed by removal of the solvent from the pores (Jiang & Cooper, 2010; Mastalerz, 2008). Microporous polymers with extremely high surface area, mesoporous polymers, macroporous polymers, and hierarchical porous polymers can be prepared by this method. Polymerizable monomers are generally the raw materials for direct synthesis. The formation of pores by direct synthesis can be summarized into two procedures. One is derived from the networks of highly cross-linked polymer chains or the space-inefficient packing of highly rigid and contorted non-network polymer chains; the other results from the reaction-induced phase separation that forms a 3D continuous polymeric gel network (Al-Muhtaseb & Ritter, 2003; Pekala, 1989). The direct synthesis methodology has precise control of the pore structure but strict requirements on the monomer structures and synthetic routes are needed (Wu et al., 2012).

In addition to above three frequently used methodologies, some uncommon synthesis methods for porous polymers include high internal phase emulsion polymerization

(Kimmins & Cameron, 2011), interfacial polymerization (Li, Yoon, & Matyjaszewski, 2010; Sun & Deng, 2005), and breath figures (Bunz, 2006). High internal phase emulsion polymerization method generates very high porosity (typically 74-95 vol%), but the mechanical strength is often weak which is not suitable for the dynamic adsorption process. Interfacial polymerization is especially suitable for synthesizing nanocapsules, while breath figures method is usually used to prepare honeycomb patterned polymer films with ordered structure (Wu et al., 2012). The synthesis of porous polymers has already become and will continue to become a thriving area of research.

2.3 Adsorption Mechanism

The interaction between biosorbents and adsorbate depends on their chemical and physical properties, such as the pH of the solution and the other components in the system (Wang & Chen, 2014). XPS and FT-IR have been widely used to provide the interaction between functional groups of the biosorbents and the metal ions (Romera, González, Ballester, Blázquez, & Muñoz, 2007). The adsorption mechanism can be concluded into two categories in accordance to interaction types: physical adsorption and chemical reduction. It is important to observe that the sorption of metal ions may involve different mechanisms depending on the composition of the solution and the pH value.

2.3.1 Physical adsorption

Physical adsorption is a process in which the electric structure of the atom or molecule is seldom changed. The physical adsorption can be summarized into chelation and ion exchange (Fomina & Gadd, 2014; Guibal, 2004).

Chelation describes a particular way that ions and molecules bind with metal ions. Chelation involves the formation of two or more separate coordinate bonds between a polydentate ligand and a single central atom (Volesky, 1990). The theory of hard and soft acids and bases, as described above, demonstrates the ability of ions to interact or enter into coordinate bonding with other ions or ligands. Chelation generally depends on the availability of outermost electrons and empty molecular orbitals (Guibal, 2004). However, such a principle is more descriptive than explanatory and is not absolute. Some behaviors will be affected by metal concentration, as well as the relative metal concentrations in mixtures where competitive effects may occur (Fomina & Gadd, 2014). Hydrated metal ion radius also plays an important role in competitive chelation as the distance from metal ions to electron donors on the adsorbent affects the Van der Waals force. In order to regenerate the adsorbent which adsorbs metal ions by chelation, an eluent that forms stronger bonds with the metal ions is needed. The chelation of metal cations by ligands in solution may result in the formation of metal anions, which therefore turns the chelation mechanism to an electrostatic attraction mechanism on protonated functional groups (Guibal, 2004). Generally, increasing pH enhances adsorption of cationic metal ions, but reduces that of anionic metal ions.

Ion exchange is an exchange of ions between two electrolytes or between an electrolyte solution and a complex. In most cases, the term is used to denote the processes of purification, separation, and decontamination of aqueous and other ion-containing solutions with solid polymeric or mineralic ion exchangers. Activity series, which is an empirical and analytical progression of metal ions, is introduced to summarize the ion

exchange order of metal ions. Ion exchange is a reversible process, and the adsorbent can be regenerated or loaded with desirable ions by washing with an excess of these ions.

2.3.2 Chemical reduction

Chemical reduction has been used to indicate precipitation taking place at the surface of the biosorbent, or within the pores of the biosorbent. Amino, hydroxyl, crosslinking agents, or grafted components can reduce metal ions in the adsorption process in certain conditions (Dambies, Guimon, Yiacoumi, & Guibal, 2001). This mechanism is widely observed in precious metal adsorption, especially silver and gold ions (Gao, Zhang, & Zhao, 2017; Gurung et al., 2014; Torres et al., 2005). It is worth noticing that chemical reduction consumes functional groups or adsorption sites permanently in the reduction reaction, therefore the adsorbents will show significant decrease in metal ion capacities after regeneration.

2.4 Modelling and simulation of fixed-bed adsorption

The batch adsorption test is commonly used to obtain and evaluate the isotherm and kinetic parameters of biosorbents, while the performance in fixed-bed systems has attracted the attention of engineers because of their potential application in the industry. The fixed-bed adsorption can process large quantities of feed solution under cyclic-batch mode. In addition, the adsorption column can effectively separate different components from liquid and easily regenerated based on the affinity of the adsorbent, which meets the need of industrial utilization (Izatt, Izatt, & Bruening, 2010; Naja & Volesky, 2006).

The amount of material adsorbed within a column depends on both position and time. As the fluid enters the bed, it comes into contact with the absorbent and the solute adsorbs. The break point occurs when the concentration of the fluid leaving the bed spikes, as unadsorbed solute begins to emerge, and the bed becomes ineffective. As the concentration wave moves through the bed, the mass transfer zone moves down the bed until it “breaks through”. The shape of the mass transfer zone, which is also called the “breakthrough curve”, depends on the adsorption isotherm, flow rate, and diffusion characteristics. Generally, with increasing flow rate and solute concentration, the break point and adsorption capacity are decreased because of insufficient contact time. The breakthrough curve is mostly observed in continuous biosorption because it reflects the conditions of the column and the feasibility and economics of the sorption phenomena.

In spite of the adsorption performance, the regeneration of biosorbents is also a significant characteristic. An elution curve is usually expressed in terms of the adsorbate concentration in the elution as a function of flow time or volume of effluent for a given bed height. Due to the selectivity and the various affinity properties of biosorbents, different components in the solution can be separated and recovered through the column. By combining the breakthrough curve and elution curve, the mathematical model can be used to provide accurate information in industrial application.

The mathematical model is a description of the mass transfer in the adsorption-desorption continuous column that predicts the breakthrough and elution curves. The model needs no experimental equipment and chemicals but gives a precise prediction based on isotherm and kinetic parameters. In the biosorption process, the column is assumed to be uni-

dimensional and have only two independent variables, time t and the column length z. The differential mass balance was introduced by Guiochon et al. (2006) to study the band profile of the components in the column, based on following assumptions:

a) The column is radically homogeneous with constant axial dispersion.
b) The mobile phase is hardly compressed and the sample components keep stable in both phases.
c) The solvent is not adsorbed in the isotherm.
d) The thermal effects and the influence of heat of adsorption on the band profile are neglected.

The differential mass balance equation can be written as:

$$\frac{\partial C_i}{\partial t} + F\frac{\partial C_{s,i}}{\partial t} + u\frac{\partial C_i}{\partial z} = D_{L,i}\frac{\partial^2 C_i}{\partial z^2} \qquad \text{Eq. (2.1)}$$

where F is the phase ratio, u is the interstitial velocity, and D_L is the axial dispersion coefficient. The first two terms on the left hand side represent the accumulation in the mobile and stationary phases, respectively; the third term is the convection; the term on the right hand side is diffusion.

When the mass transfer between two phases is fast, the concentration of the component in the stationary phase $C_{s,i}$ can be represented by q_i, and the stationary phase concentration in equilibrium with $C_{s,i}$ is:

$$C_{s,i} = q = f_i(C_1, C_2, ..., C_i, ..., C_n) \qquad \text{Eq. (2.2)}$$

and when the mass transfer kinetics is slow, such as in the liquid-solid chromatography and ion-exchange chromatography, the $C_{s,i}$ can be represented as:

$$\frac{\partial C_{s,i}}{\partial t} = g_i(C_1, C_2, ..., C_i, ..., C_n, C_{s,i}, ..., C_{s,n}) \quad \text{Eq. (2.3)}$$

The mass transfer kinetics model is combined with the mass balance equation to complete the simulation. Based on Guiochon et al. (2006), the mass transfer in the adsorption column includes following terms:

a) Radial diffusion from the center of the flow stream to the surface of biosorbents
b) Film diffusion from the mobile phase into the stationary phase
c) Diffusion from the stagnant mobile phase into the biosorbent pores
d) Adsorption-desorption, ion-exchange, and complexation

These terms are affected by temperature, pressure, velocity, concentration, molecular diffusion, and the size of biosorbents. The mass transfer kinetics can be calculated through the following models depending on different experimental conditions and assumptions: the general rate model, the lumped kinetic model, the equilibrium-dispersive model, and the ideal model.

2.4.1 The general rate model

The general rate model attempts to simultaneously consider all the possible contributions to the mass transfer kinetics, by including their contributions in the system of partial differential equations which states mass conservation and transport (Guiochon, Felinger,

& Shirazi, 2006). In this model both the inside and the outside of the biosorbents are considered, therefore two mass balance equations are needed, one for the mobile phase flowing between the particles, and the other for the stagnant mobile phase inside the biosorbents.

The mass balance equation in the mobile phase:

$$u\frac{\partial C}{\partial z}+\frac{\partial C}{\partial t}+F\frac{\partial \bar{q}}{\partial t}=D_L\frac{\partial^2 C_i}{\partial z^2} \qquad \text{Eq. (2.4)}$$

where the term $\partial\bar{q}/\partial t$ is the rate of adsorption averaged over the particle. For a spherical particle, the equation is $\frac{\partial \bar{q}}{\partial t}=\frac{\text{э}}{R_p M_F}$ where M_F is the mass flux of solute from the bulk solution to the external surface of the particle (Guiochon et al., 2006).

The mass balance of the solute inside the pores of an adsorbent particle:

$$\varepsilon_p\frac{\partial C_p}{\partial t}+(1-\varepsilon_p)\frac{\partial C_s}{\partial t}=D_p\left(\frac{\partial^2 C_p}{\partial r^2}+\frac{2}{r}\frac{\partial C_p}{\partial r}\right) \qquad \text{Eq. (2.5)}$$

where ε_p is the internal porosity of the particle, D_p is the diffusion coefficient of the solute in the particle pores, C_p is the concentration of the solute inside the pores, and C_s is the concentration of the solute adsorbed by the stationary phase. Assuming the kinetics of adsorption is fast we have:

$$C_s=K_a C_p \qquad \text{Eq. (2.6)}$$

Assuming the kinetics is slow we have:

$$\frac{\partial C_s}{\partial t} = k_a (C_p - C_p^*) = k_a (C_p - \frac{C_s}{K_a}) \quad \text{Eq. (2.7)}$$

where k_a and K_a are the adsorption rate constant and the adsorption equilibrium constant, respectively.

The predictions of the general rate model were very consistent with experimental data (Du, Yuan, & Li, 2008; Lv, Zhang, Wang, Ray, & Zhao, 2008). However, the solution for this system is very hard due to the extreme complexity of the model, which accounts for the axial dispersion, the film mass transfer resistance, the pore diffusion, and a first-order, slow kinetics of adsorption-desorption (Guiochon et al., 2006).

2.4.2 The lumped kinetic model

The lumped kinetic model is used to simplify the calculation and can be written as a kinetic derivation of the Langmuir isotherm:

$$\frac{\partial C_{s,i}}{\partial t} = k_a (q_{s,i} - C_{s,i}) C_i - k_d C_{s,i} \quad \text{Eq. (2.8)}$$

where $q_{s,i}$ is the column saturation capacity, and k_a and k_d are the rate constants of adsorption and desorption of the component. When the kinetics of adsorption-desorption is slower than the other steps of the column process, this equation can be simplified to:

$$\frac{\partial C_s}{\partial t} = k_a C - k_d C_s \quad \text{Eq. (2.9)}$$

while if the slowest step is mass transfer, the equation can be simplified to:

$$\frac{\partial C_s}{\partial t} = k_f (C - C^*) \qquad \text{Eq. (2.10)}$$

Some researchers have used lumped kinetic models and the results have shown high agreement between the experimental and calculated data with slow kinetics and the diffusion coefficient mostly equaled the axial dispersion (Bak, Thomas, & Abildskov, 2007; Pérez-Martínez, Montesinos-Cisneros, Guerrero-Germán, Guzman-Zamudio, & Tejeda-Mansir, 2015).

2.4.3 The equilibrium-dispersive model

When the mass transfer kinetics are fast but not infinitely fast, the system of mass balance equation and kinetic equation can be replaced by the following equation:

$$\frac{\partial C_i}{\partial t} + F\frac{\partial q_i}{\partial t} + u\frac{\partial C_i}{\partial z} = D_{a,i}\frac{\partial^2 C_i}{\partial z^2} \qquad \text{Eq. (2.11)}$$

where q_i is the equilibrium concentration of component i in the stationary phase and $D_{a,i}$ is the apparent dispersion coefficient which combines the axial dispersion, the non-equilibrium effects , and the finite kinetics of adsorption-desorption.

The equilibrium-dispersive model is correct if mass transfer in the chromatographic column is controlled only by molecular diffusion across the mobile phase flowing around the packing particles and if the exchange of elutes between the stationary and mobile phase is very fast (Guiochon et al., 2006). Therefore, in lab scale biosorption column it is difficult to match the calculated data with experimental data by this model.

2.4.4 The ideal model

The simplest model of nonlinear chromatography assumes that the column efficiency is infinite. There is no axial dispersion and the two phases are constantly at equilibrium. The mass balance equation simplifies to:

$$\frac{\partial C_i}{\partial t} + F\frac{\partial q_i}{\partial t} + u\frac{\partial C_i}{\partial z} = 0 \qquad \text{Eq. (2.12)}$$

This model neglects completely the influence of the mass transfer kinetics and of axial dispersion on the band profiles. The application of this model is limited due to its strict assumptions.

Several parameters in the mathematic model can be determined from empirical correlations based on some researchers (Izquierdo, Gabaldón, Marzal, & Sempere, 2010; Sulaymon, Abid, & Al-Najar, 2009). However, these correlations were acquired from specific adsorbents and experimental conditions, which have limited applicability. To obtain the optimal value of model parameters, an error of function, which is defined as the sum of square deviations of the predicted normalized concentrations with respect to the experimental ones, was used as the objective function for the optimization (Lv et al., 2008):

$$F_{(p)} = \min \sum_{i=1}^{m} \left[\frac{C_{i,\exp}}{C_0} - \frac{C_{i,\mathrm{mod}}}{C_0} \right]^2 \qquad \text{Eq. (2.13)}$$

where $C_{i,\exp}$ and $C_{i.\mathrm{mod}}$ are the experimental value and model prediction at point i of the breakthrough curve, respectively. By minimizing $F_{(p)}$, the optimal values of parameters can be determined.

Chapter 3 Selective Biosorption of Gold by Modified Cellulose

This chapter is based on and modified from the following papers:

M. Gurung, B.B. Adhikari, **X. Gao**, S. Alam & K. Inoue. (2014). Sustainability in the Metallurgical Industry: Chemically Modified Cellulose for Selective Biosorption of Gold from Mixtures of Base Metals in Chloride Media. Industrial & Engineering Chemistry Research, 53(20), 8565−8576.

Role: Dr. Manju Gurung and Dr. Birendra Babu Adhikari developed the synthesis method for the adsorbent. Dr. Manju Gurung conducted the column test and wrote the most of the manuscript. Xiangpeng Gao conducted the adsorption tests and analyzed the experimental data. Dr. Shafiq Alam and Dr. Katsutoshi Inoue supervised the experiment and reviewed the manuscript.

M. Gurung, B.B. Adhikari, **X. Gao**, S. Alam & K. Inoue. (2013). Meeting the Challenges of Sustainability: Utilization of Chemically Modified Pure Cellulose for Quantitative Separation of Gold from Mixtures of Base Metals in Acidic Solution. Proceedings of ALTA 2013 Conference, Gold Sessions, 203-213.

Role: Dr. Manju Gurung and Dr. Birendra Babu Adhikari developed the synthesis method for the adsorbent. Dr. Manju Gurung wrote the most of the manuscript. Xiangpeng Gao conducted the adsorption tests and analyzed the experimental data. Dr. Shafiq Alam and Dr. Katsutoshi Inoue supervised the experiment and reviewed the manuscript.

3.1 Abstract

In an effort to develop sustainable materials and methods for the recovery and recycling of precious metals, two different adsorbents were developed by cross-linking pure cellulose with either epichlorohydrin or concentrated sulfuric acid, and then modifying the surface with N-aminoguanidine functional groups. The adsorption behavior of these sorption materials toward Au (III) from a multicomponent mixture of Pt (IV), Pd (II), and some base-metal ions was studied in hydrochloric acid media. Both of the adsorbents exhibited outstanding selectivity toward precious metals, with a selectivity order of Au (III) >> Pd (II) > Pt (IV), over base metals in a wide range of acid concentrations. These materials contain a number of positive centers in HCl media that function as sorption active sites for chloroanionic species of Au (III), Pd (II), and Pt (IV). The chloroanionic species of the corresponding precious metals were thus adsorbed on these materials through anion-exchange coupled electrostatic interaction. The sulfuric acid cross-linked material exhibited improved selectivity and greater adsorption capacity compared to the epichlorohydrin cross-linked adsorbent as equilibrium was achieved within an hour with quantitative adsorption of Au (III). Moreover, the adsorbed Au (III) was subsequently reduced to the elemental form, yielding metallic gold particles, thereby demonstrating the considerable improvements in efficiency and effectiveness of the novel adsorbents for the recovery of gold in comparison to current commercial resins.

3.2 Introduction

The growing demand for precious metals has made the development of procedures for their recovery from primary ores and secondary resources an attractive and imperative issue. Although several methods such as ion exchange, liquid-liquid extraction, and membrane filtration are used to recover precious metals from aqueous solutions, these methods are often expensive, lacking in selectivity, and difficult to operate (Ramesh et al., 2008). Adsorption of metal ions using physically and/or chemically modified natural polymers has the superior advantage of high selectivity, low cost, and easy handling. Enriched with functional groups, modified polymers can selectively bind and concentrate metals via electrostatic interaction, ion exchange, chelation/complexation and/or chemical reduction (Guibal, 2004; Won et al., 2014).

Among biopolymers, cellulose has been attracting significant attention as a biosorbent because of its biocompatibility, outstanding physical and chemical behavior, and its abundance in nature. The hydroxyl groups of cellulose at the C-2, C-3, and C-6 atoms can be partially or even fully reacted with various reagents to afford derivatives with useful properties (Heinze & Leibert, 2001). Chemically modified cellulose has shown enormous applicability as heavy-metal adsorbents as thoroughly reviewed by some researchers (Fomina & Gadd, 2014; O'Connell et al., 2008; Won et al., 2014). Commercially available cellulose is crystalline in nature and has a poor adsorption capacity (Hall, Bansal, Lee, Realff, & Bommarius, 2010). A highly crystalline cellulose sample has a tight structure with cellulose chains closely bound to each other so that the hydroxyl groups are not easily accessible to chemical modification. Certain chemical reactions, in

particular, cross-linking and/or grafting reactions, can improve the structural stability and adsorption capability of native cellulose toward precious-metal ions. Because the adsorption of metal ions takes place mainly on the surface, increasing the sorption active sites on the surface of the polymer matrix is an effective approach to enhancing the sorption kinetics and overall sorption performance of the adsorbent. Covalent linking of amine functions has been an interesting approach for the sorption of precious metals, because the nitrogen atom is a softer base and generally prefers to interact with soft acidic precious-metal ions such as Au (III), Pd (II), and Pt (IV).

In this study, two different biosorbents were developed by cross-linking cellulose with epichlorohydrin and concentrated sulfuric acid respectively, and then chemically modifying the surface with N-aminoguanidine functional groups. The adsorption behaviors of the prepared biosorbents were studied in terms of selectivity, adsorption isotherm, and kinetics. The prepared sorbent is chemically resistant against acidic solvent, allowing it to withstand the harsh conditions to recover gold ions from mining wastes or other industrial effluents.

3.3 Materials and Methods

3.3.1 Chemicals and Materials

Reagent-grade chloride salts of various metals such as gold, palladium, platinum, iron, cobalt, nickel, copper, zinc, and lead were used to prepare stock solutions of the respective metals. The stock solutions were further diluted to the desired concentrations with 0.1 mol/L HCl to prepare the test solutions. The microcrystalline commercial

cellulose powder (Merck, Darmstadt, Germany) employed in the present study was of chromatographic grade. The thionyl chloride ($SOCl_2$), aminoguanidine hydrochloride ($CH_6N_4 \cdot HCl$), epichlorohydrin (ECH), and sulfuric acid used in this study were purchased from Sigma-Aldrich and were used as received. All other chemicals used in the experimental work were of analytical grade and were used without further purification.

3.3.2 Preparation of the Biosorbents

The adsorbents were prepared by cross-linking pure cellulose with either epichlorohydrin or concentrated sulfuric acid and then modifying the surface with N-aminoguanidine (AG) functional groups.

3.3.2.1 Epichlorohydrin Crosslinking of Cellulose

The epichlorohydrin cross-linking of cellulose was achieved by employing the procedure described by Šimkovic et al. for the cross-linking of starch. In a typical run, 30 mL of 17.5% (w/v) NaOH was added to 25 g of cellulose, and the mixture was stirred for 10 min. Then, 50 g of epichlorohydrin and 30 mL of 30% ammonium hydroxide were added sequentially, and the mixture was stirred for another 15 min. The resulting cloudy solution was then gradually heated to 338 K, where it was maintained overnight with constant stirring. Once cooled, the solid was collected by vacuum filtration and washed repeatedly with distilled water until the filtrate displayed neutral pH toward pH indicators. The collected solid was then washed with acetone, followed by an acetone/water mixture and finally distilled water. After the washed solid was dried, 26 g of cross-linked product was obtained.

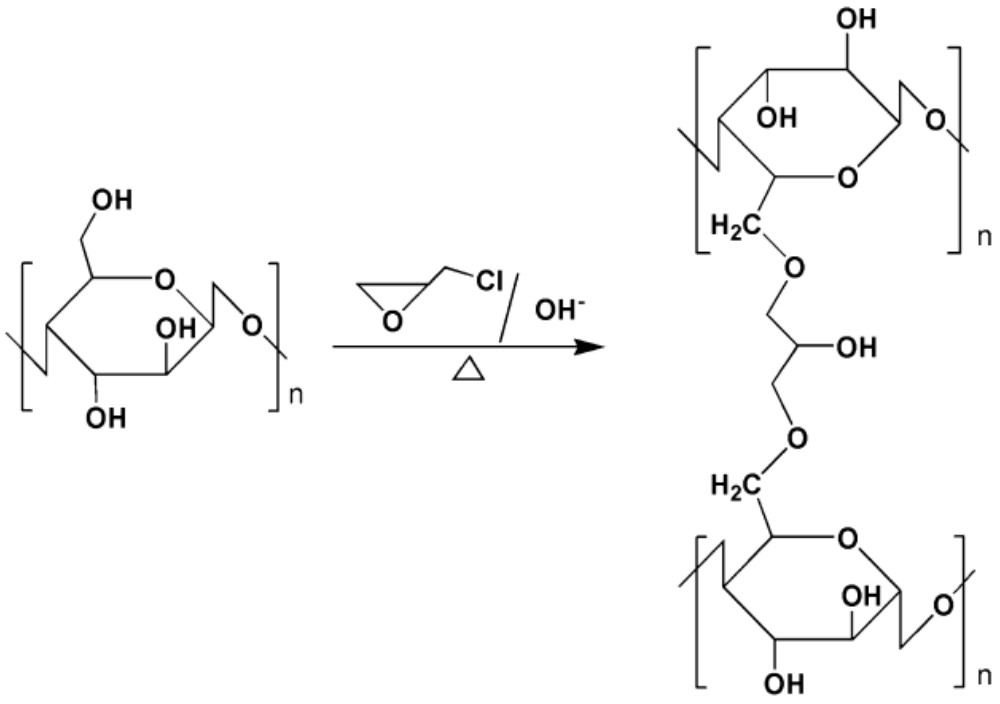

Figure 3.1 Epichlorohydrin cross-linking of cellulose

3.3.2.2 Sulfuric Acid Cross-linking of Cellulose

For the sulfuric acid cross-linking of cellulose, a mixture of 25 g of cellulose and 50 mL of concentrated sulfuric acid was first stirred at room temperature for 15 min, and then the temperature was gradually increased to 363 K. During heating, the mixture was converted to a thick paste, preventing additional stirring. Therefore, an additional 20 mL of concentrated sulfuric acid was added, yielding a considerably less viscous mixture that could be easily stirred. The entire mixture was stirred overnight at 363 K. Once this mixture had been cooled, it was slowly added to a 10% $NaHCO_3$ solution so as to neutralize the acid. The black solid was collected by vacuum filtration and washed

repeatedly with water until the filtrate was neutral toward pH indicators. After this solid was dried, 14 g of cross-linked product was obtained.

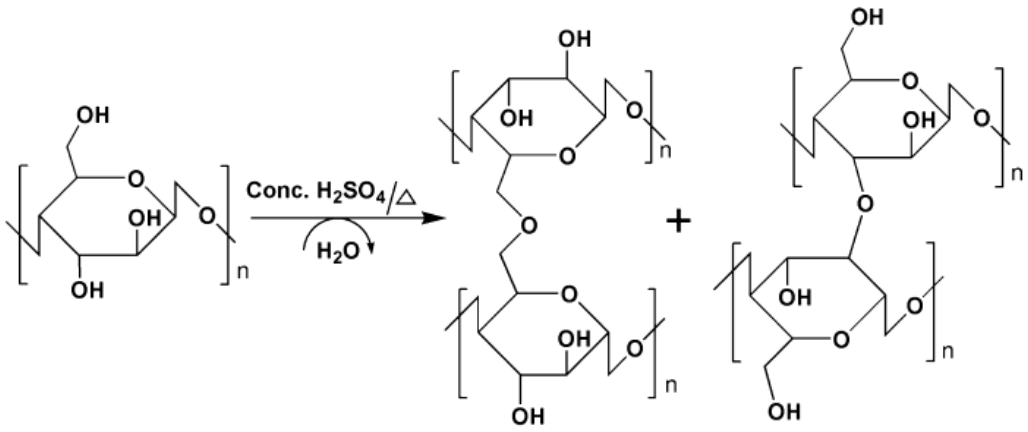

Figure 3.2 Concentrated sulfuric acid cross-linking of cellulose

3.3.2.3 Modification of Cross-linked Cellulose with Functional Groups

Surface modification of cross-linked cellulose with N-aminoguanidine (AG) was carried out according to the reaction sequence shown in Figure 3.3. In a typical run, 20 mL of thionyl chloride was slowly added to the stirred suspension of 13.0 g of ECH or concentrated sulfuric acid cross-linked cellulose in 100 mL of pyridine over a period of 2 h at room temperature, with occasional cooling of the reaction flask in ice water. After the addition of thionyl chloride, the reaction mixture was first allowed to come to room temperature and then slowly heated to a temperature of 343 K, which was maintained overnight with continuous stirring. Then, 30 mL of ice-cold water was slowly added, vacuum filtration was applied, and the solid was collected. The residue was repeatedly washed with water, followed by ethanol and then water again. After drying of the residue, the weight of product was measured and the weight loss is insignificant, which indicates

that the chlorinated cellulose was obtained in a quantitative yield. In the next step, a mixture consisting of 6.0 g of chlorinated cellulose, 3.53 g of Na_2CO_3, and 5.0 g of N-aminoguanidine hydrochloride in 80 mL of dimethylformamide (DMF) was stirred at 353 K for 24 h. Upon cooling, 50 mL of water was added, and the solid was collected by filtration. The residue was washed repeatedly with distilled water until the filtrate was neutral toward pH indicators and was then washed with ethanol. After being dried in an oven, the chemically modified cellulosic materials were obtained in almost quantitative yield. The products of epichlorohydrin cross-linked and sulfuric acid cross-linked cellulose are denoted as ECH-AG-cellulose and Sulf-AG-cellulose, respectively.

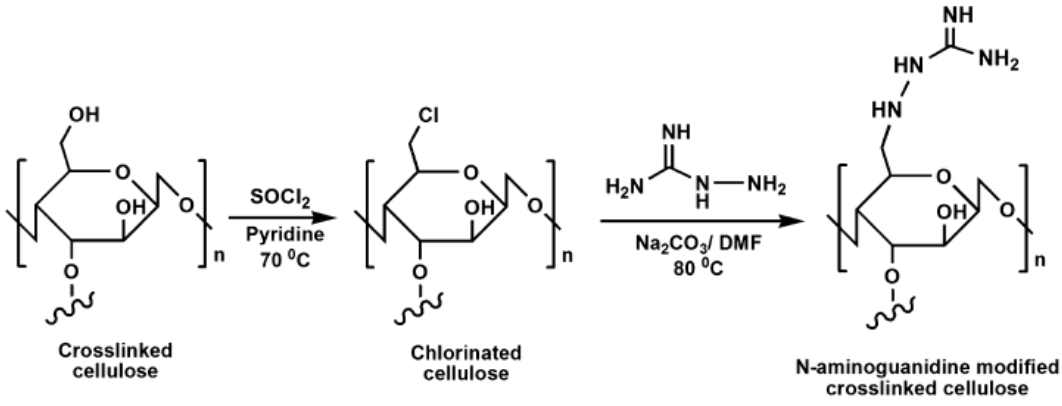

Figure 3.3 Chemical modification of cross-linked cellulose

3.3.3 Batch Adsorption Tests

Adsorption tests of various metal ions, namely, Au (III), Pd (II), Pt (IV), Fe (III), Co (II), Ni (II), Cu (II), Zn (II), and Pb (II), were carried out to observe the adsorption behaviors of the prepared adsorbents in varying HCl concentrations ranging from 0.1 to 5.0 mol/L. In a typical set, 15 mL of test solution containing the mixture of metal ions was added to

20 mg of the adsorbent, and the resulting heterogeneous mixture was agitated in a shaking incubator maintained at 303 K and 200 rpm for 24 h. The sample was then filtered to separate the adsorbent, and the concentration of metal ions was determined by inductively coupled plasma optical emission spectrometry (ICP-OES). From the measured initial and equilibrium concentrations of metal ions in solution, the percentage adsorption of different metals was evaluated using the equation

$$A(\%) = \frac{C_i - C_e}{C_i} \times 100 \qquad \text{Eq. (3.1)}$$

where C_i and C_e are the initial and equilibrium concentrations (mmol/L), respectively, of metal ions in the aqueous solution.

Adsorption isotherm tests were conducted to evaluate the maximum adsorption capacities of the prepared adsorbents for Au (III), Pd (II), and Pt (IV). In these experiments, 20 mg of the adsorbent was shaken with 15 mL of test solution containing varying concentrations of individual metal ions in 0.1 mol/L HCl at 303 K for 72 h to attain the thermodynamic equilibrium of adsorption. The amounts of metal ions adsorbed were calculated from the equation

$$q = \frac{C_i - C_e}{W} \times V \qquad \text{Eq. (3.2)}$$

where W (mg) and V (mL) are the weight of adsorbent and the volume of the test solution, respectively.

The effects of temperature and contact time on the biosorption of Au (III) were carried out at four different temperatures between 303 to 318 K. In these experiments, 150 mL of 3 mmol/L Au (III) solution prepared in 0.1 mol/L HCl was added to 200 mg of the prepared adsorbent at each temperature studied. Shaking of the heterogeneous mixture was started immediately after mixing, and a 5 mL volume of the mixture was sampled at different time intervals for the analysis of residual metal concentration in the solution. From the measured concentrations at the beginning and at any time t, the amount of metal adsorbed was calculated using the relation

$$q_t = \frac{(c_i - c_t)V - V_t\left(\sum_{k=1}^{j} c_k - tc_t\right)}{W} \qquad \text{Eq. (3.3)}$$

where q_t (mmol/g) is the amount of Au (III) adsorbed at sampling point t ($t \geq 1$); c_i and c_t (mmol/L) are the concentrations of Au (III) in the initial solution and at sampling point t, respectively; V and V_t (mL) are the initial solution volume and the sampling volume respectively; W (mg) is the weight of the dry sorbent.

3.3.4 Analytical Methods

A temperature-controlled shaking incubator (Thomas AT24R) was used to agitate the samples for the sorption experiments. The metal concentrations of aqueous samples were measured using a Perkin-Elmer Optima 5300 DV inductively coupled plasma optical emission spectrophotometer. IR spectra of the samples were recorded with a Bruker Tensor 27 FT-IR spectrometer with a Pike ZnSe MIRacle attenuated total reflectance

(ATR) accessory with Opus 4.0 software. A Leica DMLP microscope was used to take digital micrograph images of the gold-loaded adsorbent. The X-ray diffraction (XRD) pattern of the gold-loaded sample was recorded with a Rigaku Ultima-IV XRD spectrophotometer in Bragg−Brentano mode.

3.4 Results and Discussion

3.4.1 Characterization of the Biosorbents

The prepared adsorbents were characterized by FT-IR spectroscopy, as shown in Figure 3.4. The FT-IR spectrum of pure cellulose consists of a broad band with two wide peaks at 3332 and 3289 cm^{-1} due to O-H stretching. The bands at 1314, 1160, 1105, and 1029 cm^{-1} are attributed to O-H bending and both symmetrical and asymmetrical C-O-C stretching vibrations. The guanidine compounds display four characteristic peaks in the IR spectrum for the following group frequencies: N-H stretching at about 3300 cm^{-1}, C-N stretching at 1689-1650 cm^{-1}, N-H bending at about 1640 cm^{-1}, and C-N stretching at about 1300 cm^{-1} (Yumei, Jianming, & Yanmo, 1999). As expected from the corresponding group frequencies of the aminoguanidine function, new absorption bands were observed at 1683, 1629, and 1351 cm^{-1} in the IR spectrum of ECH-AG-cellulose. Similarly, significant changes were observed in the 1620-1540, 1340, and 1160-1140 cm^{-1} regions of the IR spectrum of Sulf-AG-cellulose. This corroborates the introduction of the aminoguanidine group on the cellulose matrix.

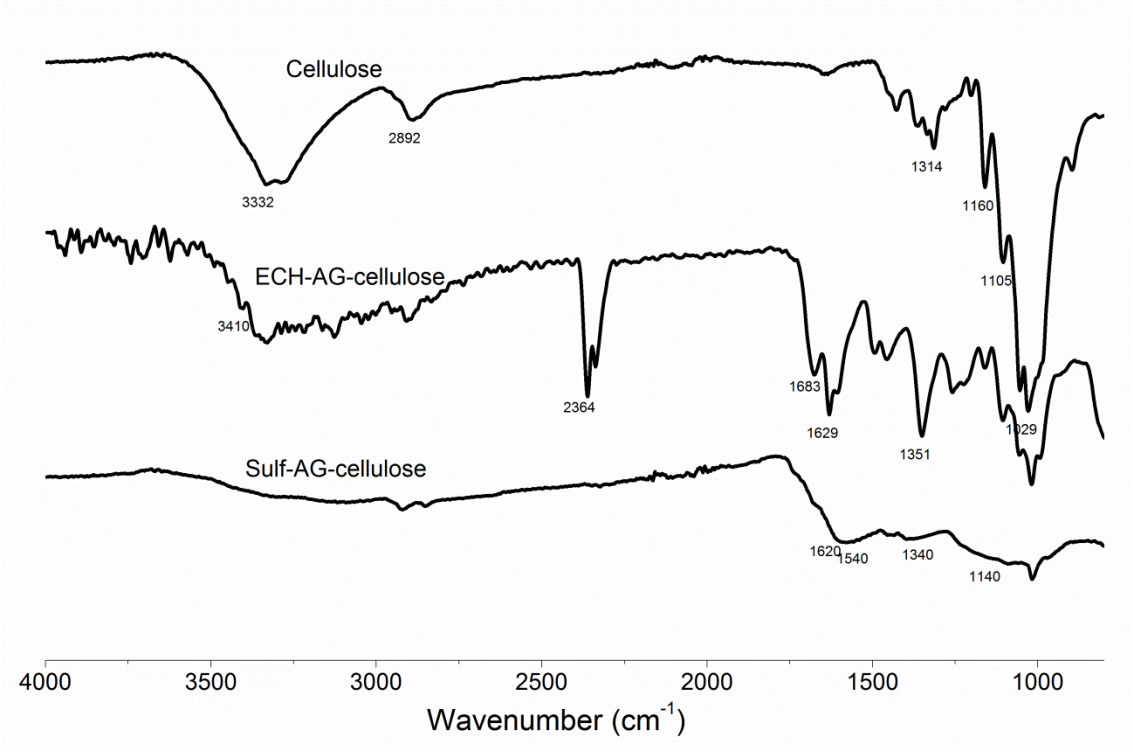

Figure 3.4 FT-IR spectra of pure cellulose, ECH-AG-cellulose, and Sulf-AG-cellulose

Once the FT-IR spectra indicated the successful modification of cross-linked cellulose with N-aminoguanidine groups, the degree of functional-group immobilization was evaluated from the nitrogen content of the material. As shown in Table 3.1, the nitrogen contents of ECH-AG-cellulose and Sulf-AG-cellulose were found to be 4.67% and 11.2%, respectively. This significant increase in nitrogen content as compared to that of pure cellulose suggests the successful immobilization of aminoguanidine functional groups on the surface of the cellulose feed material. From the observed elemental composition, the nitrogen densities of the prepared materials were calculated as 3.3 and 8.0 mol/kg of dry adsorbent for ECH-AG-cellulose and Sulf-AG-cellulose, respectively. Consequently, the

functional-group densities were 0.82 and 2.0 mol/kg for ECH-AG-cellulose and Sulf-AG-cellulose, respectively.

Table 3.1 Elemental analysis of pure cellulose, ECH-AG-cellulose, and Sulf-AG-cellulose

Material	Elemental composition (%)		N density (mol/kg)	Functional group density (mol/kg)
	C	N		
Pure cellulose	42.9	0.00	-	-
ECH-AG-cellulose	40.07	4.67	3.3	0.82
Sulf-AG-cellulose	47.6	11.20	8.0	4.0

The specific surface properties of the prepared adsorbents were evaluated by Brunauer−Emmett−Teller (BET) surface area analysis and Barrett−Joyner−Halenda (BJH) pore size and volume analysis (Table 3.2). Pure cellulose, the feed material employed in this study, is a crystalline mesoporous material. Its porosity was slightly enhanced upon treatment with ECH followed by chemical modification. Concentrated sulfuric acid treatment, on the other hand, significantly increased the porosity of the material, resulting in the formation of a macroporous adsorption material. The commercially available cellulose is microcrystalline in nature (Hall et al., 2010). The results presented in Table 3.2 indicate that the commercial cellulose and ECH-AG-cellulose were mesoporous materials whereas Sulf-AG-cellulose was macroporous in nature. Concentrated sulfuric acid treatment of cellulose ruptures some of the glycosidic linkages, destroys the rigid three-dimensional network of the polymer, and changes it to a porous material (Pangeni et al., 2012). In our case, the porosity of the sulfuric acid-treated material was enhanced nearly 300 times compared to that of the feed material. We observed the formation of porous, beadlike particles upon sulfuric acid treatment of the commercial cellulose. This phenomenon increased the porosity but decreased the specific surface area of the material.

Epichlorohydrin cross-linking, however, did not break the crystalline nature of the cellulose matrix.

Table 3.2 Surface Properties of pure cellulose, ECH-AG-cellulose, and Sulf-AG-cellulose

Material	BET surface area (m^2/g)	Total pore volume (cm^3/g)	Mean pore diameter (nm)
Pure cellulose	1.64	8.39×10^{-3}	20.41
ECH-AG-cellulose	5.02×10^{-1}	5.61×10^{-3}	44.68
Sulf-AG-cellulose	2.33×10^{-3}	3.34×10^{-3}	5736.70

3.4.2 Adsorption Behavior of the Biosorbents toward Various Metal Ions

In preliminary experiments, the adsorption behavior of commercial pure cellulose powder toward various metal ions in the mixture was examined at varying concentrations of HCl, the results indicate that none of the metallic species were adsorbed on the unmodified cellulose. Then, adsorption experiments were conducted using ECH-AG-cellulose under conditions identical to those used for the native cellulose. In this case, a notable improvement in adsorption behavior was observed. The results showing the adsorption efficiency, expressed in terms of the percentage adsorption of ECH-AG-cellulose toward various metal ions from HCl media of different concentrations, are presented in Figure 3.5(a). As can be seen in this figure, ECH-AG-cellulose exhibited good adsorption behavior toward precious metals with a selectivity order of Pd (II) ≈ Au (III) > Pt (IV). It is interesting to note that Pd (II) was adsorbed almost quantitatively from solutions with HCl concentrations of up to 1.0 mol/L. This significant enhancement in adsorption behavior toward precious metals is attributed to the contribution from the functional groups anchored on the surface of the cellulose. Figure 3.5(b) shows the results of the adsorption tests for Sulf- AG-cellulose toward various metal ions at varying HCl

concentrations. As is evident from the results, this adsorbent exhibited superior performance in comparison to ECH-AG-cellulose and a phenomenal improvement in adsorption behavior toward precious metals as compared to the native material. As can be seen in this figure, the adsorption of Au (III) and Pd (II) was quantitative up to 2 mol/L HCl concentrations and decreased very slightly with further increasing acid concentration. The sorption efficiency of the adsorbent toward Pd (II) was also enhanced when cross-linking was conducted using concentrated sulfuric acid, and the adsorbent exhibited moderate adsorption of Pt (IV) for a wide range of HCl concentrations. The metals forming stable anionic chloro complexes in HCl media exhibited decreasing adsorption behavior with increasing acid concentration (Gurung et al., 2012 & 2013). ECH-AG-cellulose also displayed similar adsorption behavior, which is likely attributable to the competitive adsorption of anions. In some cases, the adsorbents were practically nonfunctional in HCl concentrations in excess of 3 mol/L (Gurung et al., 2013). The most important point to note with regard to the adsorption behavior of Sulf-AG-cellulose is that increasing the concentration of competitive ions had almost no effect on the adsorption of precious metals and that the adsorbent performed highly efficiently for HCl concentrations of up to 5 mol/L. On the other hand, the adsorption of base-metal ions on both of the adsorbents was observed to lie at the baseline for the entire range of HCl concentrations, suggesting that the present adsorbents are outstanding materials for the adsorptive separation of precious metals from mixtures of a considerable number of base metals.

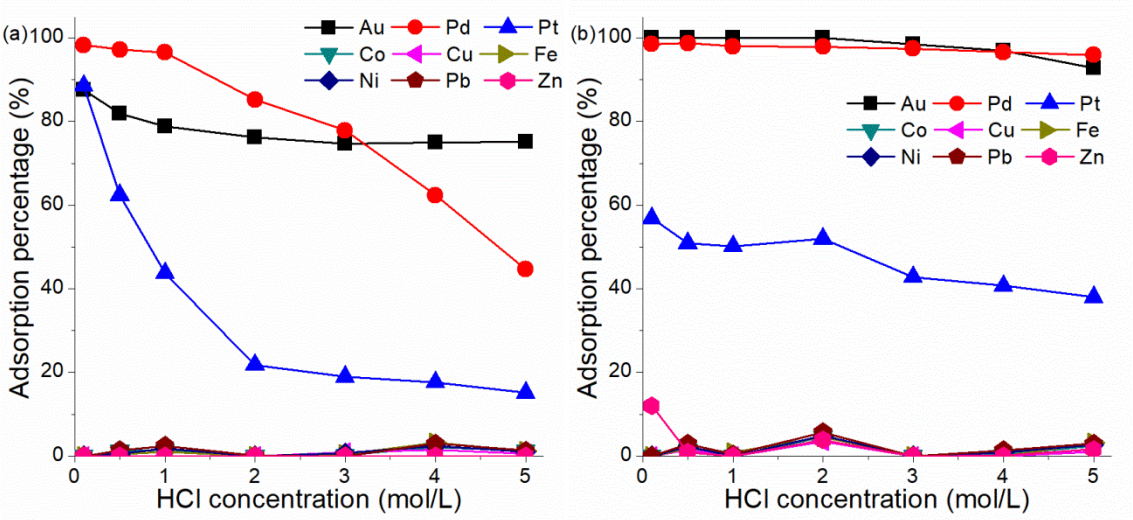

Figure 3.5 Adsorption behaviors of various metal ions on (a) ECH-AG-cellulose, and (b) Sulf-AG-cellulose

The nitrogen atoms of N-aminoguanidine functional groups attached to the surface of the cellulose are converted to positively charged centers in acidic media. Structurally, cross-linked cellulose consists of a number of ether linkages and hydroxyl groups that are also prone to undergo protonation under acidic conditions. Therefore, these adsorbents contain an enormous number of positively charged centers in contact with such solutions. Precious metals, on the other hand, are converted to chloroanionic species within the entire range of HCl concentrations studied. Consequently, the selective adsorption of precious metals on the present adsorbents is believed to be a result of anion exchange followed by electrostatic interaction. Because base metals exist as cationic species in HCl media, no preferential interactions occur, and thus, they are not adsorbed.

The superior performance of the sulfuric acid cross-linked material over the epichlorohydrin cross-linked material for adsorption of precious metals is believed to be due to the nature of the polymer matrix. As already stated, treatment of commercial

cellulose with concentrated sulfuric acid destroyed the crystalline nature of the cellulose, forming a highly porous material, but the porosity of the epichlorohydrin cross-linked material was scarcely improved from that of the feed material. Consequently, the significant improvement in adsorption efficiency of the sulfuric acid cross-linked material compared to the epichlorohydrin cross-linked material is attributed to the destruction of the crystalline nature of the cellulose, thereby producing a porous material having enhanced adsorption affinity.

3.4.3 Adsorption Isotherm

The adsorption isotherm plots of Au (III), Pd (II), and Pt (IV) on ECH-AG-cellulose and Sulf-AG-cellulose are shown in Figure 3.6. As revealed by these plots, the amounts of metals adsorbed on both of the adsorbents increased with increasing metal concentration of the test solution, which tended to approach constant values at higher concentrations corresponding to each metal species, thereby exhibiting typical monolayer-type adsorption. The maximum adsorption capacities of each adsorbent toward Au (III), Pd (II), and Pt (IV) ions were evaluated from the constant values in the plateau region of Figure 3 and are summarized in Table 3.3.

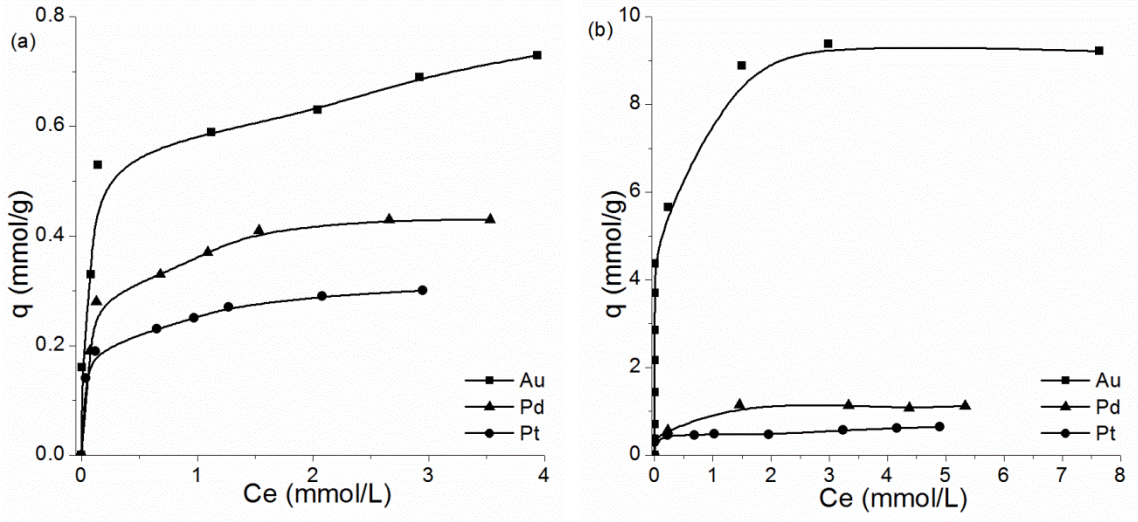

Figure 3.6 Adsorption isotherms of Au (III), Pd (II), and Pt (IV) on (a) ECH-AG-cellulose and (b) Sulf-AG-cellulose

Table 3.3 Maximum uptake capacities and isotherm parameters of cellulose-based biosorbents toward precious metals

Adsorbate	Adsorbent	q_{max} (mmol/g)		b ($\times 10^{-3}$ L/mol)
		Experimental	Calculated	
Au (III)	ECH-AG-cellulose	1.45	1.51	17.10
	Sulf-AG-cellulose	9.21	9.25	54.05
Pd (II)	ECH-AG-cellulose	1.00	1.06	14.72
	Sulf-AG-cellulose	1.12	1.12	20.24
Pt (IV)	ECH-AG-cellulose	0.53	0.54	12.72
	Sulf-AG-cellulose	0.61	0.63	4.96

3.4.4 Proposed Biosorption and Reduction Mechanism

During the sorption process, the nitrogen and oxygen containing functional groups on the cellulose-based biosorbents become the positive centers in acidic media. The major species of Au (III), Pd (II), and Pt (IV) in the experimental solutions are metal chloride anionic complexes ($AuCl_4^-$, $PdCl_4^{2-}$and $PtCl_6^{2-}$). However, the co-existing metal ions exist in their cationic forms in the acidic media (Pettit & Powell, 1999). Those positively charged metal ions interacted repulsively with the protonated functional groups, leading to a low metal uptake capacity of these transition metals and the good selectivity on Au (III), Pd

(II), and Pt (IV) in acidic conditions. The positive centers of the N-aminoguanidine functional group act as the main sorption active sites at which the anionic species $AuCl_4^-$, $PdCl_4^{2-}$, and $PtCl_6^{2-}$ replace the chloride ions and maintain electroneutrality. Similar interactions generated at positive centers due to the protonation of hydroxyl groups of cellulose cannot be overlooked. Thus, ionic interaction is considered to be primarily responsible for the adsorption of Au (III), Pd (II), and Pt (IV) on N-aminoguanidine-modified cellulose.

It is also worth noticing that Sulf-AG-cellulose has significantly high uptake capacity for Au (III) and this trend has been reported on some sulfuric acid treated biosorbents (Gurung et al., 2011; Pangeni et al., 2012; Parajuli et al., 2006). In case of biopolymers containing hydroxyl groups, the treatment of concentrated sulfuric acid took place through a dehydration reaction, leading to the formation of new ether linkages. The outstanding adsorption behavior of Au (III) with Sulf-AG-cellulose is therefore believed to be due to the structural contribution of cross-linked materials to the sorption of $AuCl_4^-$ species, which are then subsequently reduced to metallic gold with adjacent reducing functional groups as observed in the sorption process.

The Au (III) capacity of Sulf-AG-cellulose is remarkably high, which can be explained as the reduction reaction of Au (III) to metallic gold redeems the occupied sorption sites which could adsorb metal ions once exposed on the surface of the biosorbents. The formation of elemental gold can be confirmed from the XRD spectrum of dried equilibrium sample of Au (III) loaded Sulf-AG-cellulose. The peaks at 2θ of 38.2^o, 44.4^o,

64.6°, 77.5°, and 81.7° in Figure 3.7 can be indexed to the (111), (200), (220), (311) and (222) Bragg's reflections of cubic structure of metallic gold.

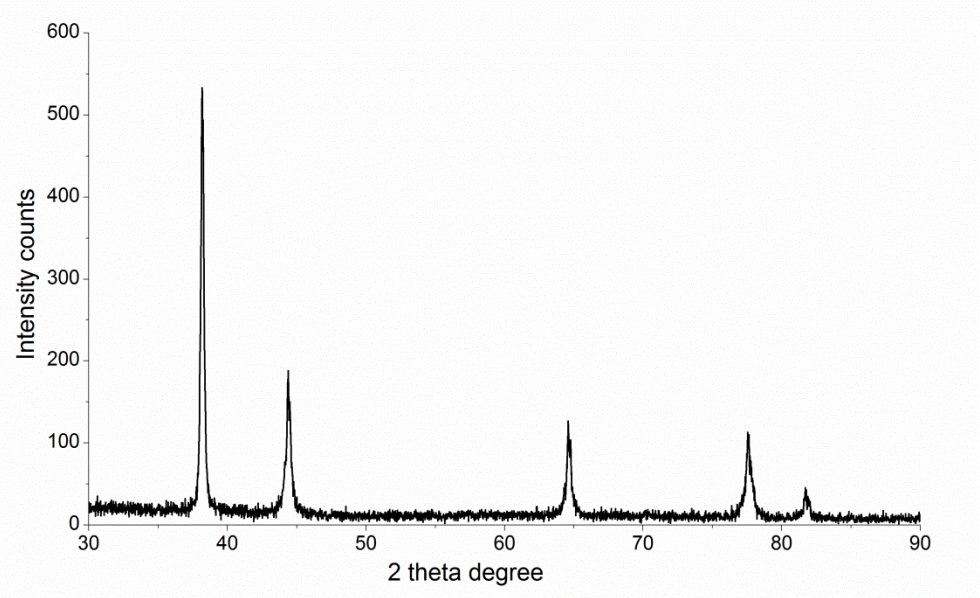

Figure 3.7 XRD spectrum of Sulf-AG-cellulose after Au(III) adsorption

Due to the strong reduction power of hydroxyl groups, the reduction of Au (III) can be achieved by the following reaction scheme:

$$2AuCl_4^- + 3RCH_2OH \rightarrow 2Au(0) + 3RCHO + 6H^+ + 8Cl^-$$

where reduction of Au (III) to Au (0) occurs through oxidation of hydroxyl to aldehyde group. This adsorption-reduction mechanism of Au (III) has also been confirmed by other research studies (Kuyucak & Volesky, 1989; Mele, Anyfantis, Fragouli, Ruffilli, & Athanassiou, 2014).

3.4.5 Effects of Temperature and Contact Time

Adsorption kinetic experiments were carried out only for Sulf-AG-cellulose on Au (III) ions. Preliminary experiments were conducted using 1 mmol/L and 3 mmol/L Au (III) solutions at 303 K, and the results are presented in Figure 3.8(a). The amount of metal adsorbed on Sulf-AG-cellulose initially increased rapidly and then gradually decreased, finally approaching a constant value after a certain period of shaking, which is the time required to reach equilibrium. It is understandable from the figure that adsorption equilibrium was attained within 1 h for 1 mmol/L Au (III) whereas it took 6 h to come to equilibrium with quantitative adsorption when the initial concentration of Au (III) was increased to 3 mmol/L.

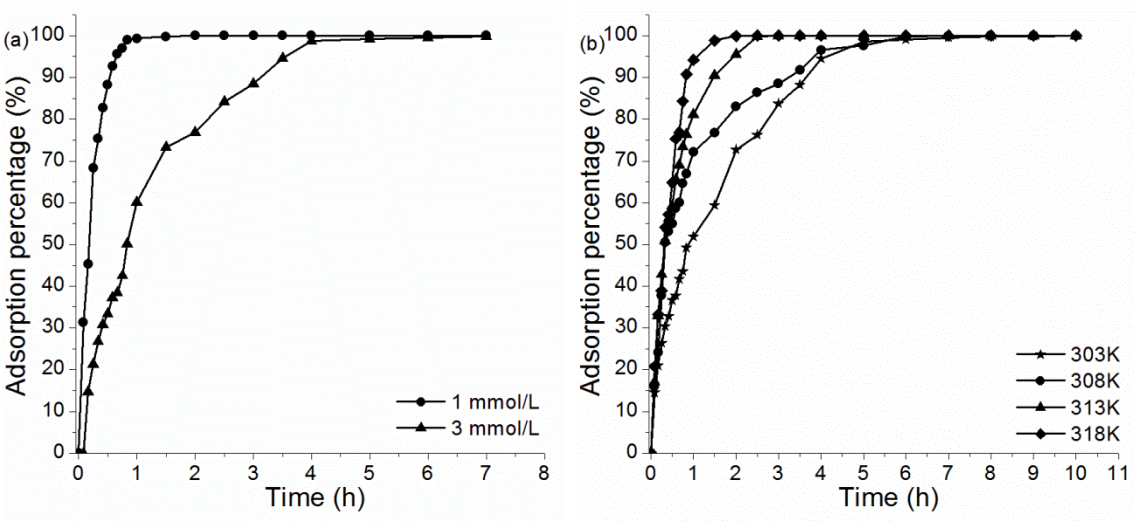

Figure 3.8 Effects of contact time and temperature of Au (III) adsorption on Sulf-AG-cellulose

The effect of temperature was studied at 4 different temperatures from 303 K to 318 K using 3 mmol/L Au (III) solutions. The results indicate that increasing temperature had a beneficial effect on the sorption kinetics of Au (III) on Sulf-AG-cellulose.

The kinetics data were analyzed in terms of pseudo-first-order and pseudo-second-order rate equations (Ho, 2006) listed below:

$$\frac{dq_t}{dt} = k_1(q_e - q_t) \quad \text{Eq. (3.4)}$$

$$\frac{dq_t}{dt} = k_2(q_e - q_t)^2 \quad \text{Eq. (3.5)}$$

The integral forms of the above rate equations are as follows:

$$q_t = q_e(1-\exp(-k_1 t)) \quad \text{Eq. (3.6)}$$

$$q_t = \frac{k_2 q_e^2 t}{1 + k_2 q_e t} \quad \text{Eq. (3.7)}$$

where, q_e and q_t are the amounts (mmol/g) of metal adsorbed at equilibrium and at time t, respectively; k_1 (h^{-1}) and k_2 (g $mmol^{-1}$ h^{-1}) are the rate constants for pseudo-first-order and pseudo-second-order equations.

The kinetic parameters for the different rate equations were determined by linear and nonlinear curve fittings using MATLAB 2014b and the results are summarized in Table 3.4. It was found that pseudo-second order rate equation provides better explanation on the sorption rate of Au (III) by Sulf-AG-cellulose.

Table 3.4 Kinetic parameters for adsorptive-reduction of Au (III) by Sulf-AG-cellulose

Initial concentration	Pseudo-first order			Pseudo-second order		
(mmol/L)	k_1 (h^{-1})	q_e (mmol/g)	R^2	k_2 (g $mmol^{-1}$ h^{-1})	q_e (mmol/g)	R^2
1.0	4.21	1.00	0.993	6.55	1.07	0.992
3.0	0.82	3.00	0.920	0.22	3.72	0.988

3.5 Conclusions

Two novel biosorbents were prepared by cross-linking pure cellulose with epichlorohydrin or sulfuric acid, and then modifying the surface with N-aminoguanidine functional groups. Both biosorbents have superior performance on the selectively adsorption toward precious metal ions from mixed metal ions solution in acidic media. The sulfuric acid cross-linked biosorbent exhibited improved selectivity and metal uptake capacity over the epichlorohydrin cross-linked biosorbent and bioreduction of Au (III) can be observed as gold aggregates. The adsorption kinetics of sulfuric acid cross-linked biosorbents was highly efficient as the equilibrium was achieved within a few hours. It can be concluded that amino-guanidine modified cellulose-based biosorbents have outstanding adsorption behavior and can be potential candidates and sustainable alternatives to commercial ion exchange resins for the separation and recovery of precious metals from acid chloride solutions.

Chapter 4 Biosorption and Reduction of Au (III) to Gold Nanoparticles by Modified Alginate

This chapter is based on and modified from the following paper:

X. Gao, Y. Zhang & Y. Zhao. (2017). Biosorption and reduction of Au (Ⅲ) to gold nanoparticles by thiourea modified alginate. Carbohydrate Polymers, 159, 108-115.

Role: Xiangpeng Gao solely worked on this study and acted as the first author of this manuscript under Dr. Yan Zhang and Dr. Yuming Zhao's guidance. Most contents of this paper was written by Xiangpeng Gao and further edited by the other co-authors.

4.1 Abstract

In this study, modified alginate biosorbent has shown a remarkably selective adsorption of Au (III) ions from multi-metallic solutions containing equal moles of Au (III), Pd (II), Pt (IV), Co (II), Ni (II) and Cu (II) ions under acidic conditions. The maximum uptake capacity of Au (III) was found to be 8.47 mmol/g at 323.15 K. Adsorption of Au (III) by modified alginate biosorbent was accompanied by chemical reduction of Au (III), leading to the formation of gold nanocrystals and microcrystals. Biosorption and reduction of Au (III) in acidic media are mediated by the electrostatic and covalent interactions between Au (III) and hydroxyl, carboxyl, amino and –C=S functional groups of modified alginate adsorbent.

4.2 Introduction

Natural polysaccharides (e.g. cellulose, alginate, chitin and chitosan) produced from plants, animals, and microorganisms offer an exciting, flexible, and largely unexplored resource for materials chemistry (Singh & Gross, 2001). Due to the unique ion-exchanging and complexing properties, polysaccharides have been used as novel biosorbents to remove heavy metal (e.g., As, Cr, Cd, Cu, Hg, Pb and Se) ions from wastewater or recover precious metals (e.g., Au, Pt, Pd and Ru) from mining effluent or electronic/catalytic wastes (Adhikari et al., 2008; Dodson et al., 2015; Fomina & Gadd, 2014; Saha & Orvig, 2010; Tran et al., 2015). Adsorption of metal ions using grated or cross-linked natural polymers has the advantages of high efficiency, easy handling, abundance in nature and low cost (Kyzas & Kostoglou, 2014). Based on the physicochemical interactions between metal ions and functional groups of the biosorbents, the binding mechanisms can be electrostatic interaction, ion exchange, chelation/complexation and/or chemical reduction (Guibal, 2014; Won et al., 2014).

Over the last decade, great efforts have been made to physically or chemically modify natural polysaccharides to improve their chemical stability, adsorption capacity, selectivity and reusability. Chemical functionalities of carbohydrate polymers can be altered by substitution reactions such as carboxymethylation (Zhang et al., 2015), acylation (Yuan, Nishiyama, Wada & Kuga, 2006), oxidation (Coseri et al., 2009), alkylation (Sarymsakov, Burkhanova, Tashpulatov & Satybaldyeva, 1997), sulfation (Freeman, Kedem & Cohen, 2008), or thiolation (Kafedjiiski, Krauland, Hoffer & Bernkop-Schnurch, 2005). Natural polysaccharides can also be chemically modified by

chain elongation via graft-copolymerization (Bhattacharya & Misra, 2004) and cross-linking (Hernández-Ortiz & Vivaldo-Lima, 2013). The fabrication methods for highly efficient natural polymer-based adsorbents were summarized in several review articles (González et al., 2011; Wang & Chen, 2009; Won et al., 2014).

Polysaccharides and their derivatives can be used not only as adsorbents, but also as reducing agents for metal ions. The hydroxyl group present in the biopolymer chains enables them to reduce the metals or semiconductor precursors. Cross-linked chitosan hydrogel (Park, Kwak, Won & Yun, 2013), modified cellulose (Gurung et al., 2014), and calcium alginate beads (Torres et al., 2005) are able to reduce Au (III) ions to metallic gold in the form of colloid nanoparticles. Moreover, the weak chemical interactions between polysaccharides and gold nanoparticles (AuNPs) ensure that the obtained nanoparticles could be easily separated, making the production more energy-efficient.

Recovery of precious metals, particularly gold from dilute solutions using polysaccharide-based adsorbents has long been a focus of study. Chitosan and cellulose are widely used as the base matrices for the adsorption of precious metal ions. Less attention has been paid to alginates which are distributed quantitatively in the cell walls of brown algae. Alginate, also called alginic acid, is a linear polysaccharide consisting of α-(1-4)-guluronic acid (G) and β-(1-4)-mannuronic acid (M) arranged in a non-regular, clockwise order along the chain. The large number of hydroxyl group on the alginate chain enables specific binding to precursor cations and thus formation of small nanoparticles (Schnepp, 2013). Additionally, the hydrophilic nature of alginate helps to stabilize the nanoparticle metal colloids.

In this study, a novel alginate-based biosorbent was prepared by gelatinization of alginate using concentrated sulfuric acid, followed by grafting of thiourea. Our experimental results indicated that the newly fabricated biosorbent is capable of selectively adsorbing Au (III) from multi-metallic solutions with extremely high uptake capacity under acidic conditions. Hydroxyl, carboxyl as well as the grafted amino and –C=S functional groups are the main binding sites for gold ions. Meanwhile, the hydroxyl group on the biosorbent is able to reduce Au (III) and precipitate Au (0) in the form of nanoparticle colloids. Such adsorptive-reduction mechanism of Au (III) by the newly prepared sorbent was proved from the XRD and XPS analyses of sorbent before and after Au (III) uptake. The prepared sorbent is chemically resistant against acidic solvent, allowing it to withstand the harsh conditions to recover gold ions from the cyanide containing leachate or other industrial effluents.

4.3 Materials and Methods

4.3.1 Chemicals and Materials

Sodium alginate, sodium bicarbonate (ACS grade) and metal chloride salts ($AuCl_3$, $PdCl_2$. $PtCl_4$, $CoCl_2$, $NiCl_2$ and $CuCl_2$) were purchased from Fisher Scientific. Concentrated sulfuric acid (70% W/W) was purchased from VWR International. Epichlorohydrin (98%) and thiourea (ACS grade) were purchased from Sigma Aldrich. The deionized water was generated from Milli-Q water purification system. All compounds were used as received.

4.3.2 Preparation of Biosorbent

The biosorbent was prepared by the gelation of sodium alginate with concentrated sulfuric acid, followed by surface modification with thiourea at the presence of epichlorohydrin (ECH). The fabrication route of ECH/thiourea modified sulfuric acid gelatinized alginate (ETSA) is illustrated in Figure 4.1. Specifically, 15.0 g sodium alginate was added to 70 mL of concentrated sulfuric acid (70% W/W) and heated to 90 ℃ for 12 h, resulting in the formation of acid-gelatinized alginate powder, which was further neutralized with $NaHCO_3$ and washed with deionized water. The solid was collected by vacuum filtration and dried in oven at 50 ℃. For surface modification of the acid-gelatinized alginate powder by thiourea, 6.0 g thiourea was firstly dissolved in 200.0 mL of 5% sodium hydroxide, 15.0 mL ECH was then added to the thiourea solution. The mixture was heated in an incubator to 70 ℃, shaking at 150 rpm for 4 h. 5.0 g acid-gelatinized alginate powder was added to the thiourea/ECH solution at 70 ℃, shaking at 150 rpm for 8 hours. The resulting solids were repeatedly rinsed in ethanol/water solution and vacuum filtered until the pH of the filtered solution was neutral. The ETSA sorbent was dried in oven at 50.0 ℃ and stored in sealed bottles for use.

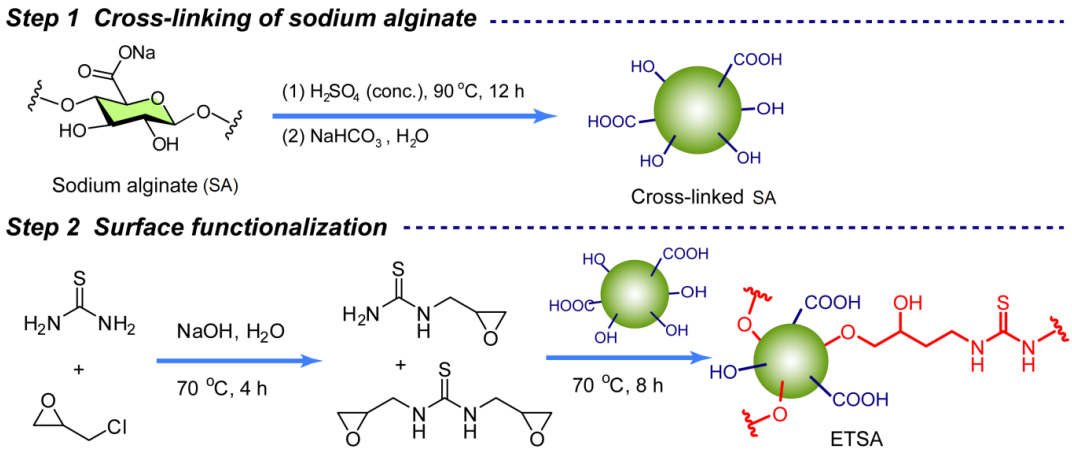

Figure 4.1 Chemical modification of sodium alginate

4.3.3 Biosorption of Au (III) from multi-metallic solutions

Multi-metallic solutions with a concentration of 0.2 mmol/L for Au (III), Pd (II), Pt (IV), Co (II), Ni (II) and Cu (II), were prepared at varying HCl concentrations (0.05 mol/L to 5.0 mol/L) to study the selective adsorption of Au (III) by ETSA,. Batch sorption experiments were conducted in an incubator shaker at 303K with 20.0 mg of dry ETSA and 15.0 mL of metal solution in 100 mL Erlenmeyer flasks, shaking at 200 rpm for 24 h. Samples of 3.0 mL solution were collected at the end of experiments and filtered for concentration measurement by inductively coupled plasma optical emission spectrometry (ICP-OES). The percentage of adsorption for each metal ion can be determined by equation:

$$A(\%) = \frac{C_i - C_e}{C_i} \times 100 \qquad \text{Eq. (4.1)}$$

where C_i and C_e are the initial and final concentrations (mmol/L) of each metal ion in the solution, respectively.

Temperature effect on the biosorption of Au (III) by ETSA was studied via batch experiments at temperatures of 303K, 313K and 323K. 15.0 mL of solutions with varying concentrations of Au (III) ranging from 0.2 mmol/L to 16.0 mmol/L in 0.1 mol/L HCl were mixed with 20.0 mg adsorbent under constant shaking at 200 rpm for 48 h. The amount of Au (III) adsorbed can be calculated by equation:

$$q = \frac{(c_i - c_e)V}{W} \qquad \text{Eq. (4.2)}$$

where W (mg) and V (mL) are the weight of adsorbent and the volume of the test solution, respectively.

The effect of contact time on the uptake of Au (III) by ETSA was investigated through batch sorption test at 303K for 24 h with an initial Au (III) concentration of 1.0 mmol/L and 8.0 mmol/L. 150 mL Au (III) solution in 0.1 mol/L HCl was mixed with 200 mg ETSA powder and shaken at 200 rpm. Samples of 5.0 mL solution were taken at scheduled time intervals and filtered for later concentration measurement by ICP-OES. The uptake of Au (III) at sampling point j can be calculated by equation:

$$q_t = \frac{(c_i - c_t)V - V_t\left(\sum_{k=1}^{j} c_k - tc_t\right)}{W} \qquad \text{Eq. (4.3)}$$

where q_t (mmol/g) is the amount of Au (III) adsorbed at sampling point t ($t \geq 1$); c_i and c_t (mmol/L) are the concentrations of Au (III) in the initial solution and at sampling point

t, respectively; V and V_t (mL) are the initial solution volume and the sampling volume respectively; W (mg) is the weight of the dry sorbent.

4.3.4 Analytical Methods

Fourier transform infrared (FT-IR) spectroscopy of ETSA before and after metal adsorption was recorded by Bruker Alpha FT-IR spectrometer (Bruker, Germany). All samples were prepared as KBr pellets and scanned in the wavenumber range of 400-4000 cm^{-1} at room temperature. Powder X-Ray diffractometry (XRD) was analyzed by Rigaku Ultima IV X-ray diffractometer with a copper X-ray source and a scintillation counter detector. X-ray photoelectron spectroscopy (XPS) analysis of ETSA before and after Au (III) binding was performed on an AXIS 165 X-ray photoelectron spectrometer (Kratos Analytical, USA) with Al Kα X-ray source. UV-visible spectra of the filtered solution after Au (III) biosorption were taken by Cary 100 Bio UV-Visible spectrophotometer (Agilent). Size distribution of AuNPs in filtered solution was determined by NanoSight NS 500 single particle zeta potential platform through the Nanoparticle Tracking Analysis (NTA) software (Malvern). The JEOL JSM-7100F (JOEL, USA) scanning electron microscope (SEM) was used to examine the outer surface and cross-section of ETSA sorbent before and after Au (III) adsorption.

4.4 Results and Discussion

4.4.1 Characterization of the Biosorbent

Figure 4.2 compares the FT-IR spectra of sodium alginate powder, sulfuric acid gelatinized sodium alginate, and ETSA powder. The characteristic peaks of sodium alginate include: 3000-3600 cm^{-1} corresponding to O-H stretching; 2916 cm^{-1} due to stretching vibrations of aliphatic C-H (Daemi & Barikani, 2012); 1594 cm^{-1} and 1405 cm^{-1} associated with asymmetric and symmetric stretching vibrations of carboxylate (COO-) group (Oomens & Steill, 2008); 1295 cm^{-1} and 1026 cm^{-1} attributed to C-O stretching of COO- and C-O-H groups, 947 cm^{-1} for O-H bending, 883 and 813 cm^{-1} due to C-H "oop" bending (Stuart, 2004). Structure changes of sulfuric acid gelatinized sodium alginate and ETSA were confirmed from their IR spectra. For acid-gelatinized sodium alginate, significant changes at 1148 and 1030 cm^{-1} are observed, associated with C-O-C stretching vibrations in the form of ester. The appearance of a new peak at 1694 cm^{-1} and the peak shifts at 1594 and 1405 cm^{-1} prove the change from carboxylate salt to carboxylic acid. Peak shift at 3000-3600 cm^{-1} from the IR spectrum of ETSA is due to the N-H stretching on the thiourea functional group. IR bands at 1514 and 1369 cm^{-1} are assigned to N-C=S group (Gavilan, Pestov & Garcia, 2009), which is indicative of the presence of thiourea functional group on the alginate matrix.

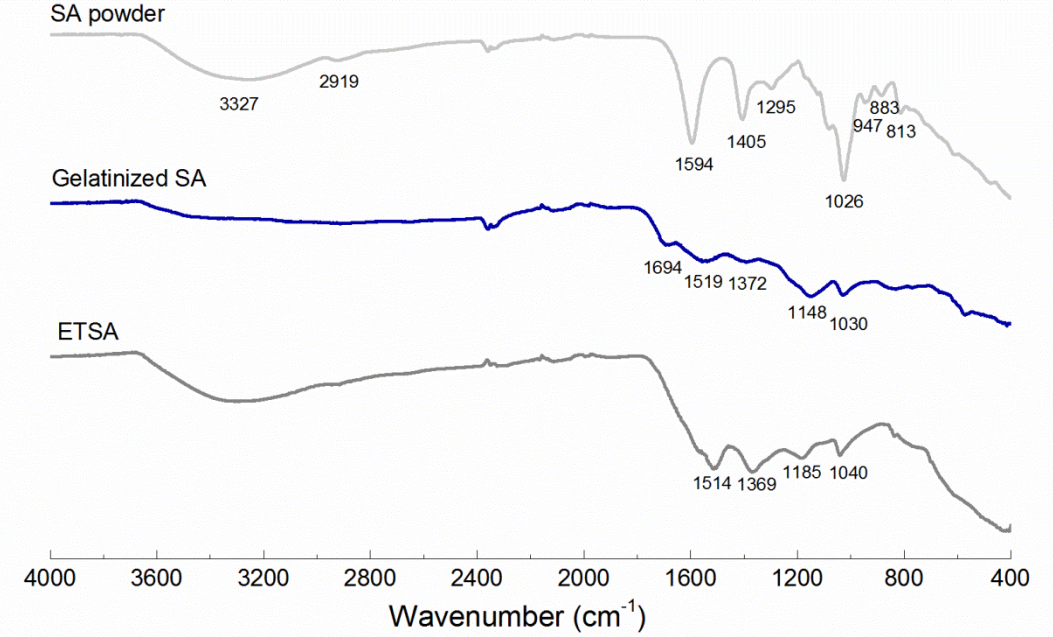

Figure 4.2 FT-IR spectra of sodium alginate, concentrated sulfuric acid gelatinized sodium alginate, and ETSA powder

4.4.2 Biosorption and reduction of Au (III)

The selective adsorption of Au (III) from multi-metallic solution by ETSA and the results are presented in Figure 4.3. As seen from Figure 4.3, ETSA powder exhibited remarkable selective adsorption toward precious metals with a selectivity order of Au (III) > Pd (II) > Pt (IV), whereas the uptake of Co (II), Ni (II) and Cu (II) is not significant under the same conditions. It is impressive that Au (III) was adsorbed efficiently by ETSA from acidic solutions with HCl concentration up to 5.0 mol/L. The potential selective sorption mechanisms of Au (III) by ETSA are explained below.

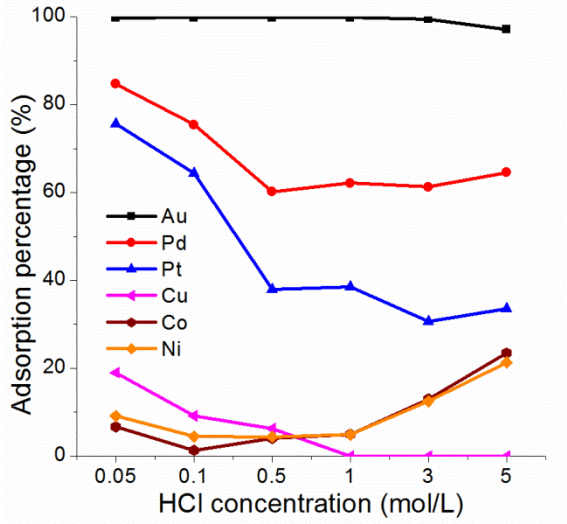

Figure 4.3 Adsorption behavior of ETSA powder towards various metal ions with varying HCl concentrations

During the sorption process, oxygen and nitrogen centered functional groups on ETSA become the positive centers by protonation in acidic media. The main species of precious metals in acidic solutions are metal chloride anionic complexes ($AuCl_4^-$, $PdCl_4^{2-}$and $PtCl_6^{2-}$). However, the coexisting metals, copper, cobalt, and nickel existed in their cationic forms (Pettit & Powell, 1999). The positively charged transition metals (Cu (II), Co (II) and Ni (II)) interacted repulsively with the protonated functional groups on ETSA. As a result, the adsorption of Cu (II), Co (II) and Ni (II) was hardly gained in acidic media. The electrostatic interaction between the negative charged metal ligands and the positive charged function groups makes ETSA selectively adsorb precious metal ions from multi-metallic solutions.

Moreover, chelation between metal chloride anionic complexes ($AuCl_4^-$, $PdCl_4^{2-}$and $PtCl_6^{2-}$) and oxygen atom from hydroxyl and carboxyl groups, nitrogen and sulfur atoms from the grafted amino and –C=S groups, also contributes significantly to the selective uptake of precious metal ions. In addition, due to the strong reduction power, hydroxyl

group on ETSA surfaces is capable of reducing Au (III) to metallic gold in line with the following reaction scheme.

$$2AuCl_4^- + 3RCH_2OH \rightarrow 2Au(0) + 3RCHO + 6H^+ + 8Cl^-$$

where reduction of Au (III) to Au (0) occurs through oxidation of hydroxyl to aldehyde group. This adsorption-reduction mechanism of Au (III) has also been confirmed by other research studies (Kuyucak & Volesky, 1989; Mele et al, 2014).

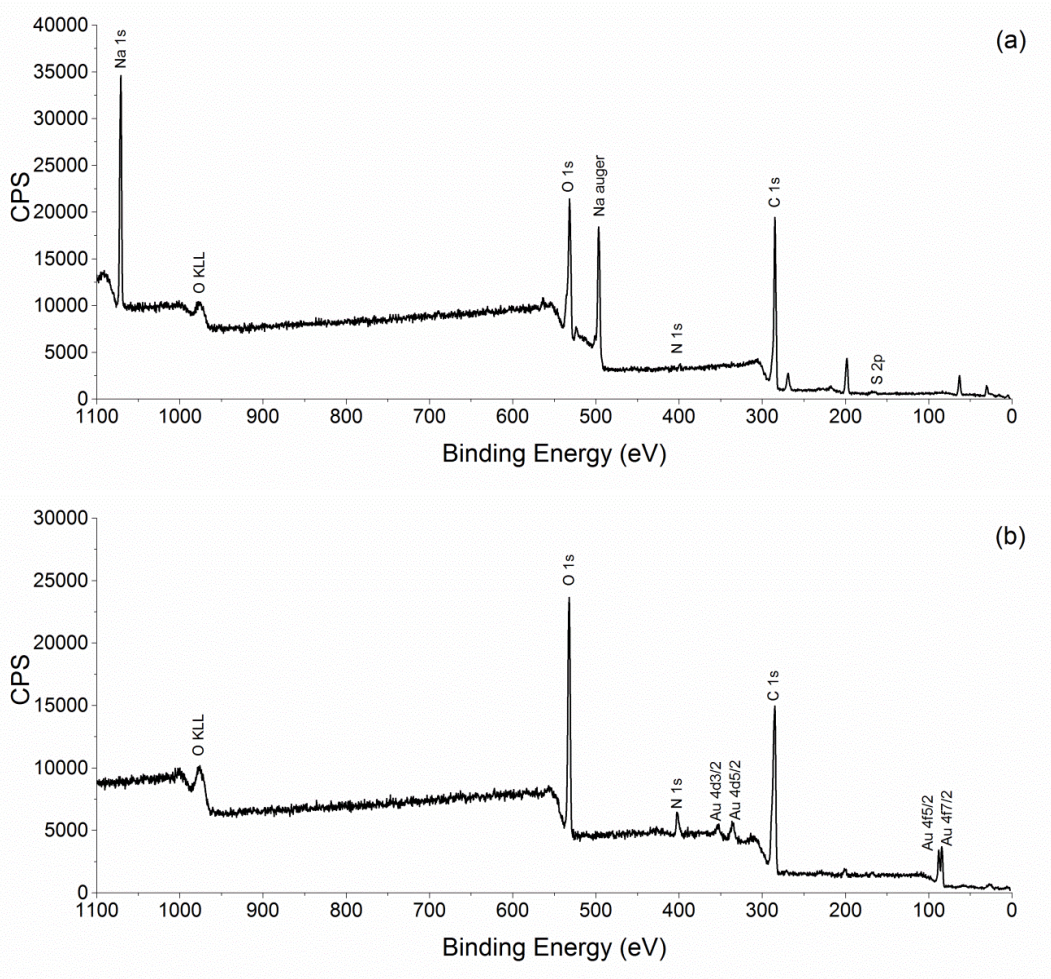

Figure 4.4 XPS survey on (a) ETSA before adsorption and (b) after gold adsorption

The aforementioned adsorption mechanism of Au (III) was examined by the X-ray photoelectron spectroscopy (XPS) analysis of ETSA before and after gold adsorption (Figures 4.4(a) & (b)). The results were calibrated using C 1s binding energy (BE) peak at 284.8 eV. New BE peaks at 546.2 eV, 352.1 eV, 334.1 eV, 87.9 eV, 83.9 eV, and 54.2 eV appeared in the survey spectrum of ETSA after adsorption. These correspond to Au 4p3/2, Au 4d3/2, Au 4d5/2, Au 4f5/2, Au 4f7/2, and Au 5p3/2, respectively, which indicate significant amount of gold has been adsorbed on ETSA. Particularly BE peak at 83.9 eV indicates the existence of metallic gold (Casaletto, Longo, Martorana, Prestianni & Venezia, 2006). High resolution XPS spectra of N 1s, O 1s and S 2p as well as their deconvoluted fitted curves are demonstrated in Figures 4.5(a)-(f) for ETSA before and after Au (III) uptake. BE peaks at 399.5 eV and 400.2 eV in Figures 4.5(a) correspond to free amino ($–NH_2$) and protonated amino ($–NH_3^+$) groups (Yong et al., 2016). After Au (III) adsorption, although both peaks shift to higher binding energy, peak shift of $-NH_3^+$ is more significant (2.1 eV to high BE), indicating the positive charged $-NH_3^+$ group is capable of attracting $AuCl_4^-$ more effectively by electrostatic interaction. The oxygen atom in ETSA exists in two chemical states, doubly-bonded oxygen (C=O) at 532.5 eV and organic C-O (oxygen in carbon chain and ether groups) at 531.2 eV as illustrated in XPS spectra of O 1s (Figure 4.5(c)) (Naumkin, Kraut-Vass, Gaarenstroom & Powell, 2012). The peak at 535.8 eV is due to sodium auger overlap. After Au (III) adsorption, peaks at 532.5 eV and 531.2 eV shift to 532.9 eV and 531.7 eV, demonstrating that oxygen acts as the electron donor when binding $AuCl_4^-$. Particularly, the intensity increase of O 1s at 532.9 eV (C=O) in Fig. 4d indicates the transition of C-O to C=O on ETSA after Au (III) adsorption, confirming the oxidation of hydroxyl group to aldehyde

group. The involvement of –C=S group in Au (III) binding is also proved from the high resolution XPS result of S 2p. Peaks at 168.8 and 167.8 eV in Figure 4.5(e) are assigned to the sulfur atoms in -SO_4^{2-} group (contaminated S) (Raj, Shanmugam, Mahalakshmi & Viswanathan, 2010). Peaks at 166.0, 163.5 and 161.2 eV are ascribed to the sulfur in –C=S group (Naumkin et al., 2012), which shifted to high BE position after Au (III) adsorption. Sulfur in –C=S group acts as an electron donor during the sorption of Au (III), which discloses that complexation is the governing mechanism for Au (III) uptake at this binding site.

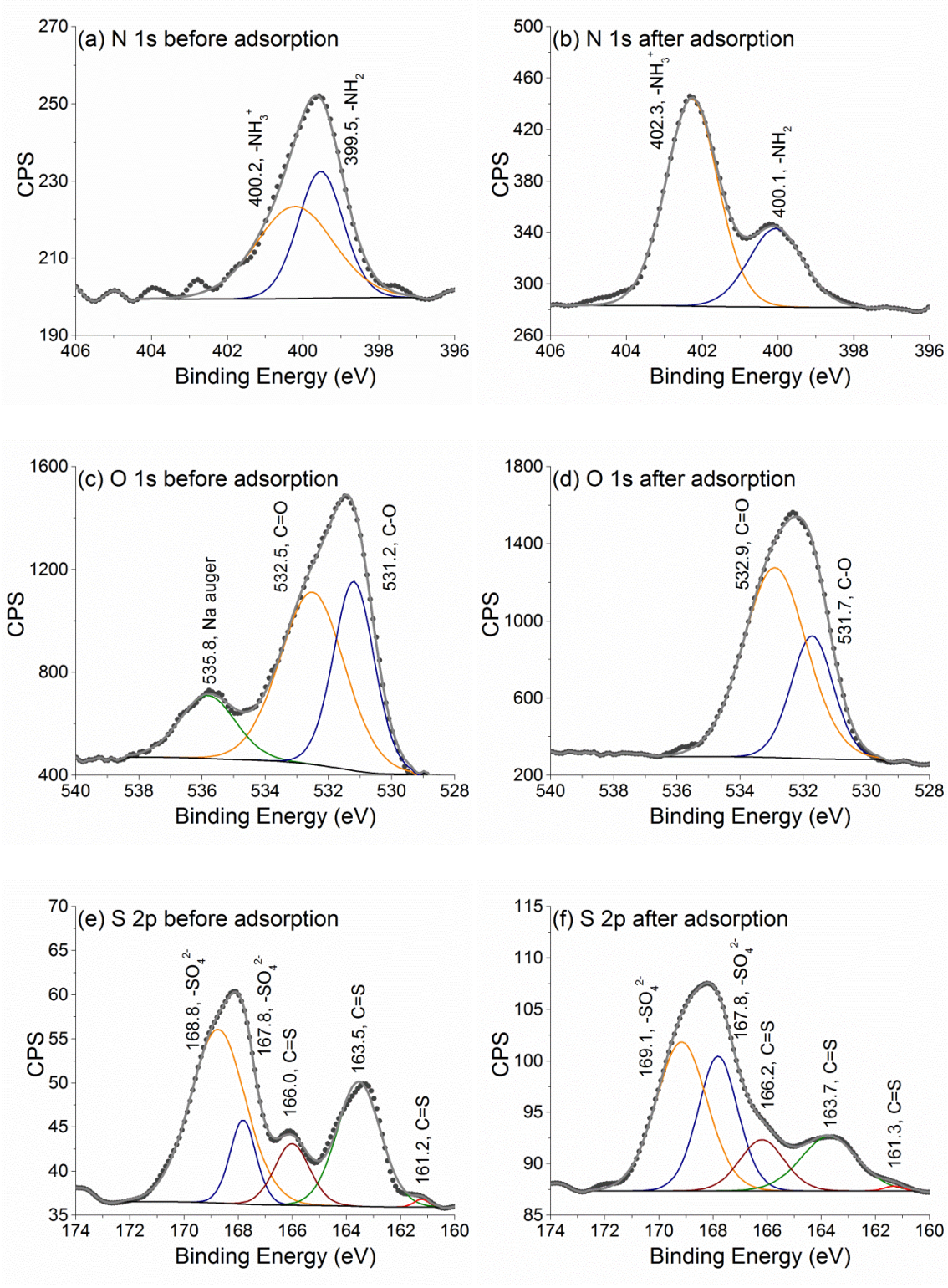

Figure 4.5 XPS high resolution spectrum on (a) N 1s before adsorption; (b) N 1s after adsorption; (c) O 1s before adsorption; (d) O 1s after adsorption; (e) S 2p before adsorption; (f) S 2p after adsorption

4.4.3 Characterization of Gold Nanoparticles

The formation of AuNPs as a result of adsorptive-reduction of Au (III) on ETSA surfaces was first experimentally detected by the appearance of color in ETSA powder, followed by the color change of the metallic solution. The color of the Au (III) solution changed from light yellow to brown and finally dark red in the process of adsorption. It is inferred that very fine gold nanoparticles were formed within few hours of adsorption as the color turned brown. After 30 hours, the fine nanoparticles agglomerated, leading to the formation of larger nanoparticles. The color of solution changed from brown to dark red accordingly. UV-Vis spectrum of the filtered colloidal gold solution (Figure 4.6(a)) shows a peak UV absorbance at wavelength of 548 nm, which renders an average size of 80 nm for the AuNPs (Haiss, Thanh, Aveyard & Fernig, 2007). Such results are consistent with the size distribution of the colloidal gold solution illustrated in Figure 4.6(b) from the analysis of NanoSight NS500. The mean particle size is about 105 nm with a highest intensity at 84 nm.

The formation of metallic gold during the biosorption of Au (III) was also proved from the XRD analysis of ETSA after Au (III) adsorption. The peaks at 2θ of 38.2^{o}, 44.4^{o}, 64.6^{o}, 77.5^{o}, and 81.7^{o} in Figure 4.6(c) can be indexed to the (111), (200), (220), (311) and (222) Bragg's reflections of cubic structure of metallic gold. These gold planes and corresponding two theta values are indexed by using the International Center for Diffraction Data (ICDD) powder diffraction files (PDF) number 04-0784 for gold. Further characterization of the ETSA after Au (III) biosorption by scanning electron microscopy (SEM) gave a visual representation of the formation of AuNPs. SEM image

presented in Figure 4.6(d) revealed the uniformly scattered AuNPs with sporadic aggregation on the surface of ETSA. Most gold particles have spherical shapes ranging from 50-200 nm. Large particles (> 1000 nm) are also present on the surface of ETSA due to the growth and aggregation of gold crystals.

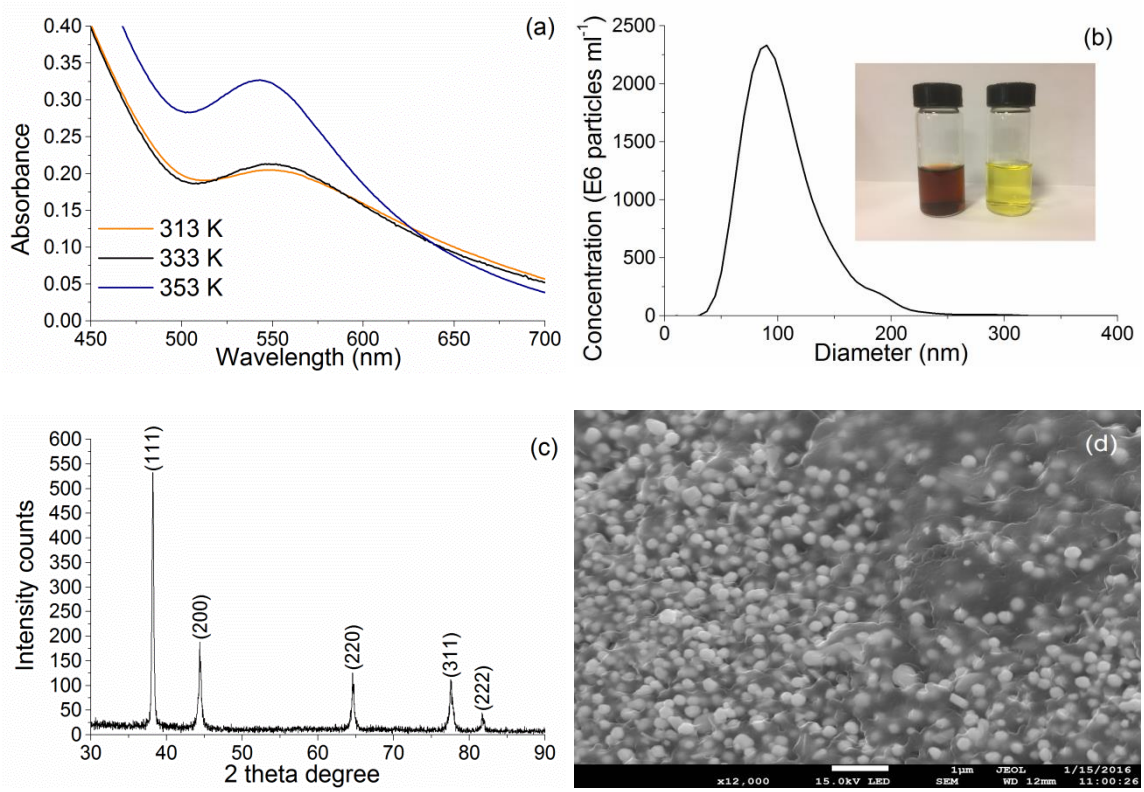

Figure 4.6 Characterization of AuNPs: (a) UV-Visible spectra of Au (III) solution after adsorption; (b) Size distribution analysis of AuNPs; (c) XRD spectrum of ETSA after Au (III) adsorption; (d) SEM image of ETSA after Au (III) biosorption

4.4.4 Effects of Temperature and Contact Time

Effects of temperature and initial Au (III) concentration on adsorptive – reduction of Au (III) was demonstrated in Figure 4.7(a). The amount of Au (III) ions adsorbed on ETSA powder increased with increasing initial concentration of the metallic solution. The maximum adsorption capacities are 6.40 mmol/g, 7.79 mmol/g, and 8.47 mmol/g at

temperatures of 303 K, 313 K and 323 K, respectively. Results in Figure 4.7(a) demonstrated that the uptake of Au (III) is increased at higher temperature and that the adsorptive-reduction of Au (III) to Au (0) on ETSA is an endergonic process.

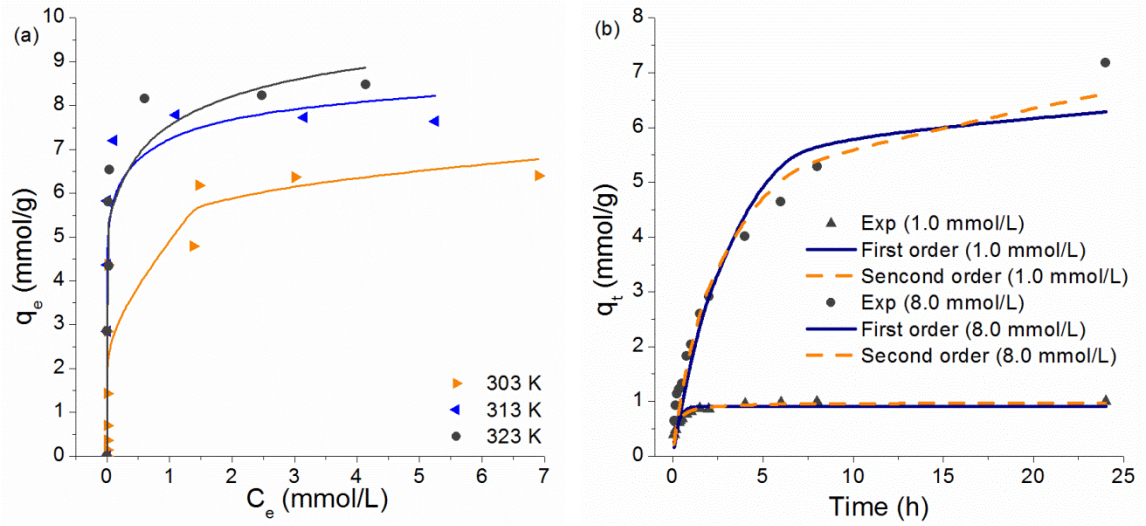

Figure 4.7 Effects of temperature and contact time on biosorption of Au (III) by ETSA

The influence of contact time on the reductive adsorption of Au (III) by ETSA was illustrated in Figure 4.7(b). The amount of Au (III) adsorbed by ETSA powder increased rapidly and approached a constant value after a certain period of shaking. The adsorption percentage reached 95.37% within the first 4 h in 1.0 mmol/L Au (III) solution and the final equilibrium was reached in 6 h. ETSA powder exhibited remarkable fast kinetics in Au (III) adsorption.

The kinetics data were analyzed in terms of pseudo-first-order and pseudo-second-order rate equations (Ho, 2006) listed below,

$$\frac{dq_t}{dt} = k_1(q_e - q_t) \qquad \text{Eq. (4.4)}$$

$$\frac{dq_t}{dt} = k_2(q_e - q_t)^2 \qquad \text{Eq. (4.5)}$$

The integral forms of the above rate equations are as follows:

$$q_t = q_e(1 - \exp(-k_1 t)) \qquad \text{Eq. (4.6)}$$

$$q_t = \frac{k_2 q_e^2 t}{1 + k_2 q_e t} \qquad \text{Eq. (4.7)}$$

where, q_e and q_t are the amounts (mmol/g) of metal adsorbed at equilibrium and at time t, respectively; k_1 (h^{-1}) and k_2 (g $mmol^{-1}$ h^{-1}) are the rate constants for pseudo-first-order and pseudo-second-order equations.

The kinetic parameters for the different rate equations were determined by linear and nonlinear curve fittings using MATLAB 2014b and the results are summarized in Table 4.1. The measured kinetic data and the model predicted kinetic results are compared and illustrated in Figure 4.7(b). It was found that pseudo-second order rate equation provides better explanation on the reductive adsorption rate of Au (III) by ETSA.

Table 4.1 Kinetic parameters for reductive adsorption of Au (III) by ETSA

Initial concentration	Pseudo-first order			Pseudo-second order		
(mmol/L)	k_1 (h^{-1})	q_e (mmol/g)	R^2	k_2 (g $mmol^{-1}$ h^{-1})	q_e (mmol/g)	R^2
1.0	3.80	0.91	0.83	5.89	0.98	0.96
8.0	0.32	6.29	0.92	0.05	7.37	0.97

4.5 Conclusions

A novel biosorbent was prepared by gelatinization of sodium alginate with concentrated sulfuric acid, followed by surface modification with epichlorohydrin/thiourea. The resulting ECH/thiourea modified sulfuric acid gelatinised alginate (ETSA) is able to selectively adsorb and reduce Au (III) to AuNPs from multi-metallic solutions under acidic conditions. ETSA is highly efficient in terms of adsorption kinetics, as the equilibrium was achieved within a few hours with quantitative adsorption in 1.0 mmol/L Au (III) solution. XRD and XPS analyses of the sorbent before and after Au (III) adsorption revealed that hydroxyl, carboxyl, pronated amino and C=S groups are the main binding sites of Au (III) and the hydroxyl group is responsible for the reduction of Au (III). Results from this study demonstrated that ETSA provides a highly efficient, cost effective and environmental-friendly pathway to recover gold ions from industrial effluents.

Chapter 5 Zinc Oxide Templating of Porous Alginate Beads for the Selective Adsorption of Au (III)

This chapter is based on and modified from the following paper:

X. Gao, Y. Zhang & Y. Zhao. (2018). Zinc Oxide Templating of Porous Alginate Beads for the Selective Adsorption of Au (III).

This manuscript is submitted to Carbohydrate Polymers and is now under review.

Role: Xiangpeng Gao solely worked on this study and acted as the first author of this manuscript under Dr. Yan Zhang and Dr. Yuming Zhao's guidance. Most contents of this paper was written by Xiangpeng Gao and further edited by the other co-authors.

5.1 Abstract

In this study, a novel porous alginate adsorbent was prepared by zinc oxide templating to selectively adsorb Au (III) ions from multi-metallic solutions under acidic condition. Due to the porous structure of the prepared sorbent, high uptake capacity and fast adsorption kinetics of Au (III) were achieved, which renders the prepared adsorbent great potential for practical applications in fixed-bed columns for large-scale applications. The adsorption of Au (III) by the prepared adsorbent led to the reduction of Au (III) to metallic gold. Adsorption and reduction of Au (III) in the process are mediated by the ionic and covalent interaction between Au (III) ions and the protonated functional groups on the modified alginate.

5.2 Introduction

Recovery of precious metals, e.g., gold (Au), platinum (Pt) and palladium (Pd) from aqueous and waste solutions has been an actively pursued research topic due to the high economic value and relative scarcity of these elements in nature (Das, 2010). Adsorption process is now recognized as an effective, efficient and economic method for the recovery of precious metals from very dilute aqueous solutions (Dodson et al., 2015; Gao, Zhang, & Zhao, 2017; Uddin, 2017). Over the past two decades, great efforts have been made to fabricate cost-effective adsorbents from natural polymers extracted from various biomass resources (Ahmaruzzaman, 2008; Bhatnagar, Sillanpää, & Witek-Krowiak, 2015; Devi & Saroha, 2017; Dodson et al., 2015; Rafatullah, Sulaiman, Hashim, & Ahmad, 2010; Uddin, 2017; Yagub, Sen, Afroze, & Ang, 2014). Biopolymer-based adsorbents show strong chelating power, good chemical stability and high adsorption selectivity and capacity due to the presence of chemical reactive groups (hydroxyl, carboxyl or amino) in polymer chains (Chassary, Vincent, & Guibal, 2004; Crini, 2005; Hokkanen, Bhatnagar, & Sillanpää, 2016). However, adsorbents prepared by the current technology, normally in the form of fine powders or nonporous hydrogels, still cannot be used as the stationary phase in fixed-bed columns for large-scale applications due to the low porosity, poor reusability and hydrodynamic limitations (Fomina & Gadd, 2014; Park, Yun, & Park, 2010; Vijayaraghavan & Balasubramaian, 2015). In this regard, preparation of porous biopolymer-based gel beads is the key to large-scale adsorption process of precious metal ions as the porous structure of gel beads not only enables fast adsorption kinetics, but also facilitates high binding capacity, high chemical stability and rapid sorbent regeneration.

Various methodologies have been developed over the past decade to prepare porous polymers and resins, including direct templating, block copolymer self-assembly, direct synthesis and high internal phase emulsion polymerization methodologies (Kailasam et al., 2010; Lou, Archer, & Yang, 2008; Mastalerz, 2008; Wu et al., 2012). Among these methods, direct templating, a molding and casting technique for the direct replication of the inverse structure of the performed templates is widely used due to its convenience in controlling the size and morphology of the porous structure (Bunz, 2006; Song & Kretzschmar, 2008). The pore size and porosity of the porous polymers fabricated by direct templating can be readily tuned by varying the size and the packing order of the colloidal templates (Wu et al., 2012).

In this study, direct templating method was employed to fabricate porous alginate gel beads for the selective adsorption of Au (III) from multi-metallic solutions. Sodium alginate, a linear biopolymer consisting of α-(1-4)-guluronic acid (G) and β-(1-4)-mannuronic acid (M) was used as the building block, whereas zinc oxide, which does not react with sodium alginate and can be easily removed by dilute hydrochloric acid was selected as the colloidal templates. We hypothesize that the uptake capacity of the prepared adsorbent can be greatly increased by grafting epichlorohydrin/thiourea onto the sodium alginate polymer chains due to the introduction of more metal binding functional groups (amino and –C=S). We also anticipate the fast adsorption kinetics of the metal ions owing to the enhanced internal mass transfer of metal ions in the porous polymer matrix. The first main objective of this work therefore is to define synthesis conditions (template dosage, crosslinker content and agitation speed, etc.) that control the properties

of interest, namely porous structure, binding capacity and adsorption kinetics. The second objective of this study is to determine the optimum environmental conditions of Au (III) adsorption and disclose the selective adsorption mechanism of Au (III) by the fabricated porous adsorbent.

5.3 Materials and Methods

5.3.1 Materials

Low viscosity alginic acid sodium salt (40-90 mPa s in 1% aqueous solution, molecular weight of 16-34 kDa, M/G ratio of 2.05)[1], zinc oxide, calcium chloride, ethanol, hydrochloric acid (35%-38%), and metal chloride salts ($AuCl_3$, $PbCl_2$, $CoCl_2$, $NiCl_2$ and $CuCl_2$) were purchased from Fisher Scientific. Sodium hydroxide pellets was purchased from VWR International. Epichlorohydrin (99%) and thiourea (ACS grade) were purchased from Sigma Aldrich. The deionized water was generated from Milli-Q water purification system. All compounds were used as received.

5.3.2 Preparation of PETA Beads

Porous epichlorohydrin/thiourea modified alginate (PETA) beads were fabricated by surface modification of sodium alginate, followed by direct templating synthesis as illustrated in Figure 5.1. During the preparation of PETA beads, sodium alginate concentration, epichlorohydrin (ECH) and thiourea contents, zinc oxide (ZnO) dosage, agitation speed, and calcium chloride ($CaCl_2$) concentration were optimized to obtain the

[1] The viscosity data were acquired from Fisher Scientific; the molecular weight was calculated by an empirical correlation provide by Ciocoiu et al. (2018); MG ratio was determined by NMR analysis (Salomonsen et al., 2009).

sorbent with high uptake capacity and anticipated porous structure. It was found that 12.0 w/v% sodium alginate, 1:2:1 mole ratio of alginate: ECH: thiourea, 15.0 w% of ZnO per unit mass of sodium alginate, 100 rpm agitation speed, and 2.0 w% $CaCl_2$ solution are the optimum synthetic conditions.

For surface modification, thiourea of 1.71 g was firstly dissolved in 30.0 ml of 5.0 w% sodium hydroxide solution, and then reacted with 3.56 ml of ECH at 70 ℃ with shaking for 4 h. Under continuous shaking, 4.0 g of sodium alginate powder reacted with ECH/thiourea solution at 70 ℃ for 8 h. To generate the porous structure, 0.6 g of ZnO powder was added to the alginate solution and stirred at 100 rpm for 2.0 min by a stand mixer, followed by sonication of 15.0 min to remove the dissolved gas bubbles from the solution. The resulting mixture was then added to 2.0 w% CaCl2 solution to form beads and aged overnight. Finally, ZnO was removed from the network using 0.1 M HCl solution and the resulting porous PETA beads were rinsed in ethanol/water solution and dried at room temperature.

To determine the effectiveness of surface grafting in enhancing the uptake capacity, porous alginate (PA) beads (12.0 w/v% sodium alginate and 15.0 w% of ZnO per unit mass of sodium alginate) were fabricated without ECH/thiourea grating. Similarly, to investigate the effect of porous structure on the adsorption kinetics, nonporous epichlorohydrin/thiourea modified alginate (NETA) beads were also prepared without ZnO templating.

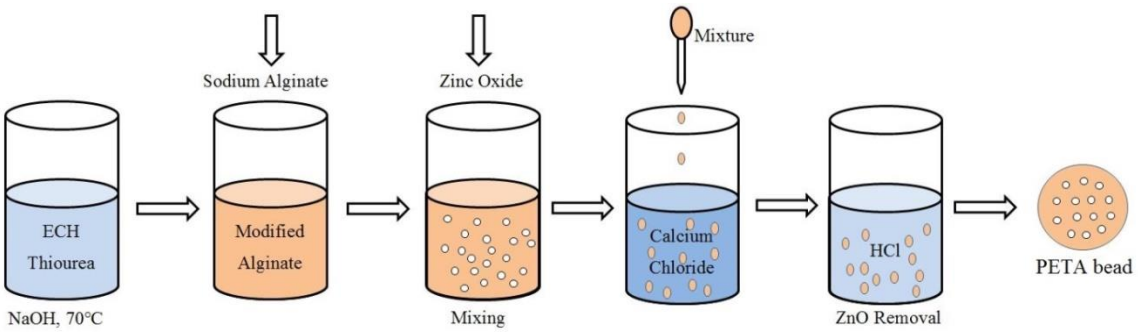

Figure 5.1 Major fabrication steps of PETA beads

5.3.3 Adsorption of Au (III) from Multi-metallic Solutions by PETA

Multi-metallic solutions with a concentration of 0.2 mmol/L for Au (III), Co (II), Pb (II), Ni (II) and Cu (II), were prepared at different HCl concentrations (0.05 to 5.0 mol/L) to study the selective adsorption of Au (III) by PETA beads. Sorption experiments were performed in an incubator shaker at 30 ℃ where 20.0 mg of dry PETA and 15.0 mL of metal solution were mixed in 100mL Erlenmeyer flasks under constant shaking for 24 hours. Samples of 5.0 mL solution were withdrawn at the end of experiments and filtered for concentration measurement by inductively coupled plasma optical emission spectrometry (ICP-OES). The percentage of adsorption for each metal ion can be determined by:

$$\text{Adsorption } \% = \frac{c_i - c_f}{c_i} \times 100 \qquad \text{Eq. (5.1)}$$

where, c_i (mmol/L) and c_f (mmol/L) are the initial and final concentrations of each metal ion in the solution, respectively.

The influence of temperature on the uptake of Au (III) by PETA was studied using batch adsorption tests at temperatures of 30 ℃, 40 ℃ and 50 ℃. Stock solutions of Au (III) were prepared by dissolving $AuCl_3$ salt in 0.1 mol/L HCl solution. 15.0 ml of stock solutions with Au (III) concentration ranging from 0.2 mmol/L to 4.0 mmol/L were mixed with 20.0 mg PETA beads under constant shaking at 200 rpm for 48 hours. The amount of Au (III) adsorbed can be calculated from Eq. 5.2,

$$q = \frac{(c_i - c_e)V}{m} \qquad \text{Eq. (5.2)}$$

where, c_i and c_e (mmol/L) are the initial and equilibrium concentrations of Au (III) in aqueous solutions, V (L) is the volume of the test solution, and m (g) is the mass of the PETA adsorbent.

The adsorption kinetics of Au (III) by PETA was investigated in a temperature-controlled incubator shaker at 30 ℃ where 150.0 ml of 1.0 mmol/L Au (III) solution at pH 1.0 was mixed with 150.0 mg PETA beads under constant shaking for 24 h. Samples of 5.0 ml solution were collected at scheduled time intervals and filtered for later concentration measurement by ICP-OES. The uptake of Au (III) at sampling point j can be calculated by Eq. 5.3.

$$q_j = \frac{(c_i - c_j)V - V_s\left(\sum_{k=1}^{j} c_k - jc_j\right)}{m} \qquad \text{Eq. (5.3)}$$

where q_j (mmol/g) is the amount of Au (III) adsorbed at sampling point j ($j \geq 1$); c_i and c_j (mmol/L) are the concentration of Au (III) in initial solution and at sampling point j,

respectively; V and V_s (L) are the initial solution volume and the sampling volume respectively; m (g) is the weight of the dry sorbent.

5.3.4 Analytical Methods

Various analytical methods have been employed to characterize the PETA adsorbent before and after Au (III) adsorption. The Fourier transform infrared (FT-IR) spectra of sodium alginate, ET alginate beads, and PETA beads were recorded by Bruker Alpha FT-IR spectrometer (Bruker, Germany). All samples were scanned in the wavenumber range of 400-4000 cm^{-1} at room temperature. Powder X-ray diffraction (XRD) analysis was performed by Rigaku Ultima IV X-ray diffractometer with a copper X-ray source and a scintillation counter detector. X-ray photoelectron spectroscopy (XPS) analysis of PETA before and after Au (III) uptake was performed on an AXIS 165 X-ray photoelectron spectrometer (Kratos Analytical, USA) with Al Kα X-ray source. The JEOL JSM-7100F (JOEL, USA) and FEI MLA 650F scanning electron microscope (SEM) systems were used to examine the outer surface and internal structure of PETA beads before and after Au (III) adsorption. Concentration of metal ions in aqueous solutions before and after metal uptake were determined by Perkin Elmer Optima 5300DV (Perkin Elmer, Canada) ICP-OES.

5.4 Results and Discussion

5.4.1 Characterization of PETA

Figure 5.2 demonstrates the FT-IR spectra of sodium alginate powder, nonporous epichlorohydrin/thiourea modified alginate (NETA) beads, and PETA beads. Main

functional groups and their characteristic peaks of sodium alginate as seen from Fig. 3 are 3000-3600 cm^{-1} corresponding to O-H stretching; 2940 cm^{-1} due to stretching vibrations of aliphatic C-H (Daemi & Barikani, 2012); 1590 cm^{-1} and 1404 cm^{-1} associated with asymmetric and symmetric stretching vibrations of carboxylate (COO^-) group (Oomens & Steill, 2008); 1085 cm^{-1} and 1030 cm^{-1} due to C-O stretching of COO^- and C-O-H groups. The grafting of ECH/thiourea to alginate is supposed to occur by reaction of hydroxyl group of the biopolymer with the epoxy group on ECH; this is confirmed from IR spectra of NETA and PETA beads. Peak shifts at 3000-3600 cm^{-1} of the IR spectra of NETA and PETA are due the N-H stretching vibrations of thiourea groups. Meanwhile, band shifts at 1404 cm^{-1} and 1085-1030 cm^{-1} stem from the N-C=S group grafted on the alginate matrix since three arbitrary regions, viz., 1570-1395 cm^{-1}, 1420-1260 cm^{-1} and 1140-940 cm^{-1} in the infrared are generally assigned to the N-C=S stretching vibrations (Gavilan et al., 2009; Rao & Venkatarachavan, 1962). Peak changes for the carboxylic acid group can be observed from the spectrum of PETA and new peaks at 1724 cm^{-1} and 1250 cm^{-1} were observed, indicating that ester was formed when hydrochloric acid was used to remove zinc oxide template from ECH/thiourea modified alginate beads. The peak at 1724 cm^{-1} is assigned to ester C=O and the IR bands at 1250 cm^{-1} and 1050 cm^{-1} are due to the ester C-O.

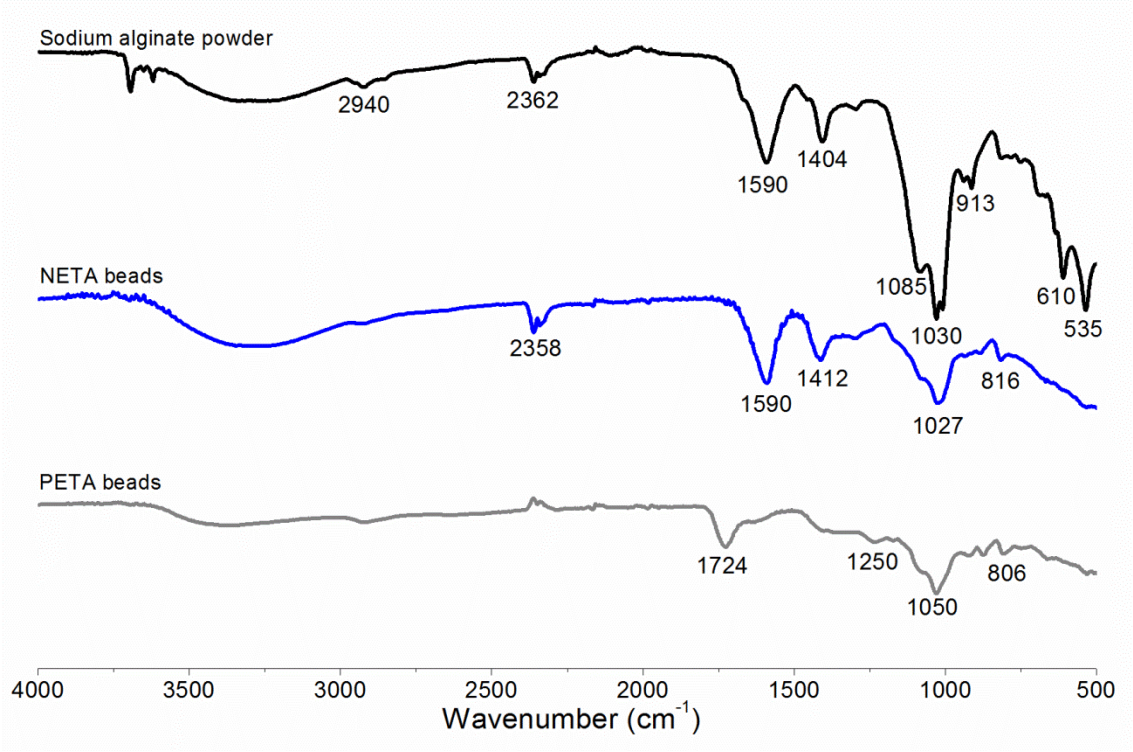

Figure 5.2 FT-IR spectra of sodium alginate, ET alginate bead, and PETA bead

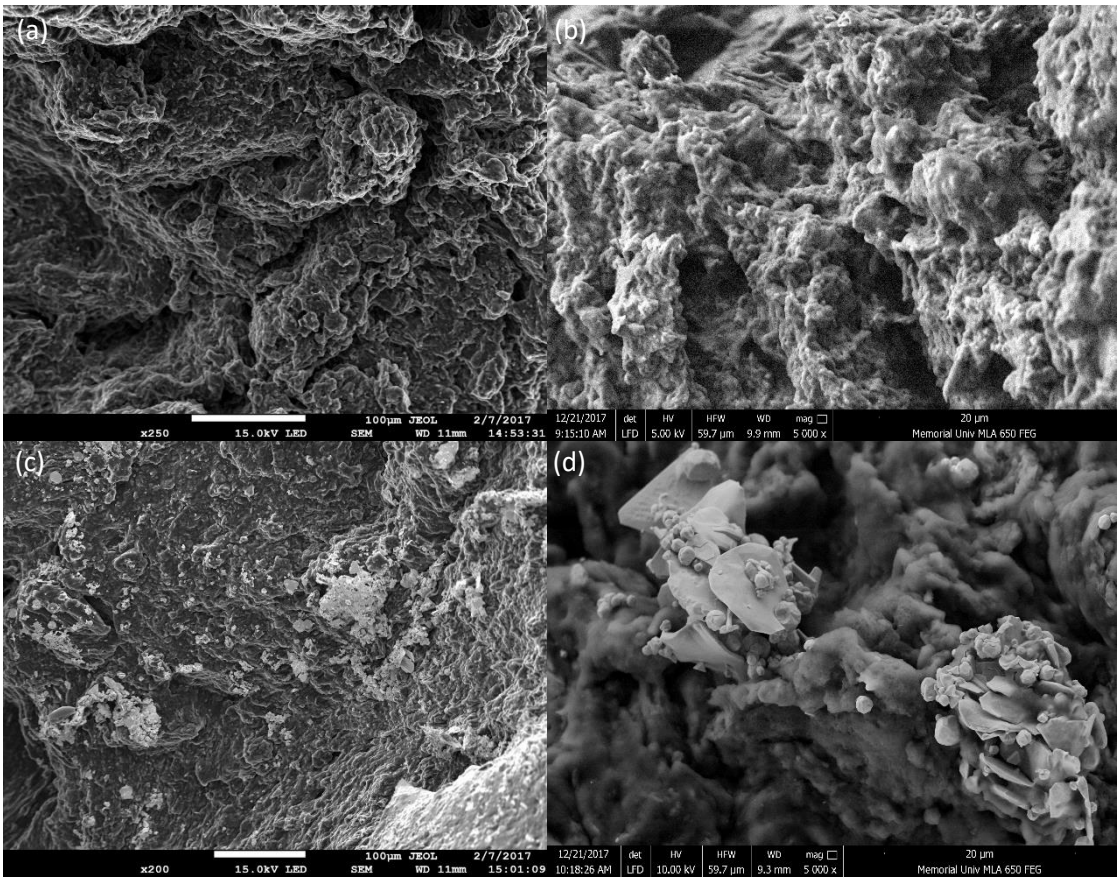

Figure 5.3 PETA beads before (a) and (b) and after (c) and (d) Au (III) adsorption

Porous structure of PETS beads is clearly illustrated from the SEM micrographs of the cross-section of PETA before and after Au (III) adsorption (Fig. 5.3). Figs. 5.3(a) and 5.3(b) are the micrographs of PETA before Au (III) adsorption; whereas Figs. 5.3(c) and 5.3(d) are for materials after Au (III) adsorption. As seen from Figs. 5.3(a) and 5.3(b), the polymeric matrix of PETA is uneven with a mass of small holes on it. However, due to the random distribution of colloidal templates in polymeric matrix, a non-uniform pore size distribution was generated for the PETA network. Very large holes are also observed in the core of the beads resulting from the air bubbles during the synthetic procedure. SEM micrographs of the Au (III)-loaded PETA shown in Figs. 5.3(c) and 5.3(d) confirm

that Au (III) was adsorbed and reduced to metallic gold on the internal surface of PETA beads, suggesting that functional groups over the entire mass of PETA beads are accessible. In addition, the tighter porous network for PETA adsorbent may explain its good stability and high chemical resistance to acidic environments.

5.4.2 Enhancement of the uptake capacity by surface grafting

The batch adsorption experiments of Au (III) by PA and PETA beads were conducted at 30 ℃ with 15.0 ml of 4.0 mM Au (III) solution (pH 1.0) being contacted with 20.0 mg of PA and PETA sorbents under constant shaking for 48h. The final uptake capacities of Au (III) by PA and PETA beads are 1.11 and 1.97 mmol g^{-1}, which indicates that surface grafting is an effective technique to increase the binding capacity of the biopolymer-based adsorbent. This result also confirmed that –C=S and protonated amino groups (under pH 1.0) play important roles in Au (III) binding.

5.4.3 Selective adsorption of Au (III) by PETA

The results of the selective adsorption of Au (III) from multi-metallic solution by PETA beads are presented in Figure 5.4. In general, PETA beads have higher uptake capacities for precious metal ions than those for Cu (II), Co (II), Ni (II), and Pb (II). Under all experimental conditions, the uptake capacity of Au (III) by PETA is roughly 40-50 % higher than those of Pd (II) and Pt (IV), which indicates the good selectivity of the prepared adsorbent for Au (III). Moreover, PETA adsorbent is capable of adsorbing precious metal ions effectively under acidic environment with HCl concentration up to 5.0 mol/L.

The good selectivity of Au (III) by PETA in acidic solutions is foreseeable. Under acidic conditions, the surface of the adsorbent is positively charged, whereas precious metal ions exhibited in the form of $AuCl_4^-$, $PdCl_4^{2-}$ and $PtCl_6^{2-}$ (Pettit & Powell, 1999). As such, the electrostatic interaction between the negative charged metal ligands and the positive charged function groups makes PETA selectively adsorb precious metal ions from solutions containing positively charged transition metals (Cu (II), Co (II), Ni (II) and Pb (II)). The strong electron accepting power makes Au (III) the winner in the competition of adsorption sites with Pd (II) and Pt (IV). Moreover, the –C=S and amino groups grafted from thiourea also provide sorption sites for $AuCl_4^-$ by complexation. In addition, Au (III) was also noticed being reduced to metallic gold by hydroxyl groups during the sorption process, following the reaction scheme listed below

$$2Au^{3+} + 3RCH_2OH \rightarrow 2Au(0) + 3RCHO + 6H^+$$

where reduction of Au (III) to Au(0) occurs through oxidation of hydroxyl to aldehyde group. This adsorption-reduction mechanism of Au (III) by PETA has been confirmed by other research studies (Gao et al., 2017; Kuyucak & Volesky, 1989; Mele et al., 2014).

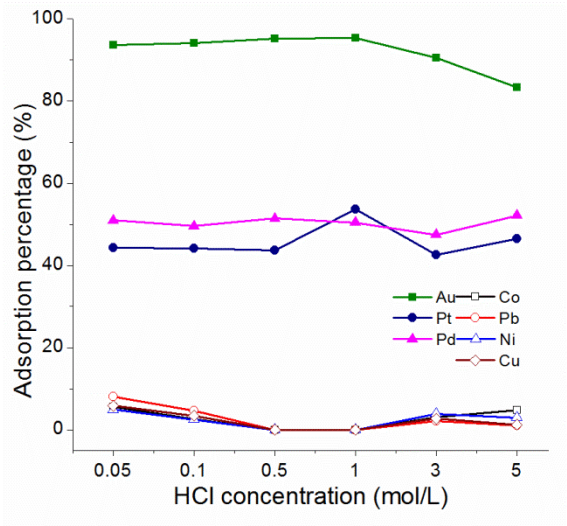

Figure 5.4 Adsorption behavior of PETA towards various metal ions with varying HCl concentrations

The adsorption mechanism of Au (III) by PETA was also studied from the X-ray photoelectron spectroscopy (XPS) analysis of the sorbent before and after gold adsorption. The results were calibrated using C 1s binding energy peak at 284.8 eV. High resolution XPS spectra of O 1s, N 1s and S 2p as well as their deconvoluted fitted curves are demonstrated in Figures 5.5(a)-(f). The oxygen atom in PETA exists in two chemical states, doubly-bonded oxygen (C=O) at 532.8 eV and organic C-O (oxygen in carbon chain and ether groups) at 532.0 eV in XPS spectra of O 1s (Fig. 5.5(a)) (Naumkin et al., 2012). After Au (III) adsorption, these two peaks shift to 533.0 eV and 532.3 eV, indicating oxygen acts as the electron donor when binding $AuCl_4^-$. BE peaks at 401.0 eV and 400.0 eV in Fig. 5.5(c) are corresponding to protonated amino ($–NH_3^+$) and free amino ($-NH_2$) groups (Yong et al., 2016). After Au (III) adsorption, both peaks shift to higher binding energy, but peak shift of $-NH_3^+$ is more significant (0.5 eV to high BE), indicating the positive charged $-NH_3^+$ group is capable of attract $AuCl_4^-$ more effectively by electrostatic interaction. The Au (III) binding by –C=S group is also confirmed from

the high resolution XPS result of S 2p. Peak at 168.7 eV in Fig. 5.5(e) is assigned to the sulfur atoms in $-SO_4^{2-}$ group (contaminated S) (Raj et al., 2010). Peaks at 166.1, 164.3 and 163.3 eV are attributed to the sulfur in –C=S group (Naumkin et al., 2012), which shifted to higher BE position after Au (III) adsorption.

Adsorption of Au (III) by PETA was accompanied by chemical reduction of Au (III) to Au (0). The precipitation of metallic gold from PETA surfaces is proved from the XRD analysis of PETA after Au (III) adsorption. The peaks at 2θ of 38.2^o, 44.4^o, 64.6^o, 77.5^o, 81.7^o, 98.1^o, 110.8^o and 115.3^o in Figure 5.6 can be indexed to the (111), (200), (220), (311), (222), (400), (331), and (420) Bragg's reflections of cubic structure of metallic gold.

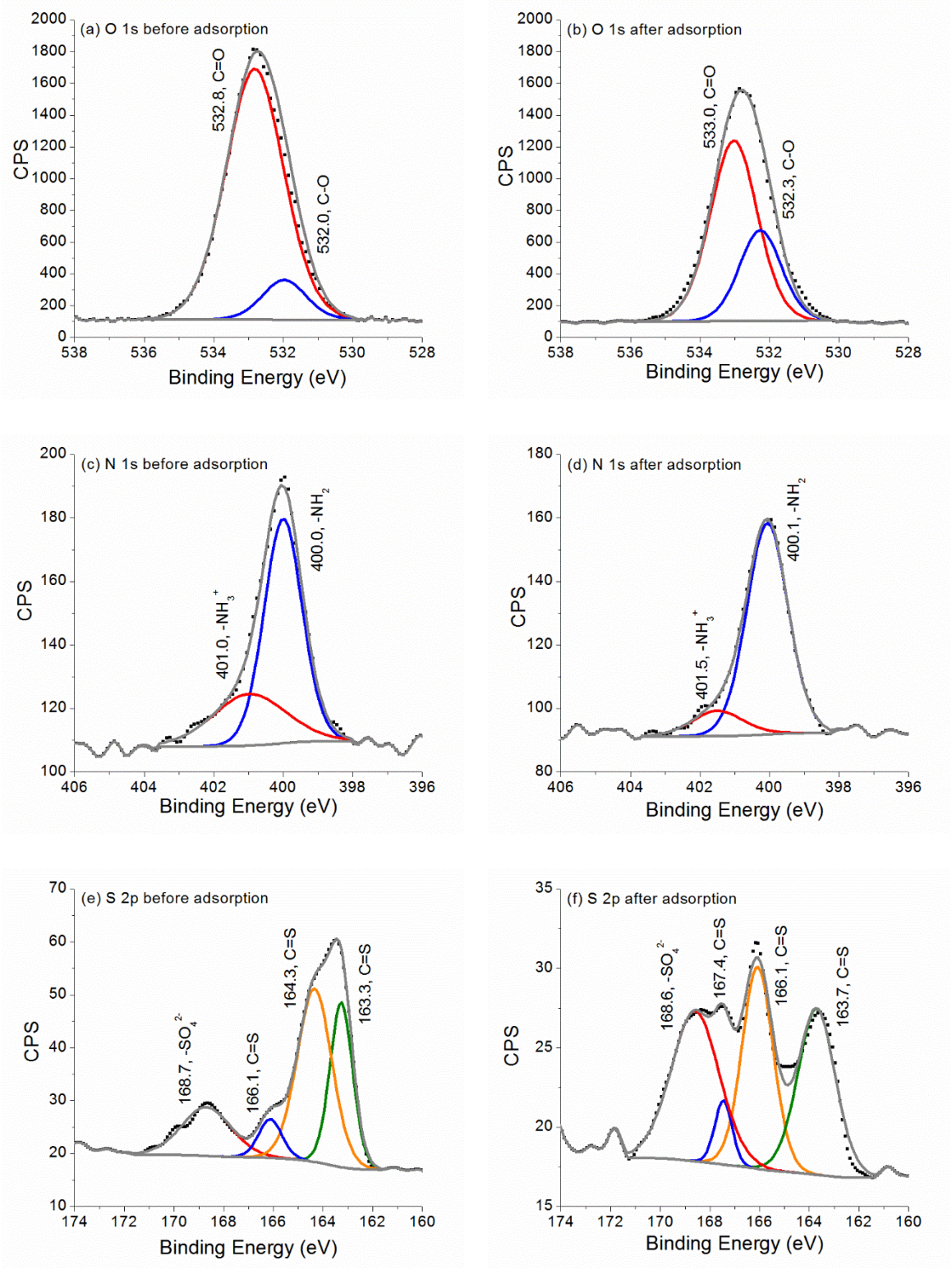

Figure 5.5 XPS high resolution spectrum on (a) O 1s before adsorption; (b) O 1s after adsorption; (c) N 1s before adsorption; (d) N 1s after adsorption; (e) S 2p before adsorption; (f) S 2p after adsorption

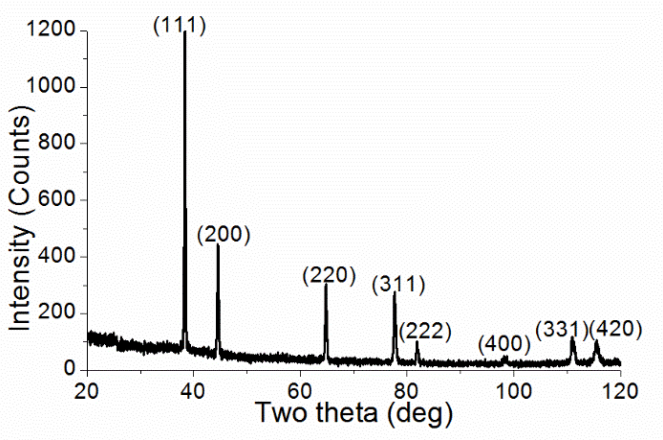

Figure 5.6 The XRD spectrum of PETA after Au(III) adsorption

5.4.4 Temperature effect on the adsorption of Au (III) by PETA

Temperature is an important operating parameter for adsorption process. Effects of temperature and initial concentration of Au (III) ions on the adsorptive–reduction of Au (III) was demonstrated in Figure 5.7. The amount of Au (III) ions adsorbed by PETA increased at higher initial concentration of the metallic solution. The maximum adsorption capacities are found to be 1.97 mmol g^{-1}, 2.07 mmol g^{-1}, and 2.30 mmol g^{-1} at temperatures of 30, 40 and 50 ℃, respectively. An increase of adsorption capacity for Au (III) was observed with the increase of temperature, which indicates the endergonic nature of the adsorptive–reduction of Au (III) to Au (0) by PETA.

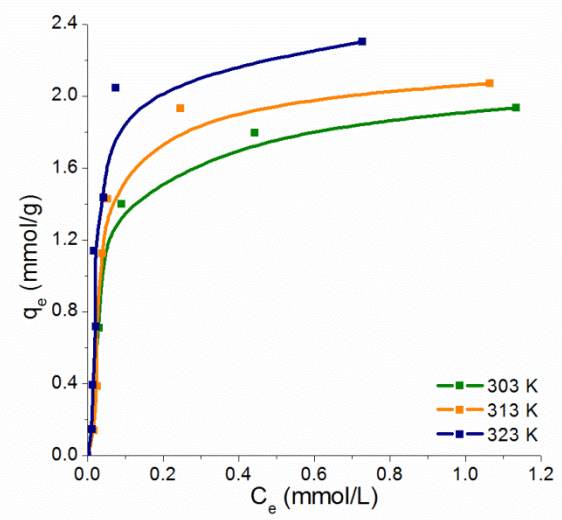

Figure 5.7 Effects of temperature on biosorption of Au (III) by PETA

5.4.5 Adsorption kinetics of Au (III) by PETA

Adsorption kinetics of Au (III) by PETA was illustrated in Fig. 5.8(a). The uptake of Au (III) by PETA increased rapidly with time, i.e., about 80% saturation was reached in 4h using an initial gold concentration of 1 mM, pH of 1.0, and temperature of 30 ℃. Final equilibrium was reached in 9h. Due to the involvement of reduction, with the spontaneous dissociation of metallic gold from the adsorbent, the released sorption sites are capable of re-adsorbing Au (III) ions from solution, leading to a slight increase in the Au (III) uptake after 12h. Fast adsorption kinetics of PETA is attributed to its porous structure. Fig. 5.8(b) compares the adsorption kinetics of Au (III) by NETA and PETA under same conditions. Results from Fig. 5.8(b) demonstrate that it takes 24h to reach 80% saturation for NETA and equilibrium is not reached within 48h. The fast adsorption kinetics of Au (III) by PETA makes this adsorbent suitable to be packed in a fixed–bed column for large-scale metal recovery process.

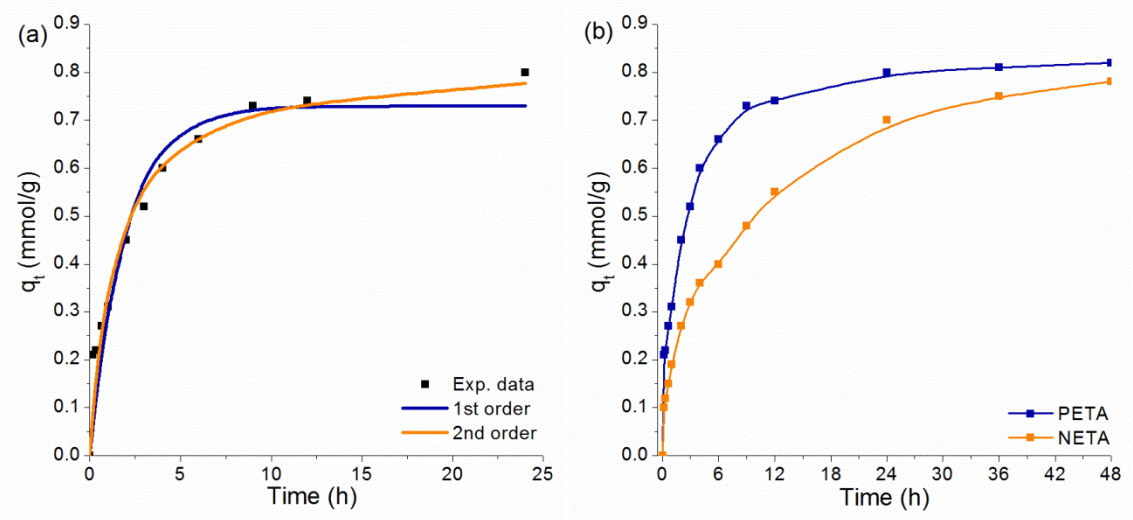

Figure 5.8 Adsorption kinetics (a) of Au (III) by PETA (b) of Au (III) by PETA and NETA

The adsorption kinetics of Au (III) by PETA were analyzed in terms of pseudo-first-order and pseudo-second-order rate equations (Ho, 2006) listed below,

$$\frac{dq_t}{dt} = k_1(q_e - q_t) \qquad \text{Eq. (5.5)}$$

$$\frac{dq_t}{dt} = k_2(q_e - q_t)^2 \qquad \text{Eq. (5.6)}$$

The integral forms of the above rate equations are as follows.

$$q_t = q_e(1-\exp(-k_1 t)) \qquad \text{Eq. (5.7)}$$

$$q_t = \frac{k_2 q_e^2 t}{1 + k_2 q_e t} \qquad \text{Eq. (5.8)}$$

where, q_e and q_t are the amounts (mmol/g) of metal adsorbed at equilibrium and at time t, respectively; k_1 (h^{-1}) and k_2 (g $mmol^{-1}$ h^{-1}) are the rate constants for pseudo-first-order and pseudo-second-order equations.

Least square regression was used to derive the kinetic parameters from experimental measurements and the results are shown in Table 5.1. The measured kinetic data and the model predicted kinetic results are compared and illustrated in Fig. 6(b). It was found that pseudo-second order rate equation provides better explanation on the adsorptive-reduction rate of Au (III) on PETA.

Table 5.1 Kinetic parameters for adsorptive-reduction of Au (III) by PETA

Pseudo-first order			Pseudo-second order		
k_1 (h^{-1})	q_e (mmol/g)	R^2	k_2 (g $mmol^{-1}$ h^{-1})	q_e (mmol/g)	R^2
0.52	0.73	0.94	0.87	0.82	0.99

5.5 Conclusions

A facile method combining surface grafting, templating and cross-linking was used to fabricate porous ECH/thiourea modified alginate (PETA) microbeads as an adsorbent to selective adsorb Au (III) ions from multi-metallic solution. Results indicated that by grafting the ECH/thiourea to biopolymer chains, the uptake capacity is increased by 77.4%. The maximum adsorption capacity of Au (III) by PETA is up to 2.30 mmol g^{-1} at 50 ℃. Analyses of PETA before and after Au (III) adsorption by XPS and XRD revealed that carboxyl, hydroxyl, protonated amino and –C=S groups are the main binding sites for Au (III), among which hydroxyl group is responsible for the bio-reduction of Au (III) to metallic gold.

Due to the introduction of the porous structure, fast adsorption kinetics of Au (III) by PETA was observed. 80% saturation was attained in 4h while equilibrium was reached in about 9h. High uptake capacity, good selectivity and fast adsorption kinetics make PETA attractive to be used as the stationary phase in fixed-bed columns for large-scale process.

Chapter 6 Modelling and Experimental Investigation of the Adsorption Breakthrough Behaviors of Pd (II) and Cu (II) by ETA Microspheres

This chapter is based on and modified from the following paper:

X. Gao, Y. Zhang & Y. Zhao. (2018). Modelling and Experimental Investigation of the Adsorption Breakthrough Behaviors of Pd (II) and Cu (II) by ETA Microspheres.

This manuscript is submitted to Journal of Chemical Technology and Biotechnology and is now under review.

Role: Xiangpeng Gao solely worked on this study and acted as the first author of this manuscript under Dr. Yan Zhang and Dr. Yuming Zhao's guidance. Most contents of this paper was written by Xiangpeng Gao and further edited by the other co-authors.

6.1 Abstract

Background: Chemically modified sodium alginate microspheres prepared by emulsion method were used as stationary phase in a fixed-bed column to selectively adsorb Pd (II) from bi-metallic solutions. The transport-dispersive model with a linear driving force kinetics equation and a pH-dependent competitive Langmuir isotherm was employed to predict the breakthrough curves of the metal ions from the fixed-bed.

Results: Good agreement between the model predictions and the experimental results under different operating conditions confirms the validity and accuracy of the mathematical model and the derived model parameters. Metal ions elute faster from the column with steeper breakthrough curves at higher flow rates and relatively higher feed concentrations. The pH value can significantly affect the competitive adsorption isotherm as well as the breakthrough curves. The fully loaded packed bed can be regenerated completely by dilute thiourea solution.

Conclusion: The microsphere adsorbent synthesized by emulsion method can be successfully applied into a fixed-bed column. The transport-dispersive model is capable of predicting the adsorption performances over a wide range of operating conditions.

6.2 Introduction

Palladium is widely used in industry for the synthesis of catalysts, electronics, and jewelry due to its specific chemical and physical properties (Awual et al., 2013; Won et al., 2014). The ever increasing demand of palladium necessitates the development of cost-effective methods to recover palladium from dilute aqueous effluents or other industrial wastes. Over the past two decades, emphasis has largely been placed on the fabrication of biopolymer based materials and their application in batch sorption process for the recovery of palladium (Pd (II)) and other precious metal ions (Brady, Tobin, & Roux, 1999; Dodson et al., 2015; Guibal, Sweeney, Zikan, Vincent, & Tobin, 2001; Park, Kwak, Won, & Yun, 2013; Won & Yun, 2013). Nonetheless, most of the biopolymer based adsorbents synthesized so far are not suitable to be packed in a fixed-bed column for large-scale processes due to their poor mechanical strength, improper particle size and/or extremely slow internal mass transport (Ahmad & Hameed, 2010; Baral et al., 2009).

Adsorbent used as stationary phase in a fixed-bed column should have uniform particle size, high density of sorption sites, high surface area, and interconnected pore morphology facilitating good internal mass transfer (Gupta, Gupta, Rastogi, Agarwal, & Nayak, 2011; Nguyen et al., 2015). Fabrication of porous biopolymer resins with uniform size distribution for the recovery precious metal ions in general and palladium in specific is thus of great importance. Although various methodologies directed at preparing porous polymer networks, including direct templating, block copolymer self-assembly, and direct synthesis have been developed, each of these methodologies has its strengths and

limitations (Wu et al., 2012). Development of facile and scalable procedures for the construction of porous biopolymer networks is appealing because of the low cost.

To date, very limited amount of work has been done on the recovery of palladium or other precious metals by biopolymer based adsorbents in dynamic systems (Won et al., 2014; Wong, Ngadi, Inuwa, & Hassan, 2018). Wang and co-workers prepared an alginate and polyethyleneimine composite by one-pot synthesis and used the adsorbent in a fixed bed column for Pd (II) recovery (Wang, Vincent, Roux, Faur, & Guibal, 2017). A semi-continuous process was recently developed for the selective adsorption of Pd (II) from polymetallic solutions using an aminophosphine oxide polymer as adsorbent. The influences of pH, the chloride concentration and the co-existing metal ions on the dynamic adsorption of Pd (II) were investigated experimentally (Pat-Espadas, Field, Razo-Flores, Cervantesb, & Sierra-Alvareza, 2016). Selective recovery of Pd (II) from industrial nitric acid extract in a fixed–bed adsorption system packed with cross-linked persimmon tannin was conducted by Yi et al, (Yi, Fan, Xie, Zhang, & Luo, 2016) who confirmed the effectiveness of the prepared sorbent in Pd (II) binding. All these studies demonstrated the efficiency and effectiveness of the biopolymer-based adsorbents in Pd (II) recovery without disclosing the dynamic features of the process. Moreover, the influences of the key operating parameters, such as flow rate, metal ion concentration and solution pH on the dynamic adsorption of metal ions were primarily studied experimentally, which is usually costly and time-consuming. As such, modeling and simulation of the dynamic adsorption of metal ions, an adaptive and predictive

methodology becomes essential (Guiochon & Lin, 2003; Lv, Zhang, Wang, Ray, & Zhao, 2008).

In this study, sodium alginate, the most abundant marine biopolymer consisting of α-(1-4)-guluronic acid and β-(1-4)-mannuronic acid was used as a building block to fabricate biopolymer adsorbent for the dynamic recovery of Pd (II) from bimetallic solutions containing equimolar Pd (II) and Cu (II) ions. The purpose of this work is twofold. Firstly, it attempts to fabricate an algal based adsorbent suitable to be used as stationary phase in fixed-bed columns. Secondly, this work aims to present an effective mechanistic model which incorporates the effects of fluid flow, metal ion concentration and solution pH on the dynamic adsorption of Pd (II) so that the developed mechanistic model is capable of predicting the dynamic sorption performance over wide operating range. Finally, the regeneration of the metal-loaded column has been studied experimentally.

6.3 Materials and Methods

6.3.1 Materials

Sodium alginate (low viscosity), ethanol, hydrochloric acid (35%-38%), calcium carbonate, acetic acid, paraffin oil, Span 85, and metal chloride salts were purchased from Fisher Scientific. Sodium hydroxide pellets were purchased from VWR International. Epichlorohydrin (99%) and thiourea (ACS grade) were purchased from Sigma Aldrich. The deionized water was generated from a Milli-Q water purification system. All compounds were used as received.

6.3.2 Synthesis and characterization of ETA Microspheres

Facile emulsion method (Baimark & Srisuwan, 2014; Chen & Subirade, 2007) was employed in this study to prepare epichlorohydrin/thiourea modified alginate (ETA) microspheres. Modified alginate was firstly obtained by reacting epichlorohydrin/thiourea solution with sodium alginate, followed by the mixing the modified alginate with calcium carbonate, paraffin oil, and Span 85 surfactant to form the emulsion solution. ETA microspheres were produced by reducing pH value of the emulsion with acetic acid, releasing calcium ions from calcium carbonate.

Specifically, thiourea solution was firstly prepared by dissolving 1.71 g thiourea in 30.0 mL of 5% sodium hydroxide solution, then 3.56 mL of epichlorohydrin (ECH) was added to the thiourea solution. The mixture was heated to 70 °C in an incubator, shaking at 150 rpm for 4 h. After that, 4.0 g of sodium alginate powder was added to the ECH/thiourea solution. The resultant mixture was kept at 70 °C and shaking at 150 rpm for 8 hours. The modified alginate solution was mixed with 20.0 mL of 25% (w/v) calcium carbonate solution and stirred at 500 rpm for 15 min until homogenous. 100.0 mL of paraffin oil with 2.0 mL of Span 85 was mixed with the solution under constant stirring at 500 rpm for 20 min. To release the calcium ions in the emulsion, 20.0 mL of paraffin oil with 10.0 mL acetic acid was added and the resulting mixture was stirred at 500 rpm for another 30 min to release the calcium ions. The reaction was stopped by adding 200.0 mL of DI water and the mixture was settled for 24 h. ETA microspheres were separated from the emulsion after washing by ethanol/water solution. The final product was collected after drying at room temperature overnight.

The functional groups of ETA microspheres were characterized by Bruker Tensor II FT-IR spectrometer (Bruker, Germany). The shape and particle size distribution of ETA microspheres were analyzed by FEI MLA 650F scanning electron microscope (ThermoFisher, USA) with mineral liberation analysis software.

6.3.3 Determination of the PZC value of ETA Microspheres

The point of zero charge (PZC) is an important parameter of adsorbent which helps to understand the selective adsorption mechanism of the competing ions under different pH values. PZC usually refers to the pH at which the surface of the adsorbent is neutral. In this study, PZC value of ETA microspheres was determined by pH drift method. To a series of 50 mL conical flasks, 20 mL of 0.1 mol/L KCl was added and the pH was adjusted from 1-7 with 1.0 M HCl or 0.1 M NaOH solutions. 15.0 mg of ETA microspheres were added and the flasks were shaken in an incubator for 24 hours. The suspensions were filtered and the equilibrium pH values were measured. The initial pH values and final pH values were plotted in figure and the intersection is the PZC value.

6.3.4 Batch Adsorption for Adsorption Isotherm

The adsorption isotherm tests were studied at 30 ℃ under pH values of 1.0, 2.0, and 3.0, respectively. The initial concentration varies from 0.2 mmol/L to 1.0 mmol/L for each metal ion. To a series of 50 mL conical flasks, 20 mg for ETA microspheres were mixed with 20 mL metal containing solution and the flasks were kept in an incubator under 200 rpm shaking for 24 hours. After filtration, the filtrates were analyzed by XRF to

determine the residue concentrations of metal ions in the solutions. The capacity of metal ions can be calculated by equation:

$$q = \frac{(C_i - C_e)V}{W} \qquad \text{Eq. (6.1)}$$

where, ci (mmol/L) and ce (mmol/L) are the initial and equilibrium concentrations of metal ions in aqueous solutions, W (mg) and V (mL) are the weight of adsorbent and the volume of the test solution, respectively.

6.3.5 Column Test

The ETA microspheres were sieved and the beads with sizes between 200-300 μm were collected for fixed-bed column adsorption. The experiment was conducted in an Omnifit Benchmark glass column with an internal diameter of 1.0 cm. ETA microspheres were packed in the column for a 2.0 cm bed depth. Blue dextran was injected into the packed bed with a flow rate of 4.0 mL/h to determine the bed voidage, ε_b. The void fraction of the packing bed is 52.74%.

In a typical adsorption experiment, an influent containing equimolar Pd (II) and Cu (II) ions was continuously fed into the column using a Masterflex L/S peristaltic pump. The effluent was collected in sample tubes by a CF-2 fraction collector and the concentrations of metal ions were measured by Rigaku supermini 200 XRF spectrometer. Due to the strong affinity of the precious metal ions with the functional groups of ETA microspheres, complete regeneration of the metal-loaded column requires the use of desorbent with extremely strong eluting power. Dilute thiourea solutions which can form stronger bonds

with these metal ions were employed as desorbent to regenerate the metal-loaded column. The saturated column was regenerated by using 0.5% thiourea or 1.0% thiourea in 0.1 M HCl at the flow rate of 4.0 mL/h. It should be addressed that both batch and the column adsorption studies were performed in duplicate and results agreed to within limits of 4.1%, which confirms the good repeatability of the experiments.

6.3.6 Mathematical Model

6.3.6.1 pH-dependent adsorption isotherm for Pd (II) and Cu (II)

In multi-component adsorption systems, the amount of one compound adsorbed at equilibrium depends on the concentrations of all the compounds present locally. Different competitive isotherm models such as Langmuir, bi-Langmuir, Toth and Langmuir–Freundlich are often explored to account for the equilibrium behaviors of multi-component systems (Jeppu & Clement, 2012; Turiel, Perez-Conde, & Martin-Esteban, 2003; Xiao & Thomas, 2004). These isotherm models are successful in describing the adsorption equilibria of nonelectrolytes (Jeppu & Clement, 2012; Umpleby, Baxter, Chen, Shah, & Shimizu, 2001). As for metal ions, variation in solution pH has a great influence on the adsorption of metal ions. None of the aforementioned isotherm models are capable of predicting pH-dependent adsorption effects in a consistent manner.

To address the pH influence on the adsorption of Pd (II) and Cu (II), modified competitive Langmuir isotherm was developed in this study to simulate the pH-dependent adsorption. In the modified model, competition between protons and metal ions to the

sorption sites is included. The competitive pH-dependent Langmuir isotherm is listed in Eq. (6.2).

$$q_i = \frac{q_m b_i c_{e,i}}{1 + b_{H^+} c_{e,H^+} + \sum_{i=1}^{2} b_i c_{e,i}} \qquad \text{Eq. (6.2)}$$

where q_i (mmol/g) is the metal uptake at equilibrium for component *i* (Pd (II) or Cu (II)), q_m (mmol/g) is the maximum metal uptake capacity of ETA adsorbent, b_i (L/mmol) is the Langmuir isotherm constant for component *i*, b_{H^+} is the Langmuir isotherm constant for protons; $c_{e,i}$ (mmol/L) is the equilibrium concentration for component *i*, c_{e,H^+} is the concentration of protons in the solution.

6.3.6.2 Fixed-bed Model

Transport-dispersive model which decouples the effect of finite mass transfer and axial dispersion has been widely used in modeling of adsorption and liquid chromatography due to the best compromise between accuracy and computational complexity (Xu, Zhu, Xu, Yu, & Ray, 2013; Zhang, Rohani, & Ray, 2008). In transport-dispersive model, mass balance equation is combined with a kinetic equation which relates the rate of variation of concentration in solid phase to solid phase concentration and the equilibrium concentration in solid phase. The column is assumed to be uni-dimensional and isothermal, the differential mass balance of each metal ion *i* and the corresponding linear driving force kinetic model are as follows:

$$\frac{\partial c_i}{\partial t} + \frac{1-\varepsilon_b}{\varepsilon_b}\frac{\partial q_i}{\partial t} + u\frac{\partial c_i}{\partial z} = D_{L,i}\frac{\partial^2 c_i}{\partial z^2} \qquad \text{Eq. (6.3)}$$

$$\frac{\partial q_i}{\partial t} = k_{f,i}(q_i^* - q_i) \qquad \text{Eq. (6.4)}$$

where ε_b is the void fraction of the packed bed, u (cm/min) is the interstitial velocity, D_L (cm^2/min) is axial dispersion coefficient, c_i and q_i represent the concentration of metal ion i in liquid and solid phases, respectively, q_i^* (mmol/g) is the solid phase concentration in equilibrium with the mobile phase concentration as described in the isotherm equation and k_f (cm/min) is the lumped mass transfer coefficient.

The initial condition for the system is:

$$\text{at } t = 0 : c_i = 0, q_i = 0 \qquad \text{Eq. (6.5)}$$

The boundary conditions are:

$$\text{at } z = 0 : D_{L,i} \left.\frac{\partial c_i}{\partial z}\right|_{z=0} = u(c_i - c_{i0}) \qquad \text{Eq. (6.6)}$$

$$\text{at } z = L : \left.\frac{\partial c_i}{\partial z}\right|_{z=L} = 0 \qquad \text{Eq. (6.7)}$$

where $c_{i,0}$ is the feed concentration of Pd (II) and Cu (II) ions. The partial differential equation was solved numerically using the method of lines in which the spatial derivatives were firstly discretized by second order finite difference method. The resulting ODEs were then solved using the stiff ODE solver ode15s in MATLAB R2016b.

6.3.6.3 Tuning Kinetic Parameters

The kinetic parameters, namely k_f and D_L, were determined by minimizing the differences between experimental breakthrough curves and simulation results obtained from solving the column model. An error function $F_{(p)}$, which is defined as the sum of square deviations of the predicted normalized concentrations from the experimental ones, was used as the objective function for the optimization:

$$F_{(p)} = \min \sum_{i=1}^{m} \left[\frac{c_{i,\exp}}{c_0} - \frac{c_{i,\mathrm{mod}}}{c_0} \right]^2 \qquad \text{Eq. (6.8)}$$

where $c_{i,\exp}$ (mmol/L) and $c_{i,\mathrm{mod}}$ (mmol/L) are the experimental value and the model prediction at point i of the breakthrough curve, respectively, c_0 is the equimolar feed concentration of Cu (II) and Pd (II) ions. By minimizing $F_{(p)}$, the optimal values of k_f and D_L was determined by employing a constraint nonlinear optimization solver, *fmincon* from MATLAB R2016b.

6.4 Results and Discussion

6.4.1 Characterization of ETA microspheres

Fig. 6.1 compares the IR spectra of sodium alginate and ETA microspheres. For sodium alginate powder, band peak at 3000-3600 cm^{-1} is corresponding to O-H stretching, 2940 cm^{-1} due to aliphatic C-H stretching vibrations (Sobkowiak, Reisser, Given, & Painter, 1984), 1593 cm^{-1} and 1408 cm^{-1} affiliated with asymmetric and symmetric stretching

vibrations of carboxylate (COO-) group (Xiao & Thomas, 2004), 1085 cm^{-1}, 1030 cm^{-1}, and 1011 cm^{-1} owing to C-O stretching of COO- and C-O-H groups. The chemical modification of sodium alginate is confirmed from IR spectrum of ETA microspheres. Band shifts at 1601 cm^{-1} and 1413 cm^{-1} are attributed to the change of carboxylate salt to carboxylic acid (Gao, Zhang, & Zhao, 2017) whereas 1556 cm^{-1} and 1010-1085 cm^{-1} are associated with the grafting of N-C=S functional group (Gavilan et al., 2009; Rao & Venkataraghavan, 1962). Peak at 872 cm^{-1} is assigned to the calcium carbonate residue (Legodi, de Waal, Potgieter, Potgieter, 2001).

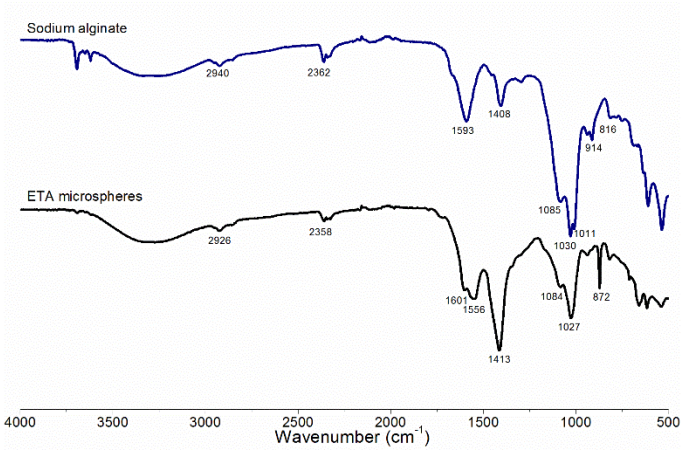

Figure 6.1 IR spectra of sodium alginate powder and ERA microspheres

The SEM image of ETA microspheres was illustrated in Fig. 6.2(a), from which uniform and spherical particles were observed. The spherical shape of the prepared adsorbent is highly desirable to be used as the stationary phase in a fixed bed column for a uniform distribution of void volume. The particle sizes observed from SEM image are consistent with those illustrated in Fig. 6.2(b) from mineral liberation analysis (MLA), rendering the mean particle size of 280-285 μm.

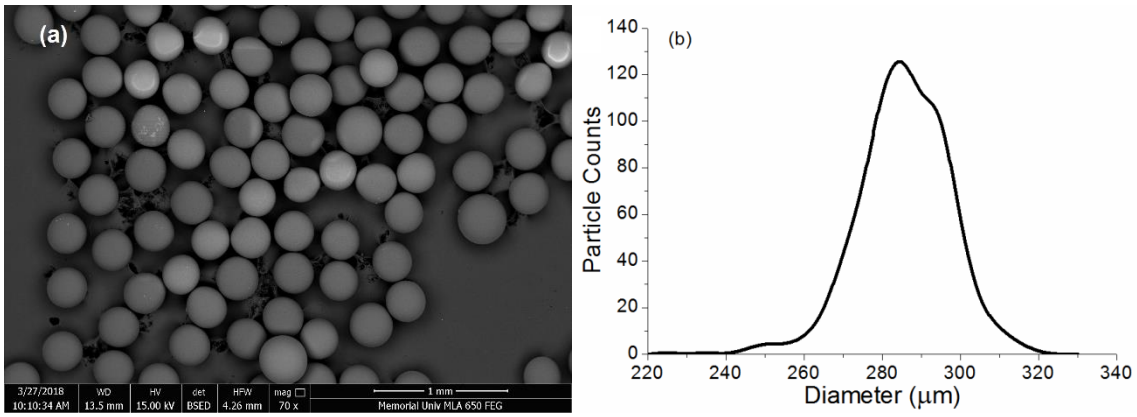

Figure 6.2 (a) SEM images of ETA microspheres (b) Size distribution of ETA microspheres

6.4.2 PZC value for ETA

Figure 6.3 shows the PZC value of ETA microspheres. When the solution pH is lower than the PZC value, the adsorbent surface is positively charged, attracting anions in the liquid phase. The Pd (II) ions are complexed with chloride ions and are negatively charged under low pH values whereas Cu (II) exists in the form of Cu^{2+}. Under this scenario, the $PdCl_4^{2-}$ ions were adsorbed by ETA microspheres via electrostatic interactions. Conversely, the ETA surface is negatively charged when the solution pH is higher than PZC. At pH 3.0, the chelation of Pd (II) and Cu (II) ions with functional groups becomes the dominated sorption mechanism and both Pd (II) and Cu (II) ions were adsorbed significantly, leading to the decrease of selectivity to Pd (II) at higher solution pH.

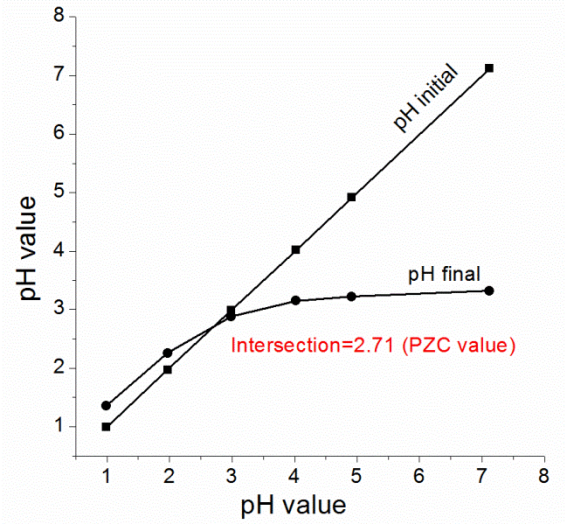

Figure 6.3 The point of zero charge value for ETA microspheres

6.4.3 Isotherm Parameters

Batch adsorption results of Pd (II) at pH values of 1.0, 2.0 and 3.0 and Cu (II) at pH 3.0 were used to determine the parameters of the competitive pH-dependent Langmuir model. Table 6.1 lists the best fitting isotherm parameters. Experimental results illustrated in Figs. 6.4(a) and 6.4(b) confirm that ETA microspheres have good selectivity to Pd (II), particularly at lower solution pH. The equilibrium uptake capacities of Pd (II) and Cu (II) both increase with the increase of metal concentrations. As seen from Fig. 6.4(a), the competitive pH-dependent Langmuir isotherm model provides accurate sorption equilibria of Pd (II) and Cu (II) well in agreement with the measured data under all pH conditions.

Table 6.1 Parameters of competitive Langmuir isotherm for Pd (II) on ETA microspheres

b_{Pd} (L/mmol)	b_{Cu} (L/mmol)	b_{H^+} (L/mmol)	$q_{\max}$ (mmol/g)
1.87	1.37	0.05	0.60

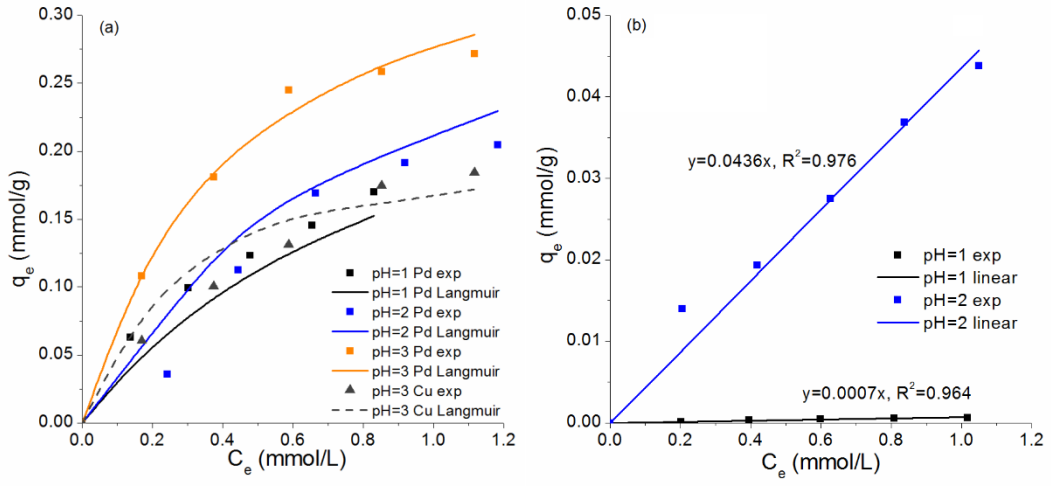

Figure 6.4 (a) Adsorption of Pd (II) and Cu (II) at different pH values; and (b) adsorption of Cu (II) at lower pH values

The uptake of Cu (II) by ETA microspheres at pH of 1.0 and 2.0 was very limited and not significantly affected by Pd (II) concentration. Therefore, the competitive Langmuir isotherm is not applicable for the adsorption equilibrium of Cu (II) at lower pH. Single component linear isotherm model is able to describe the adsorption equilibria of Cu (II) very accurately as illustrated in Fig. 4(b). The distribution coefficient under pH of 1.0 and 2.0 are 7.0×10^{-4} and 4.36×10^{-2}, respectively. Therefore, both isotherm models were used in simulating the breakthrough curves of Cu (II) at different values of solution pH.

6.4.4 Kinetic Parameters

Experimental breakthrough curves of Pd (II) and Cu (II) at c_0 of 0.2 mmol/L, solution pH of 1.0, and flow rates of 2.0 mL/h and 4.0 mL/h were used to determine k_f and D_L values by least square fitting. The best fitting values of k_f and D_L are summarized in Table 6. 2. Figure 6.5 compares the experimental and calculation results based on the optimum

kinetic parameters. It can be seen that the experimental breakthrough curves are well described by the mathematical model.

The overall mass transfer coefficient, k_f is dependent on both external mass transfer in bulk fluid and internal mass transfer in the solid phase (Guiochon et al., 2006). Most often, the internal mass transfer resistance within the solid particles dominates the process. As such, k_f value does not vary significantly with the operating conditions, such as, flow rate, feed concentration etc. In this study, the best-fitting values of k_f are almost the same for Cu (II) and Pd (II) ions.

The axial dispersion coefficient, D_L , generally includes mechanical dispersion and molecular dispersion, is directly proportional to the interstitial velocity in packed beds (Guiochon et al., 2006; Yu, Jackson, & Harmon, 1999). Empirical correlations are available to estimate the D_L values from molecular diffusivity and velocity (Izquierdo et al., 2010; Lv et al., 2008; Sulaymon et al., 2009). Based on the optimized results, the D_L values for Pd (II) and Cu (II) ions in the fixed-bed can be calculated by the following correlation equations:

$$D_{L,Pd} = 6.11 D_{m,Pd} + 3.00 u d_p \qquad \text{Eq. (6.9)}$$

$$D_{L,Cu} = 5.43 D_{m,Cu} + 7.99 u d_p \qquad \text{Eq. (6.10)}$$

where D_m (cm^2/min) is the molecular diffusion, u (cm/min) is the interstitial velocity, and d_p (cm) is the diameter of the adsorbent.

Table 6.2 Optimized kinetic parameters at different flow rates

	2.0 mL/h		4.0 mL/h	
	k_f (cm/min)	D_L (cm^2/min)	k_f (cm/min)	D_L (cm^2/min)
Pd (II)	1.10×10^{-1}	1.40×10^{-2}	1.10×10^{-1}	2.00×10^{-2}
Cu (II)	1.09×10^{-1}	3.92×10^{-2}	1.09×10^{-1}	5.51×10^{-2}

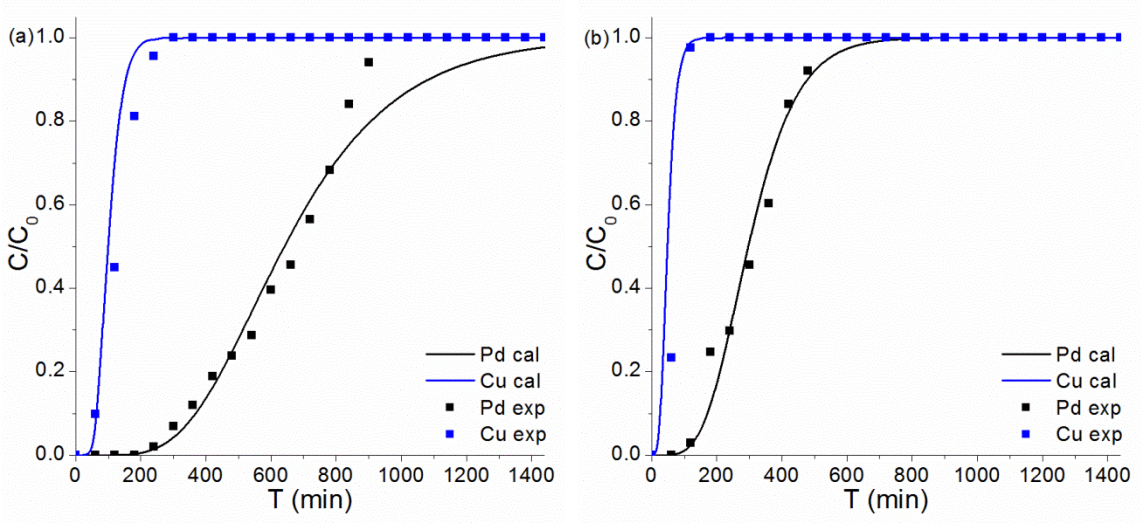

Figure 6.5 Calculated and experimental breakthrough curves at flow rates of (a) 2.0 mL/h and (b) 4.0 mL/h (Feed metal concentration of 0.2 mmol/L and solution pH of 1.0)

6.4.5 Experimental Verification of Mathematical Models

The validity of the mathematical model as well as the derived kinetic parameters was examined by comparing the simulation results and the experimental measurement at different operating conditions. Good agreements between model predictions and experimental results observed under different flow rates, feed concentrations, and solution pH, confirm the validity of the transport-dispersive model in the breakthrough adsorption.

6.4.5.1 Breakthrough Curves at Different Flow Rates

Experimental breakthrough curves at flow rates of 3.0 and 5.0 mL/h were employed to validate the simulation results using the column model and the derived isotherm and

kinetic parameters. As D_L value varies with flow rate, D_L values for Pd (II) and Cu (II) at flow rate of 3.0 mL/h used in simulation are 1.70×10^{-2} and 4.72×10^{-2} cm^2/min, respectively. At flow rate of 5.0, D_L values for Pd (II) and Cu (II) used in simulation are 2.30×10^{-2} and 6.31×10^{-2} cm^2/min, respectively. Figure 6.6 shows the simulated breakthrough curves of Pd (II) and Cu (II) at flow rates of 3.0 mL/h and 5.0 mL/h, which are in good agreement of the experimental results. This indicates that the mathematical model as well as the isotherm and kinetic parameters are accurate and valid.

The effect of flow rate on the breakthrough curves of Pd (II) and Cu (II) can be clearly seen from Fig. 6.6. At higher flow rate, both ions elute faster from the column, leading to an earlier breakthrough time (t_b) and exhaustion time (t_e). This is reasonable as the packed bed is volume-overloaded at higher flow rate and thus the time needed to reach saturation decreases. In addition, higher flow rate helps to narrow the mass transfer zone (MTZ) due to the increased migration velocity of the concentration fronts (Ruthven, 1984). As Pd (II) has stronger affinity with the solid phase than Cu (II), the reduction in MTZ is more remarkable for Pd (II), leading to much steeper breakthrough curve of Pd (II) at higher flow rate.

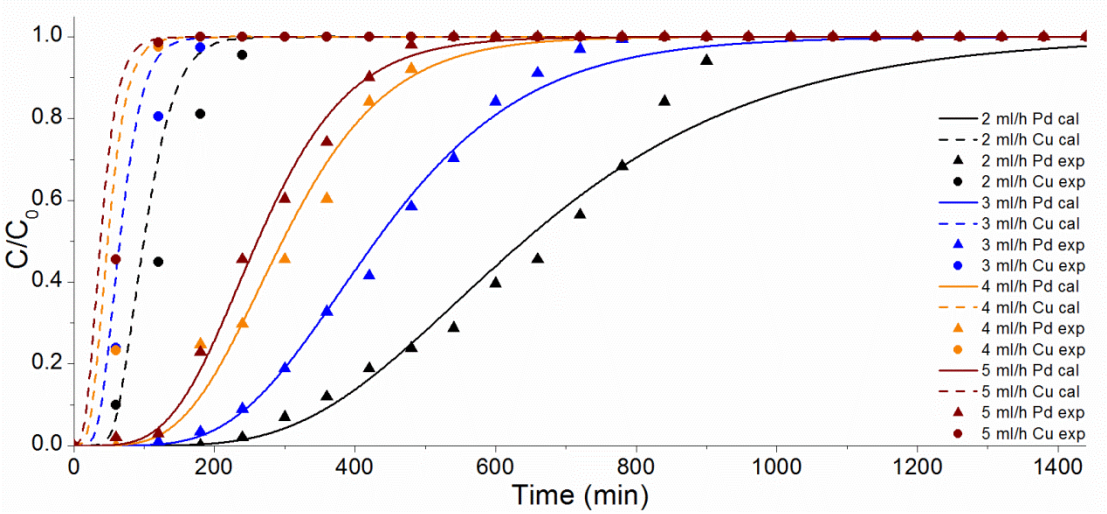

Figure 6.6 Influence of flow rate on the breakthrough curves of Cu (II) and Pd (II)
(Feed metal concentration of 0.2 mmol/L and solution pH of 1.0)

6.4.5.2 Breakthrough Curves at Different Feed Concentrations

Validation of the mathematical model was also conducted by comparing the model predicted and experimental breakthrough curves at various feed concentrations of metal ions. Likewise, the predicted breakthrough curves are completely consistent with the experimental ones (Figure 6.7), confirming the validity of the mathematical model.

Feed concentrations of metal ions have a significant influence on the breakthrough curves. It is observed from Fig. 6.7 that the breakthrough time for both ions does not vary significantly at different feed concentrations, but the exhaustion time decreases at increased feed concentration. For high initial metal ion concentration, steeper breakthrough curves are found because the equilibrium is attained faster, which would be anticipated due to the increase in the driving force of mass transfer.

In this study, lower feed concentrations (0.1, 0.2 and 0.4 mmol/L) were used in the experiments, leading to the three different equilibrium uptake amounts for each ion in the

solid phase (Refer to Fig. 6.4). Results illustrated in Fig. 6.7 reveal that complete separation of Cu (II) and Pd (II) can be achieved at higher feed concentration, with increased metal ion loading in the packed bed.

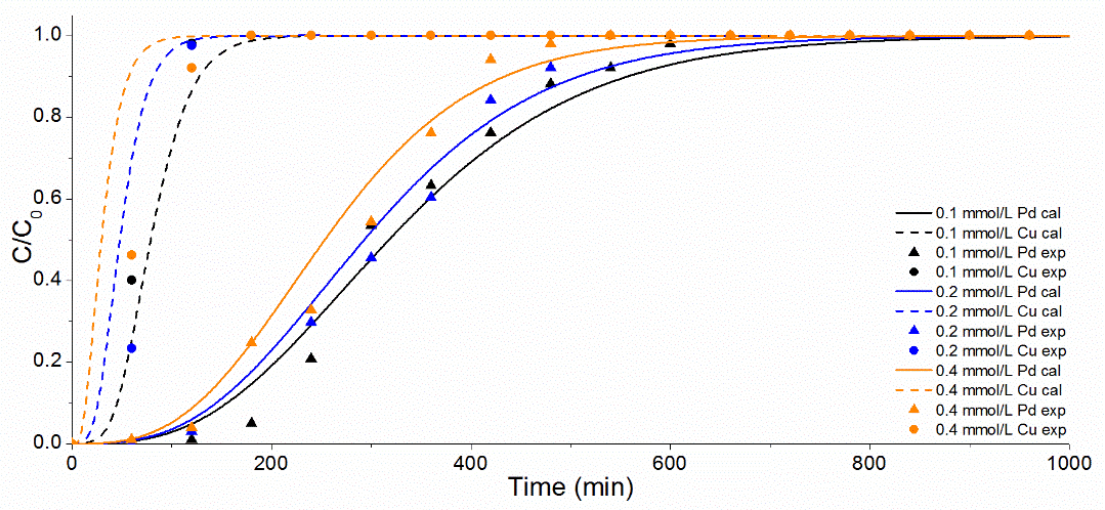

Figure 6.7 Influence of the feed metal concentration on breakthrough curves of Cu (II) and Pd (II) (Flow rate of 4.0 mL/h and solution pH of 1.0)

6.4.5.3 Breakthrough Curves at Different pH Values

The use of pH-dependent competitive Langmuir isotherm facilitates the simulation of the breakthrough curves at different pH values by using the fixed-bed model. Extremely good agreement between the model predicted and experimental breakthrough curves of Pd (II) and Cu as shown in Fig. 6.8 proves the accuracy and reliability of the column model and the derived isotherm and kinetic parameters.

We know from Fig. 6.4 that the uptake capacity of Pd (II) and Cu (II) by ETA microspheres both increase with the increase of pH. The increased uptake capacity at higher pH results in the delay of breakthrough time for both metal ions. Moreover,

breakthrough curves become more spread at higher pH due to the reduced compressing effect from protons.

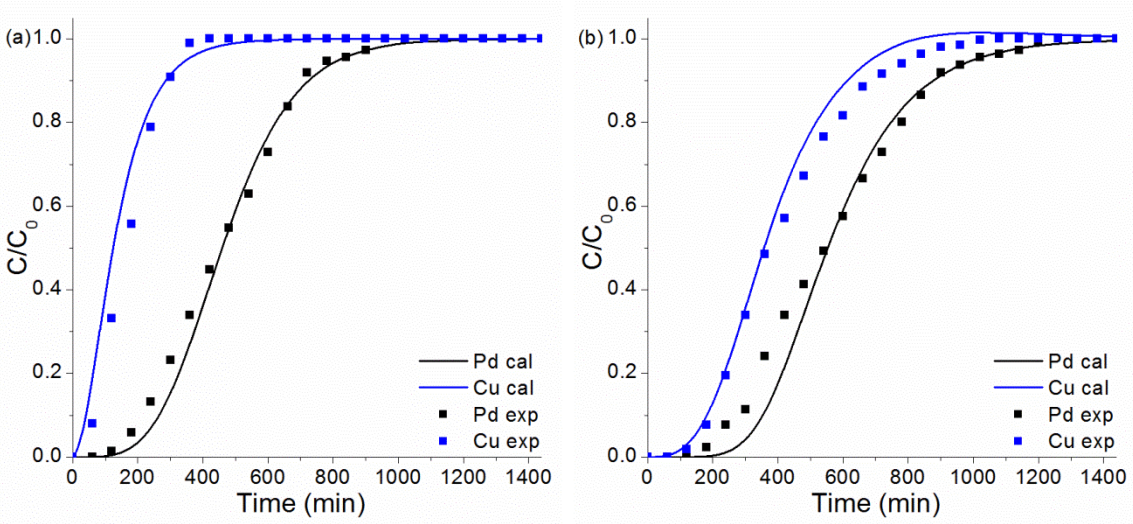

Figure 6.8 Breakthrough curves of Cu(II) and Pd (II) at solution pH of (a) 2.0 and (b) 3.0 (Feed metal concentration of 0.2 mmol/L and flow rate of 4.0 mL/h)

6.4.6 Regeneration of the ETA Bed

Regeneration of the fully loaded ETA bed was carried out to assess the reusability of the synthetic adsorbent. Figure 6.9 demonstrates the experimental desorption curves of Pd (II) and Cu (II) obtained by using two eluents with different thiourea concentrations. As seen from Fig. 6.9 the eluent with higher thiourea concentration is found to be more efficient in desorbing Pd (II) ions, whereas desorption of Cu (II) took the same time for both eluents. These results are foreseeable. The stronger affinity between Pd (II) and ETA microspheres required the use of eluent with strong elution power. Thiourea is known to have very strong chelating power with metal ions, eluent with relatively higher thiourea concentration is able to complete desorb Pd (II) ions from ETA microspheres. However Cu (II) ions have rather week affinity with the solid phase and Cu (II) ions can be readily

desorbed by liquid eluent. Results from Fig. 6.9 reveal that the packed bed of ETA microspheres can be regenerated completely and reused.

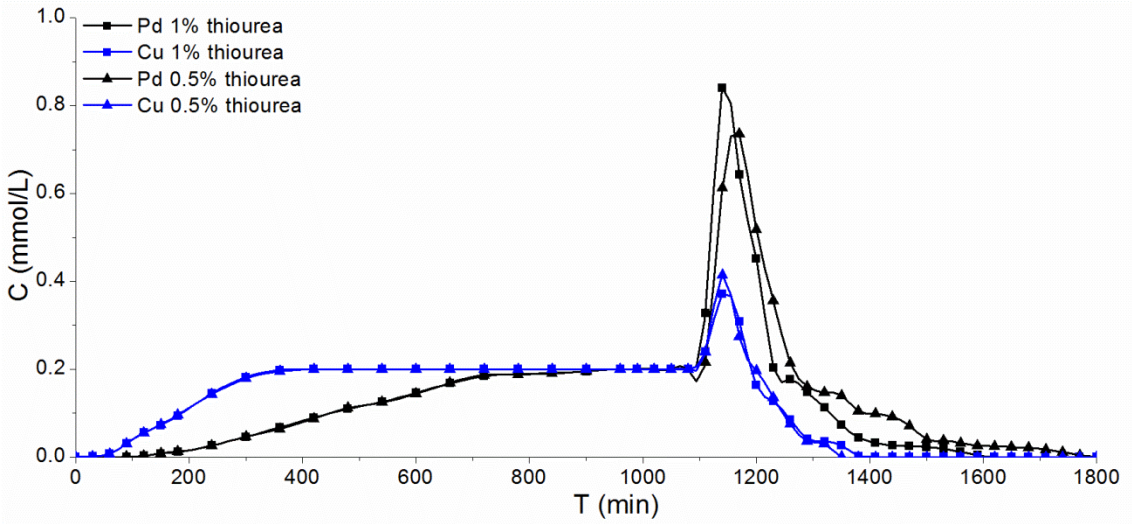

Figure 6.9 Regeneration of the metal-loaded packing bed by dilute thiourea solutions
(Feed metal concentration of 0.2 mmol/L; flow rate of 4.0 mL/h and solution pH of 1.0)

6.5 Conclusions

A transport-dispersive model was applied to describe the breakthrough curves of Pd (II) and Cu (II) ions from a fixed bed column packed with epichlorohydrin/thiourea modified alginate (ETA) microspheres prepared by emulsion method. Due to the great influence of solution pH on the adsorption behavior of metal ions, a pH-dependent competitive Langmuir isotherm was developed and incorporated into the mathematical model to predict the breakthrough curves of Pd (II) and Cu (II) under different pH values. Good agreements between model predictions and experimental results observed under different flow rates, feed concentrations, and solution pH validate the accuracy and reliability of the mathematical model and model parameters.

Experimental results reveal that metal ions elute faster from the column with steeper breakthrough curves at higher flow rate. Relatively higher feed concentration of metal ions is preferable due to the complete separation of metal ions achievable at increased metal ion loading. The effect of pH value on the dynamic adsorption of Pd (II) and Cu (II) was investigated as well. The increased uptake capacity of metal ions at higher pH results in the delay of breakthrough time and more spread breakthrough curves for both metal ions. Finally, the fully loaded ETA bed can be completely regenerated using dilute thiourea solution.

Chapter 7 Conclusion and Recommendations

7.1 Conclusions

In this study, five adsorbents were prepared from natural polysaccharides and used to selectively adsorb precious metal ions from multi-metallic solutions through either batch or dynamic fixed-bed adsorption. Powder adsorbents were prepared from both cellulose (ECH-AG-Cellulose and Sulf-AG-Cellulose) and alginate (ETSA). Sulf-AG-Cellulose and ETSA have shown great selectivity for precious metals as well as extreme high capacities for Au (III) due to an adsorption-reduction mechanism. Metallic gold was observed in the adsorption process for both adsorbents and ETSA was capable of reducing gold to gold nanoparticles. Both Sulf-AG-Cellulose and ETSA are highly efficient in adsorption kinetics, as the equilibrium can be achieved within a few hours. Several characterization methods have been applied on all three adsorbent which indicates the success modification on the cellulose or alginate backbone. XRD and XPS analyses for the sorbents before and after adsorption reveal that hydroxyl, carboxyl, pronated amino, and C=S groups are the main binding sites of Au (III) whereas the hydroxyl group is responsible for the reduction of Au (III). Gold flakes were observed for Sulf-AG-cellulose adsorbent while gold nanoparticles (AuNPs) and microcrystals were formed by ETSA adsorbent. The reduction behaviour contributes to the superior high capacity of these two adsorbents toward Au (III) ions.

To improve the physical and mechanical properties of the adsorbent, porous epichlorohydrin/thiourea modified alginate (PETA) beads were prepared using zinc oxide

as the colloidal template. The zinc oxide was finally removed by hydrochloric acid to generate porous structure which can be clearly observed from SEM images. Several synthesis conditions were optimized and the PETA adsorbent is highly efficient in selectively adsorbing Au (III) from mixed metal solution, as well as adsorption kinetics compared to nonporous adsorbent. The mechanism for Au (III) adsorption is similar as previous synthesized adsorbents.

It is found that the natural bioreduction on Au (III) makes it improper for fixed-bed column adsorption tests; therefore Pd (II) is selected as the precious metal for column study. Epichlorohydrin/thiourea modified alginate (ETA) microspheres were prepared to be applied in a laboratory fixed-bed column by facile emulsion method. A pH dependent competitive Langmuir isotherm was developed and applied in the mathematical model. A transport-dispersive model was used to simulate the breakthrough curves and experimental data were used to validate the model parameters. The mathematical model is proved to be accurate by validation results, which certifies the model can provide practical information for industrial utilization in wastewater treatment. Effects of flow rates, feed concentrations, and pH values were discussed and the results indicate that lower flow rate and lower feed concentration can extend the breakthrough and exhaust point, therefore improve the separation efficiency. The pH values of feed solution have a significant impact on the adsorption isotherm, resulting in different adsorption mechanisms and selectivity. The ETA microspheres in the fixed-bed can be regenerated by dilute thiourea solution, making the process cost-effective and easy to operate.

This research work is an important attempt to synthesis polysaccharide-based adsorbents with enhanced adsorption capacity and selectivity for precious metals, and to study the dynamic adsorption process. The selective adsorption mechanism is clearly explained with characterization analysis results, which is beneficial for further studies. ETA microspheres were successfully applied in a laboratory column, and the dynamic adsorption performance can be simulated by mathematical model.

7.2 Research Contributions

This research can be summarized and highlighted by the following contributions:

(1) Two adsorbents synthesized from cellulose (ECH-AG-cellulose and Sulf-AG-cellulose), were developed for precious metal recovery from wastewater. The adsorbents have shown outstanding selectivity for precious metals as well as high adsorption capacity. The adsorption-reduction mechanism for Au (III) was proposed based on characterization results.

(2) An experimental study was carried out to investigate the selective adsorption performance of an alginate-based adsorbent (ETSA). Gold nanoparticles were observed from the biosorption-bioreduction process. This study clearly explained the selective adsorption mechanism and gold reduction mechanism based on the FT-IR and XPS results.

(3) A porous bead adsorbent (PETA) from alginate was synthesized by direct templating method. Zinc oxide was applied as a cost-effective colloid template because it does not react with sodium alginate and can be easily removed by hydrochloric acid. The

adsorbent has good adsorption performance as well as physical structure for faster sorption kinetics. This study provides a simple and effective method to synthesize porous adsorbent from polysaccharide.

(4) To study the fixed-bed column adsorption, an adsorbent from alginate (ETA microspheres) was prepared by emulsion method. The adsorbent has relative small and uniform size (200-300 μm), which was successfully applied in a fixed-bed column to study the dynamic adsorption behaviour. A pH dependent competitive Langmuir isotherm was developed and applied in the mathematical model. A transport-dispersive model was used to predict the breakthrough curve under different flow rates, initial concentrations, and pH values. The simulated results have shown good agreement with the experimental data. Therefore, the mathematical model can be used to estimate the dynamic adsorption performance. The ETA microspheres can separate Pd (II) and Cu (II) ions from bimetallic solution in dynamic adsorption process, which provides a potential solution for large-scale precious metal containing wastewater treatment.

7.3 Publications

X. Gao, Y. Zhang, & Y. Zhao. (2018). Modelling and Experimental Investigation of the Adsorption Breakthrough Behaviors of Pd (II) and Cu (II) by ETA Microspheres. To be submitted.

X. Gao, Y. Zhang, & Y. Zhao. (2018). Selective adsorption of Hg (II) from polymetallic solutions by porous alginate gel beads. To be submitted.

X. Gao, Y. Zhang, & Y. Zhao. (2018). Biosorption of Au (III) by modified zinc oxide templated porous alginate beads. To be submitted.

X. Gao, Y. Zhang, & Y. Zhao. (2017). Selective adsorption of Hg (II) by porous chemically modified alginate beads. Persistent and Emerging Organic Pollution in Cold and Coastal Environments, October, St.John's, Canada.

X. Gao, Y. Zhang, & Y. Zhao. (2017). Biosorption and reduction of Au (III) to gold nanoparticles by thiourea modified alginate. Carbohydrate Polymers, 159, 108-115.

X. Gao, Y. Zhang, & Y. Zhao. (2016). Selective Adsorption of Au^{3+} by Epichlorohydrin/Thiourea modified porous alginate beads. AICHE annual meeting, November, San Francisco, USA.

M. Gurung, B.B. Adhikari, **X. Gao**, S. Alam, & K. Inoue. (2014). Sustainability in the Metallurgical Industry: Chemically Modified Cellulose for Selective Biosorption of Gold from Mixtures of Base Metals in Chloride Media. Industrial & Engineering Chemistry Research, 53(20), 8565−8576.

M. Hossain, **X. Gao**, & S. Alam. (2014). Application of Biomaterials in the Mining Industry. Proceedings of the 26th Canadian Materials Science Conference (CMSC 2014), June 1 – 4, Saskatoon, Canada.

M. Gurung, B.B. Adhikari, **X. Gao**, S. Alam, & K. Inoue. (2013). Meeting the Challenges of Sustainability: Utilization of Chemically Modified Pure Cellulose for Quantitative

Separation of Gold from Mixtures of Base Metals in Acidic Solution. Proceedings of ALTA 2013 Conference, Gold Sessions, 203-213, May 30 – 31, Perth, Australia.

7.4 Recommendations

Based on the current research, some improvements in terms of experiments and general understanding of adsorption are summarized below:

a) Due to the bioreduction behavior of synthesized adsorbents on Au (III), adsorbents for Au (III) cannot be completely regenerated. Therefore the application of adsorbents for gold recovery is limited. Auger electron spectroscopy analysis could be conducted to detect if adsorption has or has not occurred. Adding proper surfactant or stabilizer in the adsorption process to synthesis AuNPs within specific particle size would be of great interest.

b) The selectivity of precious metals generally took place at acidic condition, which is close to the industrial leaching process. However, the separation of precious metals in higher pH values is difficult as the selectivity decreases and some metal ions are not stable in higher pH values. Future study can focus on the recovery of precious metals in a higher pH condition, which could be applied in wastewater treatment plant, and reduces the corrosion of industrial equipment.

c) Pore formation for polymer-based adsorbent could be improved. Generating uniform pore size with ordered structure for natural polysaccharide polymers remains a difficult problem. The physical and chemical properties of polysaccharides limit the template and synthesis method for porous adsorbents. The pore size and surface area of

polysaccharides-based adsorbent cannot be detected by BET because the relative low temperature endurance for these materials. It is recommended to find a cost-effective template or synthesis method to improve the structure of the adsorbent.

d) The mathematical model for fixed-bed adsorption simplified the adsorption kinetics and isotherm. Some factors including pore diffusion and the internal mass transfer rate were simplified or neglected. Developing of new models for a precise estimation or calculation is therefore possible. Increasing experimental data points could also lead to a more precise estimation of the isotherm and kinetic parameters.

e) Surface free energies can be discussed in future study in terms of how the differences in surface free energies of adsorbents and metals can having an effect on the interfacial free energy of metal-adsorbent combinations and the relative cohesion of various metals to adsorbents.

Bibliography and References

Abdolali, A., Guo, W. S., Ngo, H. H., Chen, S. S., Nguyen, N. C., & Tung, K. L. (2014). Typical lignocellulosic wastes and by-products for biosorption process in water and wastewater treatment: A critical review. Bioresource Technology, 160, 57-66.

Aderhold, D., Williams, C. J., & Edyvean, R. G. J. (1996). The removal of heavy-metal ions by seaweeds and their derivatives. Bioresource Technology, 58 (1), 1–6.

Adhikari, C. R., Parajuli, D., Kawakita, H., Chand, R., Inoue, K. & Ohto, K. (2007). Recovery and separation of precious metals using waste paper. Chemistry Letters, 36, 1254-1255.

Adhikari, C. R., Parajuli, D., Inoue, K., Ohto, K., Kawakita, H. & Harada, H. (2008). Dimethylamine-modified waste paper for the recovery of precious metals. Environmetal Science Technology, 42, 5486−5491.

Adhikari, C. R., Parajuli, D., Inoue, K., Ohto, K., Kawakita, H., & Harada, H. (2008). Recovery of precious metals by using chemically modified waste paper. New Journal of Chemistry, 32, 1634-1641.

Ahmad, A. A., & Hameed, B. H. (2010). Fixed-bed adsorption of reactive azo dye onto granular activated carbon prepared from waste. Journal of Hazardous Materials, 175, 298-303.

Ahmaruzzaman, M. (2008). Adsorption of phenolic compounds on low-cost adsorbents: A review. Advances in Colloid and Interface Science, 143, 48-67.

Ahmed, M. M., El-Rasoul, S. A., Auda, S. H., & Ibrahim, M. A. (2013). Emulsification/internal gelation as a method for preparation of diclofenac sodium-sodium alginate microparticles. Saudi Pharmaceutical Journal, 21, 61-69.

Akar, T., & Tunali, S. (2006). Biosorption characteristics of Aspergillus flavus biomass for removal of Pb(II) and Cu(II) ions from an aqueous solution. Bioresource Technology, 97, 1780–1787.

Al-Muhtaseb, S. A., & Ritter, J. A. (2003). Preparation and properties of resorcinol-formaldehyde organic and carbon gels. Advanced Materials, 15, 101-114.

Auta, M., & Hameed, B. H. (2014). Chitosan-clay composite as highly effective and low-cost adsorbent for batch and fixed-bed adsorption of methylene blue. Chemical Engineering Journal, 237, 352-361.

Awual, M. R., Yaita, T., El-Safty, S. A., Shiwaku, H., Okamoto, Y., & Suzuki, S. (2013). Investigation of palladium(II) detection and recovery using ligand modified conjugate adsorbent. Chemical Engineering Journal, 222, 172-179.

Bailey, S. E., Olin, T. J., Bricka, R. M., & Adrian, D. D. (1999). A review of potentially low-cost sorbents for heavy metals. Water Research, 33, 2469-2479.

Baimark, Y., & Srisuwan, Y. (2014). Preparation of alginate microspheres by water-in-oil emulsion method for drug delivery: Effect of Ca^{2+} post-cross-linking. Advanced Powder Technology, 25, 1541-1546.

Bak, H., Thomas, O. R., & Abildskov, J. (2007). Lumped parameter model for prediction of initial breakthrough profiles for the chromatographic capture of antibodies from a complex feedstock. Journal of chromatography B, 848(1), 131-141.

Baral, S. S., Das, N., Ramulu, T. S., Sahoo, S. K., Das, S. N., & Chaudhury, G. R. (2009). Removal of Cr (VI) by thermally activated weed Salvinia cucullata in a fixed-bed column. Journal of Hazardous Materials, 161, 1427-1435.

Bencherif, S. A., Braschler, T. M., & Renaud, P. (2013). Advances in the design of macroporous polymer scaffolds for potential applications in the dentistry. Journal of Periodontal & Implant Science, 43, 251-261.

Benguella, B., & Benaissa, H. (2002). Cadmium removal from aqueous solutions by chitin: kinetic and equilibrium studies. Water Research, 36, 2463-2474.

Bertagnolli, C., Uhart, A., Dupin, J. C., Sliva, M., Guibal, E., & Desbrieres, J. (2014). Biosorption of chromium by alginate extraction products from Sargassum filipendula: Investigation of adsorption mechanisms using X-ray photoelectron spectroscopy analysis. Bioresource Technology, 164, 264-269.

Bhatnagar, A., Sillanpää, M., & Witek-Krowiak, A. (2015). Agricultural waste peels as versatile biomass for water purification – A review. Chemical Engineering Journal, 270, 244-271.

Bhattacharya, A. & Misra, B. N. (2004). Grafting: a versatile means to modify polymers techniques, factors and applications. Progress Polymer Science, 29, 767–814.

Brady, J.M., Tobin, J.M., & Roux, J-C. (1999). Continuous fixed bed biosorption of Cu^{2+} ions: application of a simple two parameter mathematical model. Journal of Chemical Technology and Biotechnology, 74, 71-77.

Bunz, U. H. F. (2006). Breath figures as a dynamic templating method for polymers and nanomaterials. Advanced Materials, 18, 973-989.

Casaletto, M. P., Longo, A., Martorana, A., Prestianni, A., & Venezia, A. M. (2006). XPS study of supported gold catalysts: the role of Au^0 and $Au^{+\ \delta}$ species as active sites. Surface and Interface Analysis, 38, 215-218.

Chassary P, Vincent T, & Guibal E. (2004). Metal anion sorption on chitosan and derivative materials: a strategy for polymer modification and optimum use. Reactive and Functional Polymers, 60, 137–149.

Chen, L., & Subirade, M. (2007). Effect of preparation conditions on the nutrient release properties of alginate-whey protein granular microspheres. European Journal of Pharmaceutics and Bio pharmaceutics, 65, 354-362.

Chen, Y., & Wang, J. (2012). The characteristics and mechanism of Co (II) removal from aqueous solution by a novel xanthate-modified magnetic chitosan. Nuclear Engineering and Design, 242, 452-457.

Ciocoiua, O.-N., Staikosa, G., & Vasile. C. (2018). Thermoresponsive behavior of sodium alginate grafted with poly(Nisopropylacrylamide) in aqueous media. Carbohydrate Polymers, 184, 118–126.

Cordery, J., Will, A. J., Atkinson, K., & Wills, B. A. (1994). Extraction and recovery of silver from low grade liquirs using microalgae. Minerals Engineering, 7, 1003-1015.

Coseri, S., Nistor, G., Fras, L., Strnad, S., Harabagiu, V., & Simionescu, B. C. (2009). Mild and Selective Oxidation of Cellulose Fibers in the Presence of N-Hydroxyphthalimide. Biomacromolecules, 10, 2294–2299.

Crini, G. (2005). Recent developments in polysaccharide-based materials used as adsorbents in wastewater treatment. Progress in Polymer Science, 30, 38-70.

Daemi, H., & Barikani, M. (2012). Synthesis and characterization of calcium alginate nanoparticles, sodium homopolymannuronate salt and its calcium nanoparticles. Scientia Iranica, 19, 2023-2028.

Dai, J., Ren, F., & Tao, C. (2012). Adsorption behavior of Fe (II) and Fe (III) ions on thiourea cross-linked chitosan with Fe (III) as template. Molecules, 17, 4388-4399.

Dambies, L., Guimon, C., Yiacoumi, S., & Guibal, E. (2001). Characterization of metal ion interactions with chitosan by X-ray photoelectron spectroscopy. Colloids and Surfaces A: Physicochemical and Engineering Aspects, 177, 203-214.

Das, N. (2010). Recovery of precious metals through biosorption- a review. Hydrometallurgy, 103, 180-189.

David, G., Ortega, E., Chougrani, K., Manseri, A., & Boutevin, B. (2011). Grafting of phosphonate groups onto PVA by acetalyzation. Evaluation of the anti-corrosive properties for the acetalyzed PVA coatings. Reactive and Functional Polymers, 71, 599-606.

Devi, P., & Saroha, A. K. (2017). Utilization of sludge based adsorbents for the removal of various pollutants: A review. Science of the Total Environment, 578, 16-33.

Dodson, J. R., Parker, H. L., Garc á, A. M., Hicken, A., Asemave, K., Farmer, T. J., He, H., Clark, J. H., & Hunt, A. J. (2015). Bio-derived materials as a green route for precious & critical metal recovery and re-use. Green Chemistry, 17, 1951-1965.

Donia, A. M., Atia, A. A., & Elwakeel, K. Z. (2007). Recovery of gold (III) and silver (I) on a chemically modified chitosan with magnetic properties. Hydrometallurgy, 87, 197-206.

Dong, Z., Liu, J., Yuan, W., Yi, Y., & Zhao, L. (2016). Recovery of Au (III) by radiation synthesized aminomethyl pyridine functionalized adsorbents based on cellulose. Chemical Engineering Journal, 283, 504-513.

Draghi, L., Resta, S., Pirozzolo, M.G., & Tanzi, M.C. (2005). Microspheres leaching for scaffold porosity control. Journal of Materials Science: Materials in Medicine, 16, 1093-1097.

Du, K. (2017). Ionic liquid-regenerated macroporous cellulose monolith: Fabrication, characterization and its protein chromatography. Journal of Chromatography A, 1494, 40-45.

Du, X., Yuan, Q., & Li, Y. (2008). Mathematical analysis of solanesol adsorption on macroporous resins using the general rate model. Chemical engineering & technology, 31(9), 1310-1318.

Dwivedi, A. D., Dubey, S. P., Hokkanen, S., Fallah, R. N., & Sillanpaa, M. (2014). Recovery of gold from aqueous solutions by taurine modified cellulose: an adsorptive-reduction pathway. Chemical Engineering Journal, 255, 97-106.

Dwivedi, A. D., Dubey, S. P., Sillanpaa, M., Liimatainen, H., Suopajarvi, T., Niinimaki, J., Kwon, Y. N., & Lee, C. (2015). Distinctive green recovery of silver species from modified cellulose: Mechanism and spectroscopic studies. International Journal of Biological Macromolecules, 76, 109-118.

El-Shafey, E. I. (2013). Dehydrated carbon fiber for the recovery of Pd(II) and Pt(II) from chloride aqueous solution. Separation Science and Technology, 48, 1818-1828.

Elwakeel, K. Z., El-Sayed, G. O., & Darweesh, R. S. (2013). Fast and selective removal of silver(I) from aqueous media by modified chitosan resins. International Journal of Mineral Processing, 120, 26-34.

Fernandez, M. E., Nunell, G. V., Bonelli, P. R., & Cukierman, A. N. (2014). Activated carbon developed from orange peels: batch and dynamic competitive adsorption of basic dyes. Industrial Corps and Products, 62, 437-445.

Fiset, J. F., Blais, J. F., & Riveros, P. A. (2008). Review on the removal of metal ions from effluents using seaweeds, alginate derivatives and other sorbents. Revue des Sciences de l'Eau, 21, 283-308.

Fomina, M., & Gadd, G.M. (2014). Biosorption: Current perspectives on concept, definition and application. Bioresource Technology, 160, 3-14.

Freeman, I., Kedem, A., & Cohen, S. (2008). The effect of sulfation of alginate hydrogels on the specific binding and controlled release of heparin-binding proteins. Biomaterials, 22, 3260-3268.

Fujiwara, K., Ramesh, A., Maki, T., Hasegawa, H., & Ueda, K. (2007). Adsorption of platinum (IV), palladium (II) and gold (III) from aqueous solutions onto L-lysine modified crosslinked chitosan resin. Journal of Hazardous Materials, 146, 39-50.

Gadd, G. M. (2009). Biosorption: critical review of scientific rationale, environmental importance and significance for pollution treatment. Journal of chemical technology and biotechnology, 84,13-28.

Gao, X., Zhang, Y., & Zhao, Y. (2017). Biosorption and reduction of Au (III) to gold nanoparticles by thiourea modified alginate. Carbohydrate Polymers, 159, 108-115.

Gautam, R. K., Mudhoo, A., Lofrano, G., & Chattopadhyaya, M. C. (2104). Biomass-derived biosorbents for metal ions sequestration: Adsorbent modification and activation methods and activation methods and adsorbent regeneration. Journal of Environmental Chemical Engineering, 2, 239-259.

Gavilan, K. C., Pestov, A. V., Garcia, H. M., Yatluk, Y., Roussy, J., & Guibal, E. (2009). Mercury sorption on a thiocarbamoyl derivative of chitosan. Journal of Hazardous Materials, 165, 415–426.

Gericke, M., Trygg, J., & Fardim, P. (2013). Functional cellulose beads: preparation, characterization, and applications. Chemical Reviews, 113, 4812-4836.

Ghimire, K.N., Inoue, K., Ohto, K., & Hayashida, T. (2007). Adsorptive separation of metallic pollutants onto waste seaweed Porphyra yezonsis and Ulva japonica. Separation Science Technology, 42, 2003–2018.

Ghimire, K.N., Inoue, K., Ohto, K., & Hayashida, T. (2008). Adsorption study of metal ions onto crosslinked seaweed Laminaria japonica. Bioresource Technology, 99, 32–37.

Gomes, R., Dutta, S., & Bhaumik, A. (2014). Carboxylic acid-grafted mesoporous material and its high catalytic activity in one-pot three-component coupling reaction. APL Materials 2, 113307.

González, F., Romera, E., Ballester, A., Blázquez, M. L., Muñoz, J. Á., & García-Balboa, C. (2011). Algal Biosorption and Biosorbents. In P. Kotrba, M. Mackova & T. Macek (Eds.), Microbial Biosorption of Metals (pp. 159-178). Heidelberg: Springer: Heidelberg.

Guibal, E., Sweeney, N.V.O., Zikan, M.C., Vincent, T. & Tobin, J.M. (2001). Competitive sorption of platinum and palladium on chitosan derivatives. International Journal of Biological Macromolecules, 28, 401-408.

Guibal, E. (2004). Interactions of metal ions with chitosan-based sorbents: a review. Separation and Purification Technology, 38, 43–74.

Guiochon, G., & Lin, B. (2003). Modeling for Preparative Chromatography. Academic Press, Amsterdam.

Guiochon, G., Felinger, A., & Shirazi, D. G. (2006). Fundamentals of preparative and nonlinear chromatography: Academic Press.

Gupta, V. K., Gupta, B., Rastogi, A., Agarwal, S., & Nayak, A. (2011). A comparative investigation on adsorption performances of mesoporous activated carbon prepared from waste rubber tire and activated carbon for a hazardous azo dye-Acid Blue 113. Journal of Hazardous Materials, 186, 891-901.

Gurung, M., Adhikari, B. B., Kawkita, H., Ohto, K., Inoue, K., & Alam, S. (2011). Recovery of Au (III) by using low cost adsorbent prepared from persimmon tannin extract. Chemical Engineering Journal, 174, 556−563.

Gurung, M., Adhikari, B. B., Kawkita, H., Ohto, K., Inoue, K., & Alam, S. (2012). Selective recovery of precious metals from acidic leach liquor of circuit boards of spent mobile phones using chemically modified persimmon tannin gel. Industrial & Engineering Chemistry Research, 51, 11901−11913.

Gurung, M., Adhikari, B. B., Kawkita, H., Ohto, K., Inoue, K., & Alam, S. (2013). N-Aminoguanidine modified persimmon tannin: A new sustainable material for selective adsorption, preconcentration and recovery of precious metals from acidic chloride solution. Bioresource Technology, 129, 108−117.

Gurung, M., Adhikari, B. B., Gao, X., Alam, S., & Inoue, K. (2014). Sustainability in the Metallurgical Industry: Chemically Modified Cellulose for Selective Biosorption of Gold

from Mixtures of Base Metals in Chloride Media. Industrial & Engineering Chemistry Research, 53, 8565-8576.

Haiss, W., Thanh, N. T. K., Aveyard, J., & Fernig, D. G. (2007). Determination of Size and Concentration of Gold Nanoparticles from UV-Vis Spectra. Analytical Chemistry, 79, 4215-4221.

Hall, M., Bansal, P., Lee, J. H., Realff, M. J., & Bommarius, A. S. (2010). Cellulose crystallinity-A key predictor of the enzymatic hydrolysis rate. The FEBS Journal, 277, 1571−1582.

Han, R., Zou, L., Zhao, X., Xu, Y., Xu, F., Li, Y., & Wang, Y. (2009). Characterization and properties of iron oxide-coated zeolite as adsorbent for removal of copper(II) from solution in fixed bed column. Chemical Engineering Journal, 149, 123-131.

He, H., Li, W., Lamson, M., Zhong, M., Konkolewicz, D., Hui, C. M., Yaccato., K., Rappold, T., Sugar, G., David, N. E., Damodaran, K., Natesakhawat, S., Nulwala, H., & Matyjaszewski, K. (2014). Porous polymers prepared via high internal phase emulsion polymerization for reversible CO2 capture. Polymer, 55, 384-394.

He, J., & Chen, J. P. (2014). A comprehensive review on biosorption of heavy metals by algal biomass: materials, performances, chemistry, and modelling simulation tools. Bioresource Technology, 160, 67-78.

Heeter, G., & Liapis, A. (1998). Frontal chromatography of proteins: Effect of axialdispersion on column performance. Journal of Chromatography A, 796(1), 157-164.

Heinze, T. & Leibert, T. (2001). Unconventional methods in cellulose functionalization. Progress in Polymer Science, 26, 1689−1762.

Hernández-Ortiz, J. C. & Vivaldo-Lima, E. (2013). Chapter 9: Crosslinking. In E. Saldivar-Guerra & E. Vivaldo-Lima (Eds.), Handbook of Polymer Synthesis, Characterization, and Processing (pp. 187-202). New York: Wiley.

Hillmyer, M. A. (2005). Nanoporous materials from block copolymer precursors. Block Copolymers II, 190, 137-181.

Ho, Y. S. (2006). Review of second-order models for adsorption systems. Journal of Hazardous Materials, 136, 681-689.

Hokkanen, S., Bhatnagar, A., & Sillanpää, M. (2016). A review on modification methods to cellulose-based adsorbents to improve adsorption capacity. Water Research, 91, 156-173.

Huo, H., Su, H., & Tan, T. (2009). Adsorption of Ag^{+} by a surface molecular-imprinted biosorbent. Chemical Engineering Journal, 150, 139-144.

Izatt, S., Izatt, N., & Bruening, R. (2010). Metal separations of interest to the Chinese metallurgical industry. Journal of Rare Earths, 28, 22-29.

Izquierdo, M., Gabaldón, C., Marzal, P., & Sempere, F. (2010). Sorption of copper by a highly mineralized peat in batch and packed-bed systems. Journal of Chemical Technology and Biotechnology, 85(2), 165-172.

Jang, J., Miran, W., Divine, S. D., Nawaz, M., Shahzad, A., Woo, S. H., & Lee, D. S. (2018). Rice straw-based biochar beads for the removal of radioactive strontium from aqueous solution. Science of the Total Environment, 615, 698-707.

Jeppu, G. P., & Clement, T. P. (2012). A modified Langmuir-Freundlich isotherm model for simulating pH-dependent adsorption effects. Journal of Contaminant Hydrology, 129-130, 46-53.

Jiang, J., & Cooper, A. I. (2010). Microporous organic polymers: design, synthesis, and function. Topics in Current Chemistry, 293, 1-33.

Jolly, W. L. (1984). Modern Inorganic Chemistry. New York: McGraw-Hill.

Kafedjiiski, K., Krauland, A. H., Hoffer, M. H. & Bernkop-Schnurch, A. (2005). Synthesis and in vitro evaluation of a novel thiolated chitosan. Biomaterials, 26, 819-826.

Kailasam, K., Jun, Y.-S., Katekomol, P., Epping, J. D., Hong, W. H., & Thomas, A. (2010). Mesoporous Melamine Resins by Soft Templating of Block-co-Polymer Mesophases. Chemistry of Materials. 22, 428-434.

Kanai, Y., Oshima, T., & Baba, Y. (2008). Synthesis of highly porous chitosan microspheres anchored with 1,2-ethylenedisulfide moiety for the recovery of precious metal ions. Industrial & Engineering Chemistry Research, 47, 3114–3120.

Karbstein, H. & Schubert, H. (1995). Developments in the continuous mechanical production of oil-in-water macro-emlusions. Chemical Engineering and Processing: Process Intensification, 33, 205-211.

Karmarkar, N. (1984). A new polynomial-time algorithm for linear-programming. Combinatorica, 4, 373-395.

Kim, J. K., Yang, S. Y., Lee, Y., & Kim, Y. (2010). Functional nanomaterials based on block copolymer self-assembly. Progress in Polymer Science, 35, 1325-1349.

Kimmins, S. D., & Cameron, N. R. (2011). Functional porous polymers by emulsion templating: recent advances. Advanced Functional Materials, 21, 211-225.

Klimmekand, S., Stan, H.J., Wilke, A., Bunke, G., & Buchholz, R. (2001). Comparative analysis of the biosorption of cadmium, lead, nickel, and zinc by algae. Environmental Science & Technology, 35, 4283-4288.

Kondo, K., Hirayama, K., & Matsumoto, M. (2013). Adsorption of metal ions from aqueous solution onto microalga entrapped into Ca-alginate gel bead. Desalination and Water Treatment, 51, 4675-4683.

Kostic, M. M., Milanovic, J. Z., Baljak, M. V., Mihajlovski, K., & Kramar, A. D. (2014). Preparation and characterization of silver-loaded hemp fibers with antimicrobial activity. Fibers and Polymers, 15, 57-64.

Kotoulas, K., & Kiparissides, C. (2006). A generalized population balance model for the prediction of particle size distribution in suspension polymerization reactors. Chemical Engineering Science, 61, 332-346.

Kotte, P., & Yun, Y. (2014). L-cysteine impregnated alginate capsules as a sorbent for gold recovery. Polymer Degradation and Stability, 109, 424-429.

Kousha, M., Daneshvar, E., Sohrabi, M.S., Jokar, M., & Bhatnagar, A. (2012). Adsorption of acid orange II dye by raw and chemically modified brown macroalga Stoechospermum marginatum. Chemical Engineering Journal, 192, 67–76.

Kuyucak, N., & Volesky, B. (1989). Accumulation of gold by algal biosorption. Biorecovery, 1, 189-204.

Kyzas, G. Z., & Kostoglou, M. (2014). Green Adsorbents for Wastewaters: A Critical Review. Materials, 7, 333-364.

Laus, R., Costa, T. G., Szpoganicz, B., & Favere, V. T. (2010). Adsorption and desorption of Cu (II), Cd (II) and Pb (II) ions using chitosan crosslinked with epichlorohydrin-triphosphate as the adsorbent. Journal of Hazardous Materials, 183, 233-241.

Legodi, M. A., de Waal, D., Potgieter, J. H., & Potgieter, S. S. (2001). Rapid determination of CaCO3 in mixtures utilising FT-IR spectroscopy. Mineral Engineering, 14, 1107-1111.

Li, W., Yoon, J. A., & Matyjaszewski, K. (2010). Dual-reactive surfactant used for synthesis of functional nanocapsules in miniemulsion. Journal of the American Chemical Society, 132, 7823-7825.

Liu, B., Wang, D., Yu, G., & Meng, X. (2013). Adsorption of heavy metal ions, dyes and proteins by chitosan composites and derivatives - a review. Journal of Ocean University of China, 12, 500-508.

Liu, L., Wan, Y., Xie, Y., Zhai, R., Zhang, B., Liu, J. (2012). The removal of dye from aqueous solution using alginate-halloysite nanotube beads. Chemical Engineering Journal, 187, 210-216.

Liu, Y., Goebl, J., & Yin, Y. (2013). Templated synthesis of nanostructured materials. Chemical Society Reviews. 42, 2610.

Lou, X. W., Archer, L.A., & Yang, Z. (2008). Hollow Micro-/Nanostructures: Synthesis and Applications. Advanced Materials, 20, 3987-4019.

Lu, W., Yuan, D., Sculley, J., Zhao, D., Krishna, R., & Zhou, H. (2011). Sulfonate-grafted porous polymer networks for preferential CO_2 adsorption at low pressure. Journal of the American Chemical Society, 133, 18126-18129.

Lv, L., Zhang, Y., Wang, K., Ray, A. K., & Zhao, X. (2008). Modeling of the adsorption breakthrough behaviors of Pb^{2+} in a fixed bed of ETS-10 adsorbent. Journal of colloid and interface science, 325(1), 57-63.

Mack, C., Wilhelmi, B., Duncan, J.R., & Burgess, J.E. (2007). Biosorption of precious metals. Biotechnology Advances, 25, 264–271.

Madaeni, S.S. & Mansourpanah, Y. (2003). COD removal from concentrated wastewater using membranes. Filtration and Separation 40 (6), 40–46.

Maggioris, D., Goulas, A., Alexopoulos, A. H., Chatzi, E. G., & Kiparissides, C. (2000). Prediction of particle size distribution in suspension polymerization reactors: effect of turbulence nonhomogeneity. Chemical Engineering Science, 55, 4611-4627.

Marshall, W. E., Wartelle, L. H., Boler, D. E., Johns, M. M., & Toles, C. A. (1999). Enhanced metal adsorption by soybean hulls modified with citric acid. Bioresource Technology, 69, 263-268.

Masel, R. I. (1996). Principles of adsorption and reaction on solid surfaces. Wiley Interscience.

Mata, Y. N., Torres, E., Blázquez, M. L., Ballester, A., González, F. J., & Muňoz, A. (2009). Gold (III) biosorption and bioreduction with the brown alga Fucus vesiculosus. Journal of Hazardous Materials, 166, 612-618.

Mane, S. (2016). Effect of porogens (type and amount) on polymer porosity: a review. Canadian Chemical Transactions, 4, 210-225.

Mastalerz, M. (2008). The next generation of shape-persistant zeolite analogues: covalent organic frameworks. Angewandte Chemie Internation Edition, 47, 445-447.

Mele, E., Anyfantis, G. C., Fragouli, D., Ruffilli, R., & Athanassiou, A. (2014). Localized synthesis of gold nanoparticles in anisotropic alginate structures. RSC Advances, 4, 20449-20453.

Minamisawa, M., Minamisawa, H., Yoshida, S., & Takai, N. (2005). Characterization of adsorption gels prepared from plant biomaterials. Green Chemistry, 7, 595-601.

Monteiro Jr., O.A. & Airoldi, C. (1999). Some studies of crosslinking chitosan-glutaraldehyde interaction in a homogeneous system. International Journal of Biological Macromolecules, 26, 119-128.

Naja, G., & Volesky, B. (2006). Behavior of the mass transfer zone in a biosorption column. Environmental science & technology, 40(12), 3996-4003.

Naumkin, A. V., Kraut-Vass, A., Gaarenstroom, S. W., & Powell, C. J. (2012). NIST X-ray Photoelectron Spectroscopy Database, http://srdata.nist.gov/xps/Default.aspx

Nestle, N. & Kimmich, R. (1996). NMR Microscopy of heavy metal absorption in calcium alginate beads. Applied Biochemistry and Biotechnology, 56, 9-17.

Nguyen, T. C., Loganathan, P., Nguyen, T. V., Vigneswaran, S., Kandasamy, J., & Naidu, R. (2015). Simultaneous adsorption of Cd, Cr, Cu, Pb, and Zn by an iron-coated Australian zeolite in batch and fixed-bed column studies. Chemical Engineering Journal, 270, 393-404.

Niu, H., & Volesky, B. (1999). Characteristics of gold biosorption from cyanide solution. Journal of Chemical Technology and Biotechnology, 74, 778-784.

O'Connell, D. W., Birkinshaw, C., & O'Dwyer, T. F. (2008). Heavy metal adsorbents prepared from the modification of cellulose: A review. Bioresource Technology, 99, 6709−6724.

Olson, D. A., Chen, L., & Hillmyer, M. A. (2008). Templating nanoporous polymers with ordered block copolymers. Chemistry of Materials, 20, 869-890.

Oomens, J. & Steill, J. D. (2008). Free Carboxylate Stretching Modes. The Journal of Physical Chemistry A, 112, 3281-3283.

Qin, J.J., Wai, M.N., Oo, M.H. & Wong, F.S. (2002). A feasibility study on the treatment and recycling of a wastewater from metal plating. Journal of Membrane Science 208 (1–2), 213–221.

Pangeni, B., Paudyal, H., Inoue, K., Kawakita, H., Ohto, K., & Alam, S. (2012). Selective recovery of gold (III) using cotton cellulose treated with concentrated sulfuric acid. Cellulose, 19, 381-391.

Pangeni, B., Paudyal, H., Abe, M., Inoune, K., Kawakita, H., Ohto, K., Adhikari, B. B., & Alam, S. (2012). Selective recovery of gold using some cross-linked polysaccharide gels. Green Chemistry, 14, 1917-1927.

Parajuli, D., Adhikari, C. R., Kuriyama, M., Kawakita, H., Ohto, K., Inoune, K., & Funaoka, M. (2006). Selective recovery of gold by novel lignin based adsorption gels. Industrial & Engineering Chemistry Research, 45, 8−14.

Parajuli, D., & Hirota, K. (2009). Recovery of palladium using chemically modified cedar wood powder. Journal of Colloid and Interface Science, 338, 371-375.

Park, S., Kwak, I. S., Won, S. W., & Yun, Y. S. (2013). Glutaraldehyde-crosslinked chitosan beads for sorptive separation of Au(III) and Pd(II): Opening a way to design reduction-coupled selectivity-tunable sorbents for separation of precious metals. Journal of Hazardous Materials, 248-249, 211-218.

Pat-Espadas, A.M., Field, J.A., Razo-Flores, E., Cervantesb, F.J., & Sierra-Alvareza, R. (2016). Continuous removal and recovery of palladium in an upflow anaerobic granular

sludge bed (UASB) reactor. Journal of Chemical Technology and Biotechnology, 91, 1183–1189.

Paudyal, H., Pangeni, B., Inoue, K., Kawakita, H., Ohto, K., Ghimire, K. N, & Alam, S. (2013). Preparation of novel alginate based anion exchanger from Ulva japonica and its application for the removal of trace concentrations of fluoride from water. Bioresource Technology, 148, 221-227.

Pekala, R. W. (1989). Organic aerogels from the polycondensation of resorcinol with formaldehyde. Journal of Material Science, 24, 3221-3227.

Pérez-Martínez, Y., Montesinos-Cisneros, R., Guerrero-Germán, P., Guzman-Zamudio, R., & Tejeda-Mansir, A. (2015). Batch Equilibrium and Kinetic Studies of Plasmid pCI Adsorption onto Perfusion Particles. Journal of Liquid Chromatography & Related Technologies, 38(2), 196-200.

Pettit, L. D., & Powell, K. J. (1999). IUPAC Stability Constants Database, Academic Software: Yorks.

Poon, L., Wilson, L. D., & Headley, J. V. (2014). Chitosan-glutaraldehyde copolymers and their sorption properties. Carbohydrate Polymers, 109, 92-101.

Rafatullah, M., Sulaiman, O., Hashim, R., & Ahmad, A. (2010). Adsorption of methylene blue on low-cost adsorbents: A review. Journal of Hazardous Materials, 177, 70-80.

Raj, K. J. A., Shanmugam, R., Mahalakshmi, R., & Viswanathan, B. (2010). XPS and IR spectral studies on the structure of phosphate and sulphate modified titania – A combined DFT and experimental study. Indian Journal of Chemistry, 49A, 9-17.

Ramesh, A., Hasegawa, H., Sugimoto, W., Maki, T., & Ueda, K. (2008) Adsorption of gold(III), platinum(IV) and palladium(II) onto glycine modified crosslinked chitosan resin. Bioresource Technology, 99, 3801−3809.

Rao, C. N. R., & Venkataraghavan, R. (1962). The C=S stretching frequency and the "-N-C=S bands" in the infrared. Spectrochimica Acta. 18, 541-547.

Rocher, V., Siaugue, J., Cabuil, V., & Bee, A. (2008). Removal of organic dyes by magnetic alginate beads. Water Research, 42, 1290-1298.

Romera, E., González, F., Ballester, A., Blázquez, M. L., & Muñoz, J. A. (2007). Comparative study of biosorption of heavy metals using different types of algae. Bioresource Technology, 98, 3344-3353.

Ruiz, M., Sastre, A. M., & Guibal, E. (2000). Palladium sorption on glutaraldehyde-crosslinked chitosan. Reactive and Functional Polymers, 45, 155-173.

Ruthven, D.M. (1984). Principles of Adsorption and Adsorption Processes, John Wiley & Sons, Hoboken.

Saha, B. & Orvig, C. (2010). Biosorbents for hexavalent chromium elimination from industrial and municipal effluents. Coordination Chemistry Reviews, 254, 2959–2972.

Sari, A., Mendil, D., Tuzen, M., & Soylak, M. (2009). Biosorption of palladium(II) from aqueous solution by moss (Racomitrium lanuginosum) biomass: equilibrium, kinetic and thermodynamic studies. Journal of Hazardous Materials, 162, 874-879.

Sarymsakov, A. A., Burkhanova, N. D., Tashpulatov, Y. T., & Satybaldyeva, D. T. (1997). Study of the partial O-alkylation of cotton cellulose. Chemistry of Nature Compounds, 33, 337-339.

Sathishkumar, M., Mahadevan, A., Vijiyaraghavan, K., Pavagadhi, S., & Balasubramanian, R. (2010). Green recovery of gold through biosorption, biocrystallization, and pyro-crystallization. Industrial & Engineering Chemistry Research, 49, 7129-7135.

Schnepp, Z. (2013). Biopolymers as a Flexible Resource for Nanochemistry. Angewandte Chemie International Edition, 52, 1096-1108.

Sescousse, R., Gavillon, R., & Budtova, T. (2011). Wet and dry highly porous cellulose beads from cellulose-NaOH-water solutions: influence of the preparation conditions on bead shape and encapsulation of inorganic particles. Journal of Materials Science, 46, 759-765.

Shimizu, T. & Takada, A. (1997). Preparation of Bi-based superconducting fiber by metal biosorption of Na-Alginate. Polymer gels networks, 5, 267-283.

Simkovic, I., Laszlo, J. A., & Thompson, A. R. (1996). Preparation of a weakly basic ion exchanger by crosslinking starch with epichlorohydrin in the presence of NH4OH. Carbohydrate Polymers, 30, 25-30.

Singh, S. K. & Gross, R. A. (2001). Overview: Introduction to Polysaccharides, Agroproteins, and Poly(amino acids). In R.A. Gross & C. Scholz (Eds.), Biopolymer from Polysaccharides and Argoproteins (pp. 2-20). New York: Oxford University Press.

Sobkowiak, M., Reisser, E., Given, P., & Painter, P. (1984). Determination of aromatic and aliphatic CH groups in coal by FT-IR: 1. Study of coal extracts. Fuel, 63, 1245-1252.

Salomonsen, T., Jensen, H.M., Larsen, F.H., Stefan Steuernagel, S., & Engelsen, S.B. (2009). Direct quantification of M/G ratio from 13C CP-MAS NMR spectra of alginate powders by multivariate curve resolution. Carbohydrate Research, 344, 2014–2022.

Song, J.H., & Kretzschmar, I. (2008). Colloid-templated multisectional porous polymeric fibers. Langmuir, 24, 10616-10620.

Stuart, B. (2004). Infrared Spectroscopy: Fundamentals and Applications. New York: Wiley, (Chapter 4: Organic Molecules).

Sulaymon, A. H., Abid, B. A., & Al-Najar, J. A. (2009). Removal of lead copper chromium and cobalt ions onto granular activated carbon in batch and fixed-bed adsorbers. Chemical Engineering Journal, 155(3), 647-653.

Sun, Q., & Deng, Y. (2005). In situ synthesis of temperature-sensitive hollow microspheres via interfacial polymerization. Journal of the American Chemical Society, 127, 8274-8275.

Vipin, A. K., Hu, B., & Fugetsu, B. (2013). Prussian blue caged in alginate/calcium beads as adsorbents for removal of cesium ions from contaminated water. Journal of Hazardous Materials, 258-259, 93-101.

Thomas, A., Goettmann, F., & Antonietti, M. (2008). Hard templates for soft materials: creating nanostructured organic materials. Chemistry of Materials, 20, 738-755.

Torres, E., Mata, Y. N., Blázquez, M. L., Muňoz, J. A., González, F., & Ballester, A. (2005). Gold and silver uptake and nanoprecipitation on calcium alginate beads. Langmuir, 21, 7951-7958.

Tran, R.T., Naseri, E., Kolasnikov, A., Bai, X., & Yang, J. (2011). A new generation of sodium chloride porogen for tissue engineering. Biotechnology and Applied Biochemistry, 58, 335-344.

Tran,V. S., Ngo, H. H., Guo, W., Zhang, J., Liang, S., Ton-That, C., & Zhang, X. (2015). Typical low cost biosorbents for adsorptive removal of specific organic pollutants from water. Bioresource. Technology, 182, 353-363.

Trygg, J., Fardim, P., Gericke, M., Mäkilä, E., & Salonen, J. (2013). Physicochemical design of the morphology and ultrastructure of cellulose beads. Carbohydrate Polymers, 93, 291-299.

Turiel, E., Perez-Conde, C., & Martin-Esteban, A. (2003). Assessment of the cross-reactivity and binding sites characterisation of a propazine-imprinted polymer using the Langmuir-Freundlich isotherm. Analyst, 128, 137-141.

Uddin, M. K. (2017). A review on the adsorption of heavy metals by clay minerals, with special focus on the past decade. Chemical Engineering Journal, 308, 438-462.

Umpleby, R. J., Baxter, S. C., Chen, Y., Shah, R. N., & Shimizu, K. D. (2001). Characterization of molecularly imprinted polymers with the Langmuir-Freundlich isotherm. Analytical Chemistry, 73, 4584-4591.

Vaquette, C., Viateau, V., Guérard, S., Anagnostou, F., Manassero, M., Castner, D. G., & Migonney, V. (2013). The effect of polystyrene sodium sulfonate grafting on polyethylene terephthalate artificial ligaments on in vitro mineralisation and in vivo bone tissue integration. Biomaterials, 34, 7048-7063.

Varma, A. J., Deshpande, S. V., & Kennedy, J. F. (2004). Metal complexation by chitosan and its derivatives: a review. Carbohydrate Polymers, 55, 77-93.

Vaughan, T., Seo, C. W., & Marshall, W. E. (2001). Removal of selected metal ions from aqueous solution using modified corncobs. Bioresource Technology, 78, 133-139.

Vijayaraghavan, K., & Balasubramanian, R. (2015). Is biosorption suitable for decontamination of metal-bearing wastewaters? A critical review on the state-of-the-art of biosorption processes and future directions. Journal of Environmental Management, 160, 283-296.

Vijayaraghavan, K., Won, S.W., Mao, J., & Yun, Y. (2008). Chemical modification of Corynebacterium glutamicum to improve methylene blue biosorption. Chemical Engineering Journal, 145, 1–6.

Vijayaraghavan, K. & Yun, Y. (2008). Bacterial biosorbents and biosorption. Biotechnology Advances, 26, 266–291.

Vijayaraghavan, K., Mahadevan, A., Sathishkumar, M., Pavagadhi, S., & Balasubramanian, R. (2011). Biosynthesis of Au(0) from Au(III) via biosorption and bioreduction using brown marine alga Turbinaria conoides. Chemical Engineering Journal, 167, 223-227.

Villemin, D., Moreau, B., Siméon, F., Maheut, G., Fernandez, C., Montouillout, V., Caignaert, V., & Jaffrès, P. (2001). A one step process for grafting organic pendants on alumina via the reaction of alumina and phosphonate under microwave irradiation. Chemical Communications, 20, 2060-2061.

Vipin, A. K., Hu, B., & Fugetsu, B. (2013). Prussian blue caged in alginate/calcium beads as adsorbents for removal of cesium ions from contaminated water. Journal of Hazardous Materials, 258-259, 93-101.

Volesky, B. (1990). Biosorption of Heavy Metals. Florida: CRC Pres. ISBN 0849349176.

Wang, J & Chen, C. (2009). Biosorbents for heavy metals removal and their future. Biotechnology Advances, 27, 195–226.

Wang, J & Chen, C. (2014). Chitosan-based biosorbents: Modification and application for biosorption of heavy metals and radionuclides. Bioresource Technology, 160, 129-141.

Wang, J., Wang, L., Yu, H., Zain-ul-Abdin, Chen, Y., Chen, Q., Zhou, W., Zhang, H., & Chen, X. (2016). Recent progress on synthesis, property and application of modified chitosan: An overview. International Journal of Biological Macromolecules, 88, 333-344.

Wang, L., Peng, H., Liu, S., Yu, H., Li, P., & Xing, R. (2012). Adsorption properties of gold onto a chitosan derivative. International Journal of Biological Macromolecules, 51, 701-704.

Wang, S., Vincent, T., Roux, J.C., Faur, C., & Guibal, E. (2017). Innovative conditioning of algal-based sorbents: Macro-porous discs for palladium sorption. Chemical Engineering Journal, 325, 521-532.

Wang, Y. & Li, F. (2011). An emerging pore-making strategy: confined swelling-induced pore generation in block copolymer materials. Advanced Materials, 23, 2134-2148.

Widmer, R., Oswald-Krapf, H., Sinha-Khetriwal, D., & Schnellmann, M. (2005). Global Perspectives on e-Waste. Environmental Impact Assessment Review, 25, 436−458.

Won, S. W., Kotte, P.,Wei, W., Lim, A., & Yun, Y. S. (2014). Biosorbents for recovery of precious metals. Bioresource Technology, 160, 203-212.

Wong, S., Ngadi, N., Inuwa, I. M., & Hassan, O. (2018). Recent advances in applications of activated carbon from biowaste for wastewater treatment: A short review. Journal of Cleaner Production, 175, 361-375.

Wu, D., Xu, F., Sun, B., Fu, R., He, H., & Matyjaszewski, K. (2012). Design and preparation of porous polymers. Chemical Reviews, 112, 3959-4015.

Xiao, B., & Thomas, K. M. (2004). Competitive adsorption of aqueous metal ions on an oxidized nanoporous activated carbon. Langmuir, 20, 4566-4578.

Xu, J., Zhu, L., Xu, G., Yu, W., & Ray, A.K. (2013). Determination of competitive adsorption isotherm of enantiomers on preparative chromatographic columns using inverse method. Journal of Chromatography A, 1273, 49-56.

Xu, M., Yin, P., Liu, X., Dong, X., Xu, Q., & Qu, R. (2013). Preparation, characterization, adsorption equilibrium, and kinetics for gold-ion adsorption of spent buckwheat hulls modified by organodiphosphonic acid. Industrial & Engineering Chemistry Research, 53, 8114-8124.

Yagub, M. T., Sen, T. K., Afroze, S., & Ang, H. M. (2014). Dye and its removal from aqueous solution by adsorption: A review. Advances in Colloid and Interface Science, 209, 172-184.

Yi, Q., Fan, R., Xie, F., Zhang, Q., & Luo, Z. (2016). Recovery of Palladium (II) from nitric acid medium using a natural resin prepared from persimmon dropped fruits residues. Journal of the Taiwan Institute of Chemical Engineers, 61, 299-305.

Yong, S. K., Skinner, W. M., Bolan, N. S., Lombi, E., Kunhikrishnan, A., & Ok, Y. S. (2016). Sulfur crosslinks from thermal degradation of chitosan dithiocarbamate derivatives and thermodynamic study for sorption of copper and cadmium from aqueous system. Environmetal Science and Pollution Research, 23, 1050-1059.

Yu, D., Jackson, K., & Harmon, T. (1999). Dispersion and diffusion in porous media under supercritical conditions. Chemical engineering science, 54(3), 357-367.

Yuan, H., Nishiyama, Y., Wada, M., & Kuga, S. (2006). Surface acylation of cellulose whiskers by drying aqueous emulsion. Biomacromolecules, 7, 696-700.

Yumei, Z., Jianming, J., & Yanmo, C. (1999). Synthesis and antimicrobial activity of polymers guanidine and biguanidine salts. Polymer, 40, 6189−98.

Yunus, I. S., & Tsai, S. L. (2015). Designed biomolecule-cellulose complexes for palladium recovery and detoxification. RSC Advances, 5, 20276-20282.

Zhang, S., Xu, F., Wang, Y., Zhang, W., Peng, X., & Pepe, F. (2013). Silica modified calcium alginate-xanthan gum hybrid bead composites for the removal and recovery of Pb (II) from aqueous solution. Chemical Engineering Journal, 234, 33-42.

Zhang, M., Zhang, Y., & Helleur, R. (2015). Selective adsorption of Ag^{+} by ion-imprinted O-carboxymethyl chitosan beads grafted with thiourea-glutaradehyde. Chemical Engineering Journal, 264, 56-65.

Zhang, Y., Rohani, S., & Ray, A. K. (2008). Numerical determination of competitive adsorption isotherm of mandelic acid enantiomers on cellulose-based chiral stationary phase. Journal of Chromatography A, 1202, 34-39.

Zhao, X.S., Su, F., Yan, Q., Guo, W., Bao, X., Lv, L., & Zhou, Z. (2005) Templating methods for preparation of porous structures. Journal of Materials Chemistry, 16, 637-648.

Zhou, L., Wang, Y., Liu, Z., & Huang, Q. (2009). Characteristics of equilibrium, kinetics studies for adsorption of Hg (II), Cu (II), and Ni (II) ions by thiourea-modified magnetic chitosan microspheres. Journal of Hazardous Materials, 61, 995-1002.